DOKUZ EYLÜL UNIVERSITY
GRADUATE SCHOOL OF NATURAL AND APPLIED SCIENCES

PRODUCTION AND CHARACTERIZATION OF HIGH ENTROPY ALLOYS (HEA) BY VACUUM ARC MELTING (VAM) METHOD

by

SAADET GÜLER

September, 2022
İZMİR

PRODUCTION AND CHARACTERIZATION OF HIGH ENTROPY ALLOYS (HEA) BY VACUUM ARC MELTING (VAM) METHOD

A Thesis Submitted to the
Graduate School of Natural and Applied Sciences of Dokuz Eylül University
In Partial Fulfillment of the Requirements for the Degree of Doctor of Philosophy in Metallurgical and Materials Engineering, Metallurgical and Materials Engineering Program

by

SAADET GÜLER

September, 2022
İZMİR

Ph.D. THESIS EXAMINATION RESULTS FORM

We have read the thesis entitled **PRODUCTION AND CHARACTERIZATION OF HIGH ENTROPY ALLOYS (HEA) BY VACUUM ARC MELTING (VAM) METHOD** completed by **SAADET GÜLER** under supervision of **Assoc. Prof. Dr. Esra Dokumacı ALKAN** and we certify that in our opinion it is fully adeaquate, in scope and in quality, as a thesis for the degree of Doctor of philosophy.

Assoc. Prof. Dr. Esra DOKUMACI ALKAN

Supervisor

Asst. Prof. Dr. Murat ALKAN

Thesis Committee Member

Asst. Prof. Dr. Tolga TAVŞANOĞLU

Thesis Committee Member

Prof. Dr. Mücahit SÜTÇÜ

Examining Committee Member

Assoc. Prof. Dr. Ahmet TURAN

Examining Committee Member

Prof.Dr. Okan FISTIKOĞLU

Director

Graduate School of Natural and Applied Sciences

ACKNOWLEDGEMENTS

First of all, I would like to express the sense of gratitude to my advisor Assoc. Prof. Dr. Esra Dokumacı ALKAN for her constructive ideas, help, constant support, guidance and contributions during my PhD research.

I would also like to thank my committee members, Assist. Prof. Dr. Murat ALKAN and Assist. Prof. Dr. Tolga TAVŞANOĞLU for reviewing my work and offering valuable suggestions and sharing their visions about the content of my thesis.

I wish to extend my sincere thanks to Assoc. Prof. Dr. Aslı Çakır, Assoc. Prof. Dr. Mustafa EROL, Prof. Dr. Mücahit Sütçü for their collaboration in the laboratory studies and for sharing their valuable experiences with me.

In addition, I would like to thank Asst. Yaşar ORBAY, Asst. M. Batıkan KANDEMİR, Specialist Uğur Can Özöğüt, Asst. Dr. Ramazan DALMIŞ, Asst. Dr. Çağrı KILINÇ, Asst.Dr.Serhan KÖKTAŞ, Asst. Özgür Yasin KESKİN and Dilan UĞURLUER for their support and friendships. Besides, I would like to thank Asst. Ahmet YAVAŞ, Asst. Metehan ATAGÜR, and Asst. Merve TORMAN for their collaboration in the laboratory studies and kind friendships who are my colleagues in my department. The authors are pleased to acknowledge the financial support for this research from TUBITAK (The Scientific and Technological Research Council of Turkey, Project No. 118M204). The authors would like to thank the advisor of this project, Assistant Professor Dr. Nuri SOLAK for his support with the usage of the Thermo-Calc software.

Finally, I would like to thank my mother, Şennur GÜLER, and my father, Himmet GÜLER, who contributed to my success. Special thanks to my dear sister Gizem GÜLER, who encouraged me to progress in my scientific journey and always supported me on this path.

Saadet GÜLER

PRODUCTION AND CHARACTERIZATION OF HIGH ENTROPY ALLOYS (HEA) BY VACUUM ARC MELTING (VAM) METHOD

ABSTRACT

High entropy alloys (HEA) are a new generation alloy group that, unlike conventional alloys, contains basic alloying elements in ratios of at least 5 elements to or near co-atoms. In the triple phase diagram, the composition lines of high entropy alloys are in the center of the diagram, unlike conventional alloys. This situation directly changes the thermodynamic structure, morphology, type of phases to occur and all properties of the material of the new generation alloy. These alloys are multi-component structures that have the potential to exhibit properties useful for engineering applications.

Within the scope of this thesis, by examining the production AlCoCrFeNiTix of high entropy alloys, it is aimed to create phase diagrams of AlCoCrFeNiTix alloys, which were created for the first time in the literature. AlCoCrFeNiTix of high entropy alloys heat treatment behavior, characterization of these alloys, various properties, and to facilitate the determination of the predicted phases to occur in future studies. The AlCoCrFeNiTiX series designed with CALPHAD has been produced using the arc melting method of high entropy alloys. Heat treatment was applied to the selected samples among the produced samples. In the thesis study, the phase structure, morphology, thermal properties, and hardness properties of these alloys were examined in detail. In line with this information, a phase diagram of the AlCoCrFeNiTix high entropy alloy system, which was created under balanced cooling conditions, was obtained.

Keywords: High Entropy Alloy, Vacuum Arc Melting, Heat Treatment, CALPHAD, Phase Diagram

YÜKSEK ENTROPİLİ ALAŞIMLARIN (YEA) VAKUM ARK ERGİTME (VAM) YÖNTEMİ İLE ÜRETİMİ VE KARAKTERİZASYONU

ÖZ

Yüksek entropili alaşımlar (YEA) , geleneksel alaşımlardan farklı olarak en az 5 elementin eş-atom veya eş-atom oranına yakın oranlarda temel alaşım elementi içeren yeni nesil bir alaşım grubudur. Üçlü faz diyagramında yüksek entropili alaşımların kompozisyon çizgileri, geleneksel alaşımların aksine diyagramın merkezinde yer alır. Bu durum, yeni nesil alaşımın termodinamik yapısını, morfolojisini, meydana gelecek fazların türünü ve malzemenin tüm özelliklerini doğrudan değiştirir. Bu alaşımlar, mühendislik uygulamaları için yararlı özellikler sergileme potansiyeline sahip çoklu bileşenlerden oluşan yapılardır.

Bu tez çalışması kapsamında, yüksek entropili alaşımların üretimi,ısıl işlem davranışları, bu alaşımların karakterizasyonu, çeşitli özellikleri incelenerek literatürde ilk kez oluşturulan AlCoCrFeNiTix alaşımların faz diyagramlarının oluşturulması ve ileriki çalışmalarda oluşacak tahmini fazların belirlenebilmesinde kolaylık sağlanması amaçlanmıştır. CALPHAD ile tasarlanan AlCoCrFeNiTiX serisi yüksek entropili alaşımların ark ergitme yöntemi kullanılarak üretilmiştir. Üretilen numuneler arasından seçilen numunelere ısıl işlem uygulanmıştır. Tez çalışmasında, bu alaşımların faz yapısı, morfolojisi, termal özellikleri ve sertlik özellikleri detaylıca incelenmiştir. Bu bilgiler doğrultusunda, AlCoCrFeNiTix yüksek entropili alaşım sistemine ait dengeli soğuma koşullarında oluşturulan bir faz diyagramı elde edilmiştir.

Anahtar kelimeler: Yüksek Entropili Alaşım, Vakum Ark Ergitme, Isıl İşlem, Termodinamik Yaklaşım(CALPHAD), Faz diyagramı

CONTENTS

Page

PH.D. THESIS EXAMINATION RESULTS FORM iii
ACKNOWLEDGEMENTS iii
ABSTRACT iv
ÖZ v
LIST OF SYMBOLS ix
LIST OF FIGURE x
LIST OF TABLE xiii

CHAPTER 1 - INTRODUCTION 1

CHAPTER 2 - HIGH ENTROPY ALLOYS 4

2.1 General Definition of High Entropy Alloys 4
2.2 Four Main Effects in High Entropy Alloys 11
2.2.1 High Entropy Effect 11
2.2.2 Lattice Distortion Effect 12
2.2.3 Sluggish Diffusion Effect 14
2.2.4 Cocktail Effect 16
2.3 Production Methods of HEAs 17
2.3.1 Production from the Solid State 18
2.3.2 Production from the Liquid State 19
2.3.2.1 Vacuum Arc Melting 20
2.3.2.2 Bridgman-Stockbarger 23
2.3.2.3 Vacuum induction method 24
2.3.3 Production from the Gas State 25
2.4 Notation of High Entropy Alloys 25
2.5 Solid solutions, intermetallics and intermetallic compounds in HEAs 26
2.5.1 B2 phases 27
2.5.2 $L1_2$ phases 27
2.5.3 Intermetallic 28

2.5.4 Sigma phases 29
2.5.5 Laves phases 30
2.5.6 Intermediate Compounds 31
2.6 Application Areas of High Entropy Alloys 32
2.7 Design of High Entropy Alloys 33
2.7.1 Method of Empirical Calculation 33
2.7.2 Atomistic approaches 34
2.7.3 Thermo-Calc Software 34
2.8 Literature survey 36

CHAPTER 3 - MATERIALS AND METHOD 44

3.1 Materials 44
3.2 Thermo-Calc Software for AlCoCrFeNiTi$_X$ HEAs 46
3.3 Production of AlCoCrFeNiTi$_X$ HEAs 48
3.4 Characterization of produced AlCoCrFeNiTi$_X$ HEAs 51

CHAPTER 4 - RESULTS AND DISCUSSION 53

4.1 CALPHAD Results 53
4.2 Arc Melting Result of AlCoCrFeNiTi$_X$ HEAs 56
4.2.1 XRD Results 56
4.2.2 SEM/EDS Results 59
4.2.3 DTA Results 63
4.2.4 Hardness Results 68
4.3 Heat Treatment Result of AlCoCrFeNiTi$_X$ HEAs 71
4.3.1 XRD Results 71
4.3.2 SEM Results 74
4.3.3 DSC Results 76
4.4 Phase Diagram Result of AlCoCrFeNiTi$_X$ HEAs 78

CHAPTER 5 - CONCLUSION 81

CHAPTER 6 - FUTURE RECOMMENDATIONS 84

REFERENCES 85

LIST OF SYMBOLS

Sconf	: Configurational Entropy
Smix	: Configurational Entropy
Hmix	: Entropy of Mixing
ΔHmix	: Enthalpy of Mixing
ΔGmix	: Gibbs Free Energy of Mixing
$\bar{r}$	: Average Atomic Radius
δ	: Atomic Size Difference
R_i	: Radius of i^{th} Element
Tm	: Melting Point
HEA	: High entropy alloys

LIST OF FIGURES

Figure 1.1 Schematics of ternary and quaternary systems depicting parts of the phase diagram that are relatively understood (green) at the corners and somewhat less well known (white) in the middle. 1
Figure 2.1 Timeline of the growth of metals and metal alloys in terms of the amount of elements, as well as the most important uses of HEAs. 6
Figure 2.2 Illustration of ΔSconf values calculated depending on the composition in the ternary alloy system. 8
Figure 2.3 Types of alloys in the alloy world based on configurational entropy). 11
Figure 2.4 The deformed lattice of a solid solution with 10 distinct primary elements and two vacancies. 13
Figure 2.5 Variation of the hardness of alloy AlxCoCrCuFeNi with Al content. 17
Figure 2.6 Production methods of high entropy alloys. 18
Figure 2.7 Schematic of mechanical alloying. 19
Figure 2.8 Schematic representation of the arc melting furnace. 21
Figure 2.9 Microstructure images of cylindrical AlCoCrFeNi alloy obtained by arc melting and subsequent casting into copper crucible: a) and b) coaxial dendrites in the center, c) surface-to-center cast structure, d) columnar dendrites in the transition zone 22
Figure 2.10 Schematic illustration of phase separation during solidification of AlCoCrCuFeNi HEA by splat quenching and casting. 23
Figure 2.11 Schematic view of the Bridgman solidification method..... 24
Figure 2.12 a) x = 0.5, b) x = 1.0, c) x = 1.5 and d) x = 2 SEM images of $AlCo_xCrFeMo_{0.5}Ni$ alloy 30
Figure 2.13 Unit cell of Laves phase with $MgZn_2$ structure (Mg atoms are green). . 31
Figure 2.14 XRD results as-cast, remelted, and annealed HEAs of AlCoCrFeNiTi0.5 40
Figure 2.15 AlCoCrFeNiTi0.5 HEA micrographs a)As-cast; b)remelted; c)annealed. (DR: dendrite; ID:interdendrite; CW:cell wall) 41
Figure 2.16 XRD analysis results of AlCoCrFeNiTix HEA before high temperature oxidation test. 42

Figure 2.17 XRD analysis results of AlCoCrFeNiTix HEA after high temperature oxidation test. 42
Figure 2.18 XRD analysis results of AlCoCrFeNiTix (Ti00, Ti03, Ti05)..... 43
Figure 3.1 The process of creating the model tree for calculations. 46
Figure 3.2 Entering boundary conditions into the model tree created for the calculations. 47
Figure 3.3 The cooling behavior occurring at equilibrium conditions..... 48
Figure 3.4 The cooling behavior occurring at non-equilibrium conditions 48
Figure 3.5 a) Weighing process of the prepared powders and b) Mixture of the prepared powders..... 49
Figure 3.6 a)Edmund Bühler brand VAM device, b)arc melting process, and c)cooling of melted samples 50
Figure 3.7 a) Cutting samples, and b) measuring the dimensions of the cut samples 50
Figure 3.8 Heat treatment stages of the produced samples. a) holding process, b) cooling in the furnace c) cooling in water 51
Figure 4. 1 Possible phases to occur under balanced cooling conditions and their quantities, respectively a) X=0.0, b) X=0.2, c) X=0.4, d) X=0.6, e) X=0.8, and f) X=1.0 in AlCoCrFeNiTi$_X$ HEAs..... 53
Figure 4.2 Phase diagram of AlCoCrFeNiTi$_X$ high-entropy alloy formed according to Scheil Solidification Simulations under non-eqilibrium conditions 55
Figure 4.3 XRD analysis of as-cast AlCoCrFeNiTi$_X$-based HEAs: a) full scan, b) magnified sections 57
Figure 4.4 SEM micrographs of as-cast AlCoCrFeNiTi$_X$ based HEAs where (a) X = 0.0, (b) X = 0.2, (c) X = 0.4, (d) X = 0.6, (e) X = 0.8, and (f) X = 1.0 60
Figure 4.5 Image depicting the microstructure and phase compositions of the AlCoCrFeNiTix alloy as recognized via EDS (a)Ti0.0,b) Ti0.2, c) Ti0.4, d) Ti0.6, d) Ti0.8, and e) Ti1.0 magnification 15.00Kx)..... 63
Figure 4.6 Differential thermal analysis (DTA) curves a)Ti0.0 and b)Ti0.2 based HEAs 65
Figure 4.7 Differential thermal analysis (DTA) curves c)Ti0.4 and d)Ti0.6 based HEAs 66

Figure 4.8 Differential thermal analysis (DTA) curves e)Ti0.8 and f)Ti1.0 based HEAs 67
Figure 4.9 The microhardness values of AlCoCrFeNiTix HEAs 68
Figure 4.10 The XRD patterns of as-heat treated a)Ti0.0-based HEA 71
Figure 4.11 The XRD patterns of as-heat treated b)Ti0.2, and c)Ti1.0-based HEA . 73
Figure 4.12 The SEM micrographs of as-heat treated Ti0.0, Ti0.2, and Ti1.0-based HEA 74
Figure 4.13 DSC curve of Ti0.0, Ti0.2, and Ti1.0-based HEAs..... 76
Figure 4.14 The phase equilibrium diagram of the AlCoCrFeNiTi_X (0<x<2) system (Thermo-Calc software calculations) 78
Figure 4.15 The phase equilibrium diagram of the AlCoCrFeNiTiX (0 < x < 2) system (■ = literature articles with ● = experimental findings) 79

LIST OF TABLES

Table 2.1 Configurational entropy values in R depending on the number of alloying elements in alloys with equiatomic ratio. 8
Table 2.2 Configurational values for elemental phases, compounds, intermediate phases, and random solid solutions are compared. 12
Table 2.3 Diffusion parameters for nickel in different FCC matrices 15
Table 2.4 Binary mixture enthalpies of atom pairs in Al-Co-Cr-Cu-Fe-Ni alloys (kJ/mol) 28
Table 3.1 Physical characteristics of chosen elements for the multi-principle alloying system. 44
Table 3.2 Calculated alloy composition ratios 45
Table 3.3 Initial weights of powders prepared by pelleting 45
Table 3.4 Initially weight of the pellet .....**Hata! Yer işareti tanımlanmamış.**
Table 3.5 Average of the final weights of the melted alloy series 50
Table 4.1 Microhardness values of AlCoCrFeNiTix HEAs from different phase regions (Area 1:Dark area, and Area 2: bright area) 69

CHAPTER 1

INTRODUCTION

Most conventional alloy systems consist of at least two major elements.The mechanical, corrosion, magnetic, and electrical properties of the alloy produced by adding minor alloying elements to the main element can be improved. However, this type of alloying strategy forces researchers to increase the alloy configuration and conduct research on multi-component systems. However, they noticed that little information is available about the phase diagrams of multicomponent systems. The concept of high entropy alloys (HEA), proposed in early 2004, made it possible to investigate the phase diagrams of multicomponent systems. The HEA concept has started to offer a new field for producing new alloys with unique properties that cannot be achieved with conventional alloy systems. High entropy alloys (HEA) are defined as alloys containing five or more basic alloying elements at or near equi-atom ratios. The basic principle of HEA is that high mixing entropy favors solid solution formation compared to the intermetallic compound formation, thereby increasing the high temperature stability of alloys. As demonstrated in Figure 1.1, alloy systems with high entropy are situated at or around the phase diagram's center, maximizing configuration entropy(Murty, Ranganathan, Yeh, & Bhattacharjee, 2019).

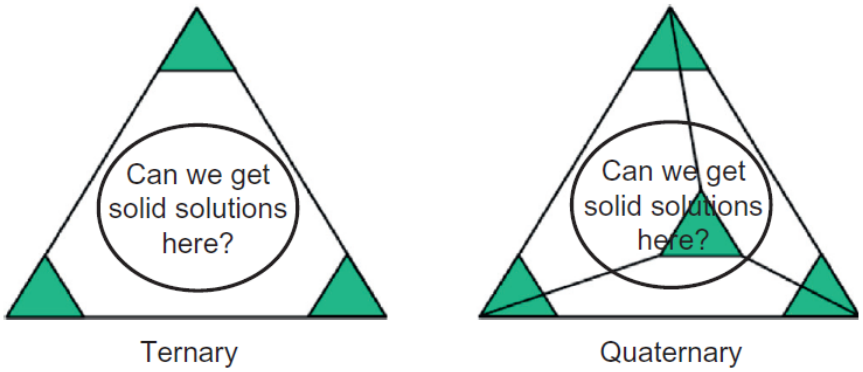

Figure 1.1 Schematics of ternary and quaternary systems depicting parts of the phase diagram that are relatively understood (green) at the corners and somewhat less well known (white) in the middle (Murty et al., 2019)

In general, high entropy alloys are also called equiatomic or near equiatomic alloys. They are structures containing single or double solid solution phases that do not contain any stable intermetallics due to their higher configuration entropies (Sconf). In addition, they are alloys that can be produced by preserving their phase structure even at high temperatures. This situation is contrary to the known Gibbs phase rule. According to this rule, the tendency of the intermediate phases increases as the number of components increases. The reason why these alloys do not comply with the rule is that the results of mixing entropy is higher than that of conventional alloys. Consequently, this is one of the primary reasons why the HEA idea is getting more attention in material research studies. Another argument is that the number of elements in HEAs may be expanded. In this way, the ability to vary the atomic proportions of alloying elements across a broad range enables the availability of an infinite number of alloy combinations. Consequently, it becomes feasible to find novel materials with desirable qualities. In most cases, the most notable characteristic of newly found materials is their mechanical qualities. In the past and present, applications needing high strength at room temperature and elevated temperatures have used Ni-based, Co-based, and Ti-based alloys. Nonetheless, the manufacturing and material costs of these alloys are rather expensive. In addition to these alloys, high entropy alloys with multiple superior properties have started to be developed(J. W. Yeh et al., 2004).

In order to examine the various properties of these alloys, it is necessary to determine the phases formed in the structure of the alloys. Determining the structures of the phases forming the alloy at room temperature or at high temperatures will help to detail the usage areas of these alloys. In this way, by looking at the phase diagrams of the developed alloys, the usage areas of these materials will be determined. Within the scope of this study, chapter 2 begins by reviewing high entropy alloys, some formation rules, the four primary effects of high entropy alloys, the production methods of these alloys, their areas of use, and computer-aided programs used during the design of alloys. In Chapter 3, $AlCoCrFeNiTi_X$-based HEAs with different stoichiometries were manufactured using vacuum arc melting (VAM) and heat treatment processes.

In Chapter 4,the alloy series formed was examined in detail. Also, the phase diagram has been generated under equilibrium and non-equilibrium cooling conditions associated with this alloy series for the first time. Experimental studies and literature findings have examined the accuracy of the generated phase diagrams. Finally, future recommendations are highlighted in Chapter 5.

CHAPTER 2

HIGH ENTROPY ALLOYS

2.1 General Definition of High Entropy Alloys

Till date, about 30 practical alloy systems based on Fe, Al, Cu, Ti, Mg and Ni have been developed. These alloys are typically built on one major element and other alloying elements are added in small amounts to modify the properties (J. W. Yeh, 2006). Most of the high-performance alloys used today were developed in 1975s due to the inadequacy of conventional alloys. In 1981s, Brian Cantor and her student have being developed a $Co_{20}Cr_{20}Fe_{20}Mn_{20}Ni_{20}$ alloy containing multiple essential elements by going beyond the concept of "traditional alloy". Then, in 1995, Jien-Wei Yeh et al. started to carry out various studies with the arc melting technique, predicting that the high mixing entropy caused by the combination of multiple essential elements would increase the mixing between the components. On the contrary, the number of phases formed in the structure are reduced(Gao, Liaw, Yeh, & Zhang, 2016). Following the studies carried out by different teams, studies on high entropy alloys have been issued since 2004.

Recently, high entropy alloys or multicomponent alloys have great attention with their unique compositions, microstructures, and various tunable superior properties. HEAs are described based on their composition and entropy. According to the definition based on composition, HEAs consist of at least five major components. Each of the major elements should have a concentration between 5 and 35 at. percent. Additionally, HEAs may include small components that should be below 5 percent (Tsai & Yeh, 2014). This formation creates high mixing entropy and prevents the formation of intermetallic phases. Instead of intermetallic phases, it causes the formation of simple face-centered cubic (FCC) or body-centered cubic (BCC) or mixed solid solutions. The fact that HEAs have superior properties compared to conventional alloys has drawn the attention of researches to a great extent (Dong, Lu, Kong, Zhang, & Li, 2013; Nayan et al., 2014; Y. Zhang, 2019).

Each major alloying element that makes up high entropy alloys has concentrations between 5% and 35%. Besides of these main compounds, HEAs can contain additional elements in small proportions (below 5%). In addition to the main elements, HEAs can contain other elements in small proportions below 5%. These alloys are defined as HEAs. Solution or solid melt forming states have considerably higher mixing entropy than conventional alloys (Bhattacharjee et al., 2014; Cantor, Chang, Knight, & Vincent, 2004; Srivatsan & Gupta, 2020). The entropy of the mixture is often mentioned in high entropy alloys. Current information on metallurgical concepts and binary and ternary phase diagrams states that multiple elements can form complex phases and brittle microstructures and intermetallic compounds. Contrary to this expected situation, experimental studies shows that high mixing entropy eased the formation of solid melt phases of these alloys. This resulted in a reduction in the number of phases formed in the structure HEA alloys are materials with high strength, high ductility and high resistance to wear, corrosion and oxidation (S. Guo & Liu, 2011; Tsai & Yeh, 2014; K. Zhang & Fu, 2012; Y. Zhang, 2019). While the results obtained with the production of HEAs are found to be suitable in terms of chemical stability, microstructure and magnetic, high mechanical and thermal properties attract attention.

Especially in terms of providing strength and mechanical standards, they have become an alloy type that is interested in the automotive and aviation sectors, which are in continuous development as a necessity of the technology age. Another reason for this interest is that the elements to be used and their ratios create thousands of combinations. When evaluated from this point of view, it is foreseen that it will allow the material sector to gain a lot of new alloys. Figure 2.1 shows the evolution of high entropy alloys and other metal alloys over time.

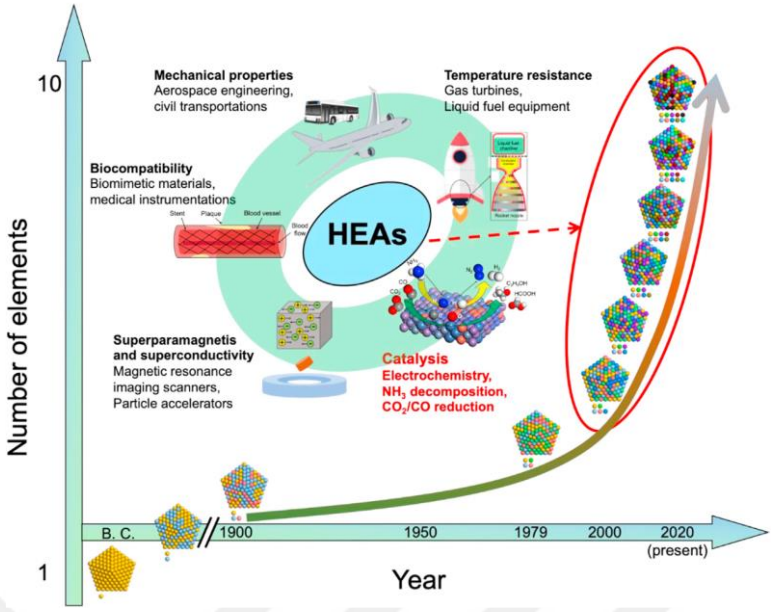

Figure 2.1 Timeline of the growth of metals and metal alloys in terms of the amount of elements, as well as the most important uses of HEAs (K. Li & Chen, 2021)

Before investigating core properties and main structure of high entropy alloys, the concept of entropy should be understood. Thermodynamics; mainly deals with the relationship between three important variables: Temperature (T), Volume (V) and Pressure (P). According to the 2nd law of thermodynamics, the total entropy of the system and the environment increases in any process that occurs spontaneously. In the equation, S is entropy, Q is heat flux, and T is absolute temperature. (Matsushita & Mukai, 2018).

$$dS = \frac{dQ}{T} \tag{2.1}$$

Entropy can be thought of as molecular disorder or molecular randomness. When the disorder of a system increases, the positions of the molecules will become uncertain, and the entropy of the system will increase. The system's entropy is related to the total number of microscopic states in which the system can exist. This number is known as the thermodynamic probability(w), and its relation to entropy is given by the Boltzman equation:

$$\Delta S_{conf} = k_B \ln w \tag{2.2}$$

Here, k_B=1.38×10^{-23} J/K is the Boltzmann constant and w is the number of methods that cause the available energy to be mixed or shared among the particles in the system. Every spontaneous process in the universe always tends to increase entropy. This is because the free energy of the system tends to go into a lower state. This occurs by increasing entropy.

$$\Delta G_{mix} = \Delta H_{mix} - T\Delta S_{mix} \quad (2.3)$$

where ΔGmix is the Gibbs free energy of mixing, ΔHmix is the enthalpy of mixing, ΔSmix. In this equation, an increase in entropy will decrease the Gibbs free energy, and statistically, every spontaneou(random) process in the universe is expressed as ΔS>0 or ΔG<0. The entropy of mixing consists of four parts: structural, vibrational, magnetic dipole, and electronic disorder. Based on theoretical predictions, it was decided that structural entropy has been detected the most effective among these four components (Murty et al., 2019; Y. Zhang et al., 2014). For a solid solution with a certain number of compounds, n, the structural entropy change is:

$$\Delta S_{conf} = -R \sum_I^n X_I \ln(X_I) \quad (2.4)$$

where "R (8.314 J/K mol)" is the gas constant and X_i is the molar content of component "i". For atomically equivalent or equimolar alloys, the structural entropy value reaches its maximum. Therefore, final equation for each mole is as follows.

$$\Delta S_{conf} = kB \ln w = -R \left(\frac{1}{n}\ln\left(\frac{1}{n}\right) + \frac{1}{n}\ln\left(\frac{1}{n}\right) + \ldots + \frac{1}{n}\right) = R \ln N \quad (2.5)$$

The structural entropy also increases when the number of elements increases. The structural entropy values that change as a function of alloy composition in a three-component system are shown in Figure 2.2.

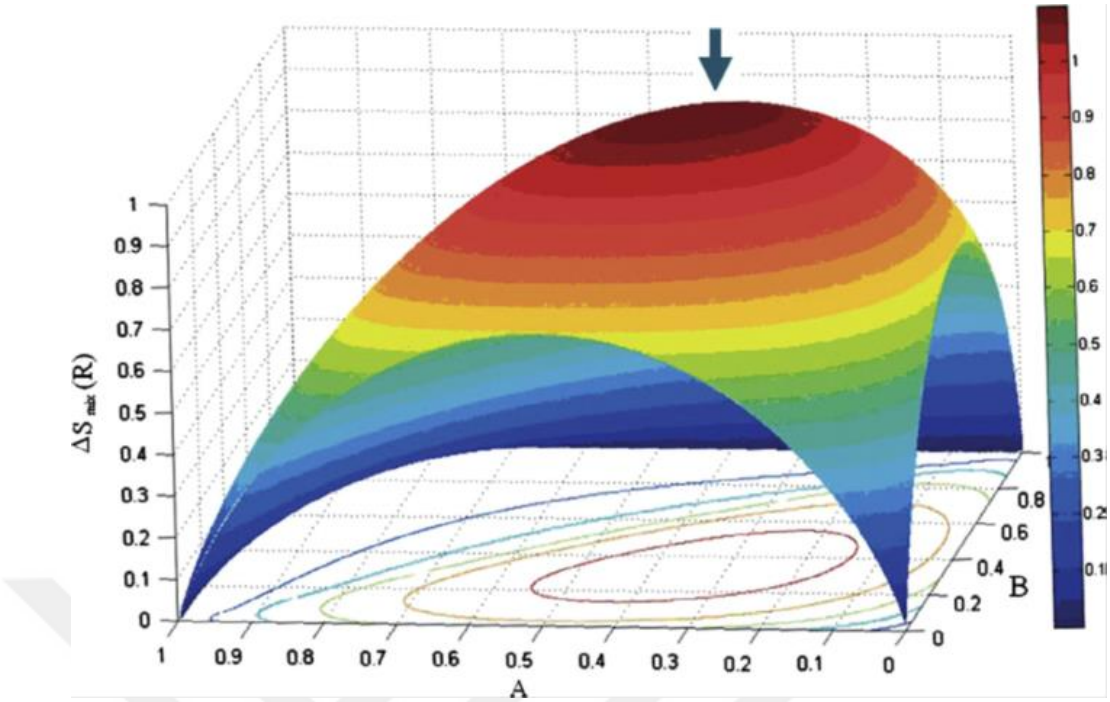

Figure 2.2 Illustration of ΔSconf values calculated depending on the composition in the ternary alloy system (Y. Zhang, Zhou, Lin, Chen, & Liaw, 2008)

In alloys with co-atomic composition; The highest structural entropy value to be reached in the ternary alloy system was calculated as 1.1×R. Therefore, the presence of more constituent elements in the alloy raises the structural entropy to an even higher level. For an atomically equivalent alloy with five elements, ΔSconf = 1.6×R. In Table 2.1, the structural entropy values that change depending on the number of elements in alloys with equiatomic ratio are given as the ratio of the gas constant R.

Table 2.1 Configurational entropy values in R depending on the number of alloying elements in alloys with equiatomic ratio(J.-W. Yeh, 2016)

n	1	2	3	4	5	6	7	8	9
ΔS_{conf}	0	0.69	1.10	1.39	1.61	1.79	1.95	2.08	2.20

As the number of elements in the alloy increases, the configurational entropy of the alloy in the equiatomic ratio also increases. The entropy change (ΔSconf) during the melting of metals, transition from solid phase to liquid phase, approximately equals to gas constant, R. This situation is known as the “Richard Rule”. Also, the enthalpy change (ΔHconf) during melting is proportional to ΔSconf:

$$\Delta H_{conf} = \Delta S_{conf} \times T_m \quad (2.6)$$

Looking at the difference in the number of bonds between solid and liquid, it is assumed that the configurational enthalpy of one mole of solid is equivalent to the energy that is necessary to break about 1/12 of all bonds in a tight-packed structure. From this point of view, it can be said that the $T_m \times R$ value is equal to approximately 1/12 of the bond energy of a mole solid in a tight-packed structure. As a result, it is seen that the entropy of the mixture (R per mole) is large enough to reduce the value of the mixture's free energy (R×T) (J.-W. Yeh, 2016).

If the strain energy caused by atomic size difference is neglected, the two main factors that determine the state of equilibrium are mixture entropy and mixing enthalpy due to chemical bonds. On the contrary to positive and negative enthalpies of mixing which are the driving forces for formation of the decomposition state and to form compounds, respectively, mixing entropy is the driving force to generate a random solid solution. Therefore, the equilibrium state depends on the relative enthalpy and entropy values of the different states being highly relative to each other. For instance, ratio of the formation enthalpies to their respective melting temperatures of two strong intermetallic compounds, NiAl and TiAl, yields 1.38×R and 2.06×R, respectively. According to solid solution formation or formation of two separate phases, the highest mixture entropy values were obtained in case of intermetallic compound formation. This shows that it is with the driving force to form compounds with high entropy. The ratios of the enthalpy of formation to the melting temperature of copper are 1.06×R and 1.15×R. For this reason, it is considered that the probability of solid solution formation in the system increases if the entropy of a mixture (1.5×R per mole) is relatively large relative to the enthalpy of the mixture. As shown in Table 2.1, the configurational entropy of a 5-element alloy is 1.61×R. Thus, a system with at least five elements will be more likely to form a solid solution. Solid solutions with a high degree of the disorder are easier to obtain, although in most cases no random solid solution is formed. Therefore, the high mixing entropy increases the mutual solubility of the elements in the alloy with each other and effectively reduces the number of phases, especially at high temperatures (Murty et al., 2019; J.-W. Yeh, 2016).

Based on the given information, “high entropy alloys” can be defined as either based on composition or based on configurational entropy. Firstly, HEAs are defined as alloys containing at least five major elements, each with an atomic percentage of 5 to 35%. The atomic percentage of all minor contributions, in these alloys, is below 5%. Secondly, HEAs are defined as alloys with configurational entropies greater than 1.5R, regardless of whether they are single-phase or polyphase at room temperature. Although both definitions cover a wide range of alloys, they often intersect. Compositions in regions where the two definitions do not overlap are also considered as HEA. Therefore, an alloy with a composition that fits only one of these two definitions is also considered as HEA(Gao et al., 2016).

Based on these definitions of HEAs, it can be understood that the main principle behind the HEAs with more than one main element is the high mixing entropy, which is used for increasing the formation of solid solution phases and preventing the formation of intermetallic compounds. This principle is extremely important for avoiding the complexity and fragility in HEAs. Also, the high mixing entropy ensures the appropriate handling of the most of the HEAs in terms of production, processes, analyze, and use. Mixing entropy is the only factor among various thermodynamic factors that increases when number of principal components increases. For alloys with very basic elements, the name “high entropy alloys” are considered appropriate (Murty et al., 2019).

Since 1.5 R is the lower configurational entropy limit for high entropy alloys, MEAs (Medium Entropy Alloys) and LEAs (Low Entropy Alloys) are also defined to distinguish the strength of the effect of mixing entropy. For separation, 1R is the boundary value between medium entropy alloys and low entropy alloys. Related definitions are demonstrated in Figure 2.3.

.

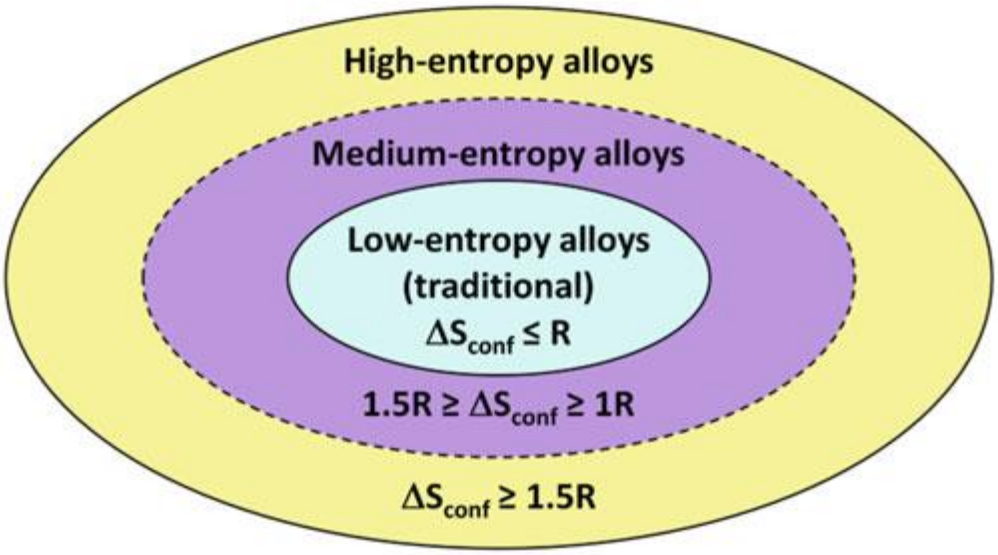

Figure 2.3 Types of alloys in the alloy world based on configurational entropy(Murty et al., 2019)

2.2 Four Main Effects in High Entropy Alloys

So many variables influence the mechanical, microstructural, and other properties of HEAs. However, the most prevalent "core effects" include a high entropy effect, a slow diffusion effect, a severe lattice distortion effect, and a cocktail effect (J. W. Yeh, 2013; Y. Zhang et al., 2014).

In summary, high entropy simplifies the microstructure, therefore, in principle, FCC and BCC play the most important role in forming solid solutions. Material properties including mechanical, physical and chemical properties are affected by lattice distortion. The effect of slow diffusion enhances the formation of amorphous or nanocrystalline structures. The cocktail effect plays a crucial role in creating a composite effect with the interactions of different elements. All the factors mentioned make HEAs have numerous features and are suitable for many applications(Y. Zhang, 2019).

2.2.1 High Entropy Effect

High entropy is the parameter that effects HEA production the most. This phenomenon differs HEAs from conventional alloys in that it causes simple solid

solution phases to form (Murty et al., 2019). This theory indicates that the free energy of solid solutions diminishes as Sconf. increases. This facilitates the production of solid solution phases at increasing temperatures, especially in the production of alloys. As the solubility of candidate elements increases, the resulting number of phases in HEAs decreases. Solid solution phases have a larger mixing entropy than intermetallic compounds in conventional alloy systems (Table 2.3). Due to the greater number of primary elements in HEAs, the difference in mixing entropy between solid solution and intermetallic compounds is relatively substantial. Consequently, HEAs have greater solid solution stability, especially at higher temperatures. As the temperature increases towards higher temperatures, the degree of ordered structure in the HEA diminishes. Consequently, even if these alloys demonstrate ordered structure in the casting state, the ordered structure in the alloy turns into solid solution at high temperatures. Besides, when the enthalpy of formation of intermetallic compounds is high enough at higher temperatures, the effect of the enthalpy of the alloy will surpass the effect of high entropy. Instead of solid solution phases, intermetallic compounds will be stable phases in this instance (Tsai & Yeh, 2014).

Table 2.2 Configurational values for elemental phases, compounds, intermediate phases, and random solid solutions are compared.(J.-W. Yeh, 2016)

Comparative states	Elemental Phases	Compounds	Intermediate Phases	Random Solid solution
ΔH_{mix}	0	Larger negative	Less large negative	Medium negative
ΔS_{mix}	0	0	Medium	$-R\sum_{i}^{n} X_i \ln(X_i)$
ΔG_{mix}	0	Larger negative	Larger negative	Larger negative

2.2.2 Lattice Distortion Effect

Due to the multi-elemental nature of HEAs, the traditional concept of the structure needs to be expanded to the concept of multi-element structure rather than one or two element-based structures. Since every compound is entirely dissolved in the matrix and every atom has neighbor atoms that vary in atomic radius, the lattice of alloy stretches and stresses. Figure 2.4 shows a solid solution with a distorted lattice that has 10 different principal elements and two vacancies spots. (Ng, Guo, Luan, Shi, & Liu, 2012; Senkov, Wilks, Miracle, Chuang, & Liaw, 2010).

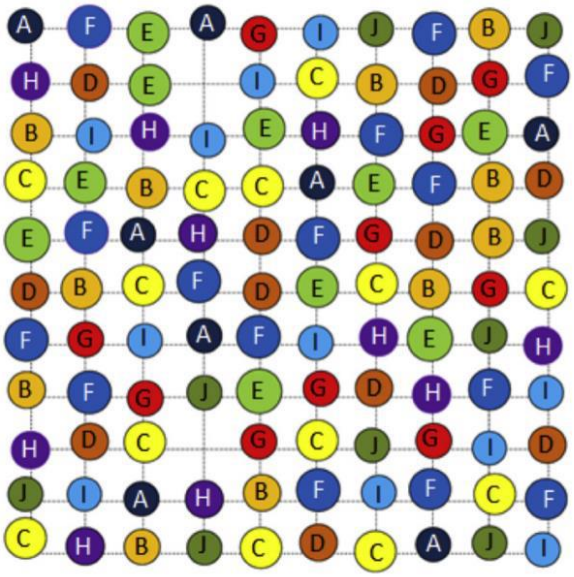

Figure 2.4 The deformed lattice of a solid solution with 10 distinct primary elements and two vacancies (Tsai & Yeh, 2014)

The difference of the binding energies and the crystal structure of the constituent elements and the variances in the atomic radius of the constituent elements cause an increase in lattice distortion. According to research by Senkov et al., FeCoCrNiMn equiatomic high entropy alloys exhibit an FCC crystal structure and a Vickers hardness of 1192 MPa under homogeneous conditions, compared to a rule of mixing calculation of 864 MPa. Additionally, MoNbTaVW equiatomic refractory high entropy alloys has BCC crystal structure and Vicker hardness of 5250 MPa which is approximately three times higher than the Vickers hardness of 1596 MPa obtained by the rule of mixture. These results proves that the solid solution hardening occurs more in BCC alloys than the FCC alloys(Senkov et al., 2010).

2.2.3 Sluggish Diffusion Effect

Diffusion is simply the displacement of atoms due to temperature. The groups with the highest diffusion values are pure metals and then other alloys. In high entropy alloys, diffusion values are at lower levels. Diffusion values are at lower levels in high entropy alloys (Gao et al., 2016).

Phase transformations: depend on the balanced distribution of the elements by the common diffusion action throughout the phase. Diffusion is restricted in high entropy alloys because atomic movements are prevented due to the lattice distortion. During casting process of high entropy alloys, phase separation during cooling is prevented at the high temperatures. For this reason, phase separation is prevented up to low temperatures. Also because of this reason, high entropy alloys sometimes form structures with nanoprecipitates. Yeh et al. conducted studies on the void formation and compositional decomposition in high entropy alloys. As a result of these studies, the diffusion coefficients of pure elements, stainless steel and high entropy alloys were compared. As a result, in the three types of alloy systems mentioned, as high entropy alloys < stainless steels < pure metals diffusion rates were determined (J. W. Yeh, 2006; Y. Zhang et al., 2014).

Phase transformation and diffusion kinetics are relatively slower in HEAs than the conventional alloys. This situation should be analyzed from two perspectives. First, the neighbors of atoms at all lattice points are slightly different. For this reason, the jumping of the previous and next neighboring atoms into the spaces is different. The difference in local atom configurations results in different bonds and different local energies for each point. As the atom switches to a low-energy point, it becomes trapped and has a low probability of moving its place out of that point. Conversely, if the atom switches to a high-energy point, the atom has a high probability of jumping to the original point. Both of these events slow down the diffusion process(Tsai & Yeh, 2014).

In the second scenario, the diffusion rates of elements in high alloys change. Each element has different activity level in which some of them are significantly lower. These elements have lower success rates in moving into spaces. However, for phase transformations, it is essential to have coordinated diffusion of the elements, which only obtained if compound element have similar activity levels. For example, the nucleation and growth of a new phase require the redistribution of elements to reach the desired composition. Grain growth allows all elements to combine and migrate through the grain boundaries successfully. In such cases, the slow movement of the elements has a limiting effect on the transformation. Table 2.3. gives the diffusion parameters of the nickel atom in different matrices.

Table 2.3 Diffusion parameters for nickel in different FCC matrices (Tsai and Yeh, 2014)

Solvated	System	D_0 (10^{-4} m^2/s)	Q (kj/mol)	Tm (K)	Q /Tm	D_{Tm} (10^{-13} m^2/s)
Ni	CoCrFeMnNi	19.7	317.5	1607	1.1975	0.95
	Fe-15Cr-20Ni-Si	4.8	310	1705	0.1818	1.53
	FCC Fe	3	314	1812	0.1733	2.66
	Co	0.43	282.2	1768	0.1596	1.98
	Ni	1.77	285.3	1728	0.1651	4.21
	Fe-15Cr-20Ni	1.5	300	1731	0.1733	1.33

The slow diffusion effect will affect nucleation, growth, distribution and new phase morphology in diffusion-controlled phase transformations. This situation; will provide control of microstructure and properties and the formation of supersaturated fine precipitates. In addition, high recrystallization temperature will provide advantages such as reduced grain coarsening and high creep resistance. As a result, slow diffusion

has a positive effect on high entropy alloys' metallurgical properties. For example, a combination of fine precipitate, grain structure and strength and toughness can be improved. With its high creep resistance, the service life of parts operating at high temperatures can be increased behavior (Tsai & Yeh, 2014; Gao et al., 2016; Murty et al., 2019).

2.2.4 Cocktail Effect

For metallic alloys, the ability to obtain properties that cannot be achieved based on any one element by mixing many elements is called cocktail effect. The properties of the elements that make up the alloy are highly effective on how the properties of HEAs could be. So that, by courtesy of the cocktail effect, changing the alloys' composition results in the significant adjustment of alloy properties. For instance, using elements with low density will reduce the density of the alloy. But, the elements interactions with each other must be taken into the consideration as well as individual properties of the each component (Miracle et al., 2014; Y. Zhang et al., 2014).

In concentrated solid solutions, each phase can often be seen as a composite in atomic scale. The properties of composites cannot be determined only from the fundamental properties of the elements. They also can be determined from the lattice distortion of the composite and the interactions of all elements within the composite. Therefore, the cocktail effect is composition, crystal structure, lattice distortion, and the overall effect of microstructure. For example, light metals should be used for light alloys; refractory elements can help to achieve high melting points and oxidation-resistant alloys need the addition of Al, Cr or Si in their composition(Cheng et al., 2017).

In high entropy alloys, the interaction between these elements should be considered as well as the properties of the elements in the composition. For example, although aluminum (Al) with a low melting point is a soft element, the addition of aluminum can increase the hardness of high entropy alloys. In Figure 2.4, it is shown that the hardness of AlxCoCrCuFeNi alloy increases as the percentage of Al in the alloy increases. This increase in hardness is caused by both the hard BCC phase formation

and the strong bonding of aluminum with other elements due to its large atomic size. The properties of high entropy alloys depend not only on the average properties of the main elements but also include the effect of inter-elemental reactions and lattice distortions (Tsai & Yeh, 2014).

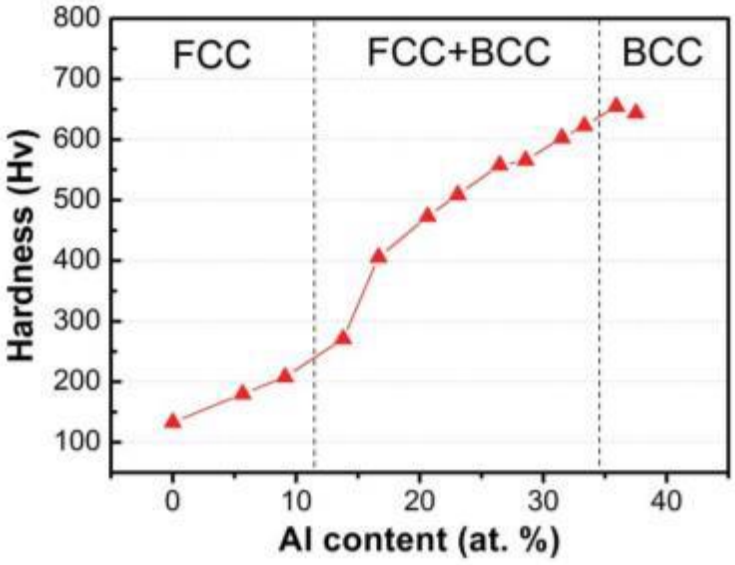

Figure 2.5 Variation of the hardness of AlxCoCrCuFeNi with change of Al content (Tsai & Yeh, 2014)

2.3 Production Methods of HEAs

Microstructural and physicochemical characteristics of high entropy alloys are the most important factors determining the production methods to be preferred in these alloys. Alloy compositions, melting points and purity levels of the elements change the production methods to be preferred (Y. Zhang et al., 2014).While producing these special alloys, the most preferred production method is the casting method. In this method, high entropy alloys are produced by casting in arc melting furnaces, melting furnaces using argon gas or standard melting furnaces in a vacuum environment (Butler & Weaver, 2016; Fujieda et al., 2015). Vacuum arc melting (VAE) and vacuum induction melting (VIM) methods are frequently used in vacuum melting. In addition, methods such as production from solid-state and gas-state are also used in the production of HEAs.

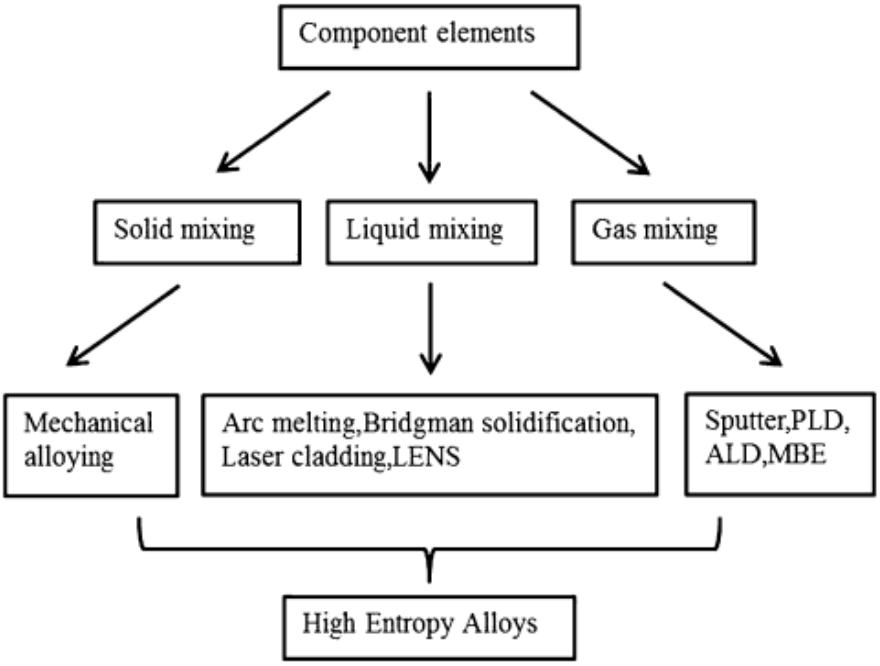

Figure 2.6 Production methods of high entropy alloys (Tsai & Yeh, 2014)

2.3.1 Production from the Solid State

Many polycrystalline materials are synthesized by mixing the alloying elements at room temperature and then condensing them at a high temperature. Powder production and subsequent operations, including as mixing, sintering, hot/cold pressing, extrusion, and rolling, are typical of solid-state manufacturing procedures (Alshataif, Sivasankaran, Al-Mufadi, Alaboodi, & Ammar, 2020). The most common method of obtaining HEA powders is the mechanical alloying (MA) method (Fig.2.7). Mechanical alloying is a method that emerged as versatile production technique applied for the production of micron or nano-sized powders and for obtaining various metallic alloys with different melting temperatures The biggest disadvantage of the mechanical alloying system is that the expected phases do not occur in the alloys produced. The reason for this is that mechanical stress strains occur at the nanoscale. It is not possible to predict the phases that will occur (Vaidya, Muralikrishna, & Murty, 2019).

In this method, cold welding and grinding methods are used repeatedly for breaking the elements into the powder in order to obtain desired alloy combination. While the first applications of the mechanical alloying method were the production of alloys strengthened by oxide dispersion, later on, this method is used for production of metastable materials like nanocrystalline metals and alloys, semi-crystals, and amorphous materials (Gao et al., 2016).

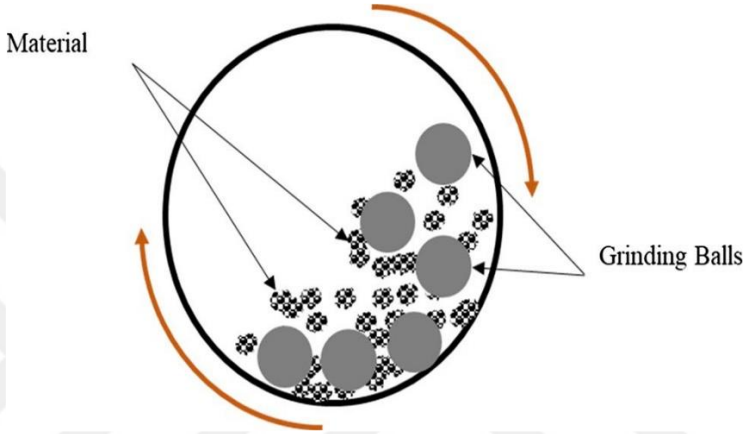

Figure 2.7 Schematic of mechanical alloying (Alshataif et al., 2020)

In general, in mechanical alloying performed at room temperature and below does not encounter the potential problems encountered in liquid state methods such as casting and melting. For example, in liquid state production of the alloys, it is difficult to handle the elements with different melting or evaporation temperatures, but those alloys can be easily produced by using mechanical alloying method. Moreover, in the densification stage of nanocrystalline alloy powders produced by mechanical alloying, to prevent the grain growth caused by exposing powders to elevated temperatures for long time in conventional sintering method, various rapid sintering techniques such as spark plasma sintering (SPS) and microwave sintering are generally used (Alshataif et al., 2020; Murty et al., 2019).

2.3.2 Production from the Liquid State

In terms of liquid state production of high entropy alloys, casting is the most widely used method. In the production of HEAs by casting method, the alloys are generally

resolidified by melting several times. The purpose of applying these processes repeatedly is to provide homogeneity in the alloy structure. However, in the casting technique, inhomogeneous structures may occur between the surfaces and centers of the alloys due to the rapid solidification and the difficulty of solidification control. This situation can create different microstructural properties between the alloy surface and its center. In addition, unavoidable casting defects such as segregation, microscopic and macroscopic stresses, cracks, and pores can directly affect the mechanical properties of high entropy alloys. After the casting processes, annealing processes may be needed in order to eliminate these defects and to provide homogenization in the structure. There are many methods as liquid state production methods: Vacuum Arc Melting, Vacuum Induction Melting, Bridgman solidification, Self-propagating high-temperature synthesis (Y. Zhang, 2019).

2.3.2.1 Vacuum Arc Melting

The most well-known liquid state production method is vacuum arc melting (VAM). The schematic representation of a typical furnace is given in Figure 2.6. In this method, electrically controlled arc melting furnace is used for very high process temperatures (>3000°C). Most of the elements with high melting points can be mixed with this type of furnace in their liquid state. However, alloys with low melting temperatures (such as Mg, Zn, Mn) can evaporate easily. For alloys containing these elements, the arc furnace may not be the best choice for composition control (Murty et al., 2019; Y. Zhang, 2019).

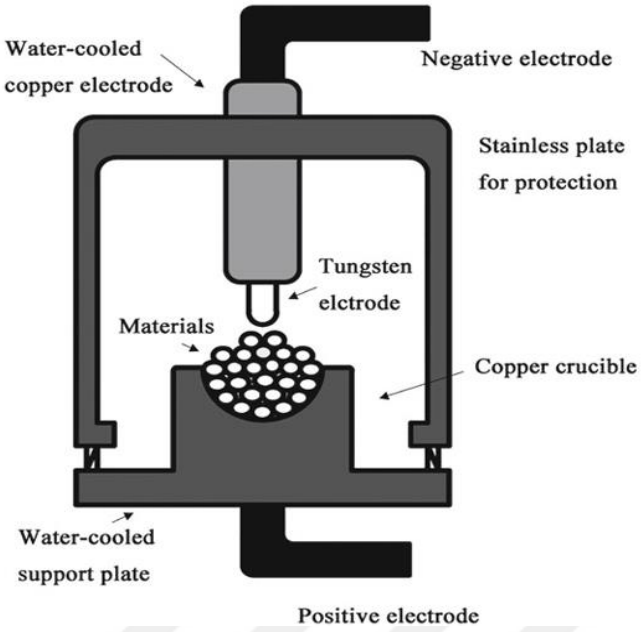

Figure 2.8 Schematic representation of the arc melting furnace (Y. Zhang, 2019)

With the arc melting method, which has many advantages such as low energy consumption, time-saving and low porosity rates, cylindrical ingots can be produced successfully at high cooling rates. However, the problem of the arc melting method is that, because of the rapid solidification, there isn't any control on the solidification process.

In the literature, arc melting method has been used to prepare AlCoCrFeNiTix high entropy alloys exhibiting BCC solid solution structures. With this method, alloys with very high fracture strength were obtained. In another study, it was found that the mechanical properties of AlCoCrFeNi were significantly improved by decreasing the sample size and thus increasing the cooling rate. If microstructure of the AlCoCrFeNi alloy (Figure 2.7) is examined for different regions from the surface to the center. it is seen that an inhomogeneous structure is formed after melting from fine grains (region A) to columnar dendrites (region B) and then to coarse-coaxial dendrites (region C) (Gao et al., 2016).

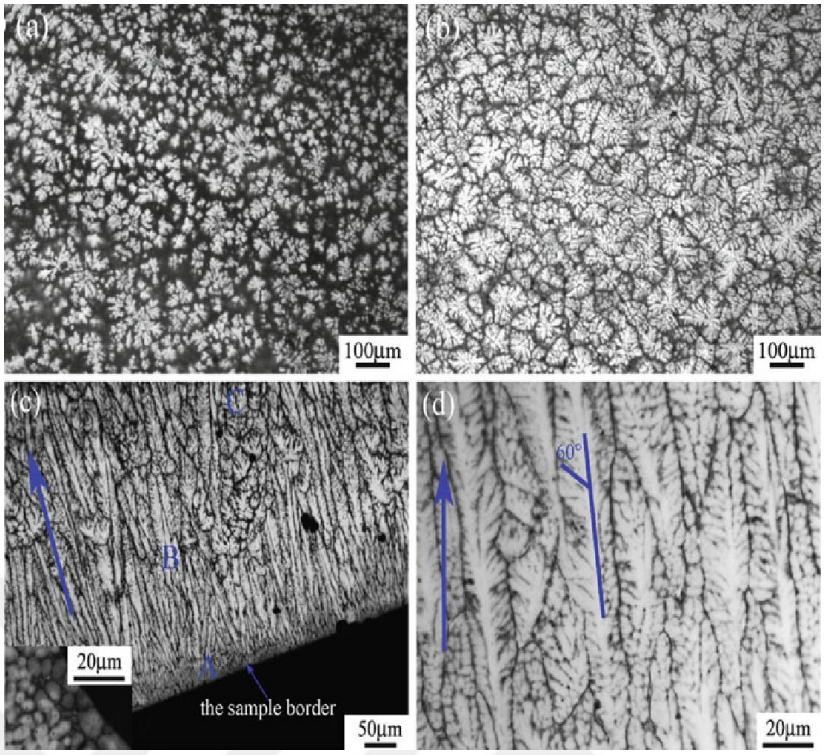

Figure 2.9 Microstructure images of cylindrical AlCoCrFeNi alloy obtained by arc melting and subsequent casting into copper crucible: a) and b) coaxial dendrites in the center, c) surface-to-center cast structure, d) columnar dendrites in the transition zone (Gao et al., 2016)

Singh et al.(S. Singh, Wanderka, Murty, Glatzel, & Banhart, 2011) have researched the development of microstructures of HEAs based on the cooling rate (Figure 2.8). Results indicates that the phase segregation during solidification of high entropy alloy is caused by splat quenching (cooling rate:10^6–10^7 K s^{-1}) and by casting processes (cooling rate 10–20 K s^{-1}).

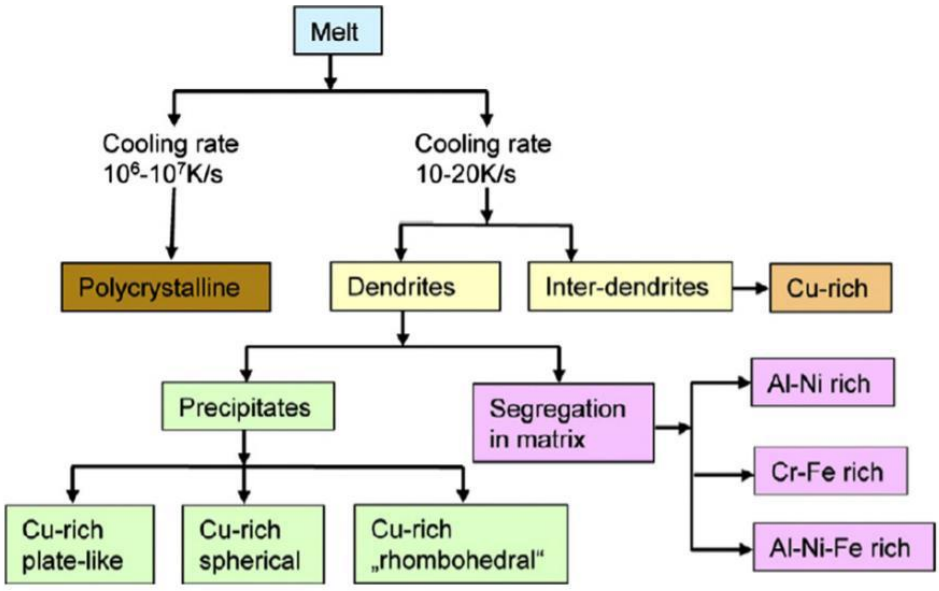

Figure 2.10 Schematic illustration of phase separation during solidification of AlCoCrCuFeNi HEA by splat quenching and casting (S. Singh et al., 2011)

The basis of the vacuum induction method, which is another of the liquid state production techniques, is similar to the arc melting method, but the power that provides melting here is the Eddy current. The Bridgman technique, which is another method, is characterized by heating and cooling the ceramic mold with the help of radiation and is especially preferred for property improvement by controlling the microstructure of high entropy alloys.

2.3.2.2 Bridgman-Stockbarger

Another liquid state production technique used apart from the casting method is the Bridgman solidification method, also known as the Bridgman-Stockbarger method (Fig.2.8). This method was first used in the production of single crystal ingots (S. G. Ma, Zhang, Gao, Liaw, & Zhang, 2013). In the process, which is generally used in the production of single-crystal materials, the materials are heated to their melting temperature and slowly cooled starting from the side where the core crystal is located at the end of the container. A single crystal starts to grow on the core, continues to grow gradually on same crystallographic orientation and starts elongating and forming into the container. In this production method, the process can be selected vertically or

horizontally. The Bridgman method is also a frequently used process in the production of semiconductor crystals.

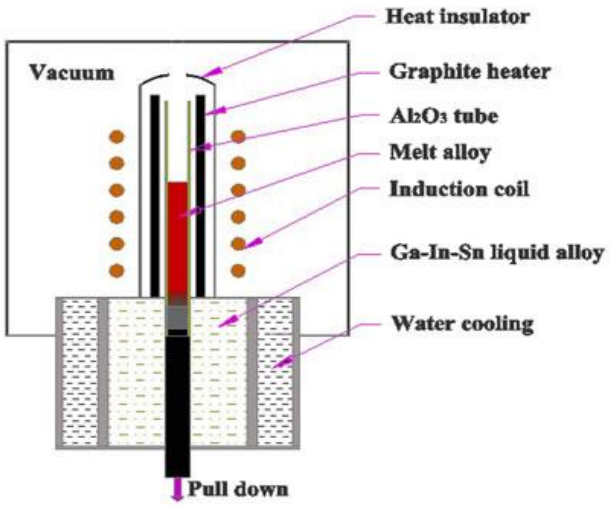

Figure 2.11 Schematic view of the Bridgman solidification method (S. G. Ma et al., 2013)

Cui et al. have been solidified AlCoCrFeNi high entropy alloys vertically by Bridgman method. As a result of the study, it was observed that directional solidification causes coarse dendritic structure and the concentration difference decreases in the dendritic and interdendritic regions (Cui, Wang, Wang, & Fu, 2011).

2.3.2.3 Vacuum induction method

Vacuum induction melting is a method frequently used in the production of metallic alloys, especially in the production of high alloy steels and superalloys. It is a process designed especially for alloys that are required to be produced in an environment free from O_2 and N_2 elements. A vacuum induction melting furnace contains a melting crucible inside a steel shell which is connected to a high-speed vacuum system. the heating and cooling coils are placed in the middle of the furnace and the crucible covered with refractory. The furnace is heated by electric current passing through a series of induction coils. The coils are made of copper tube cooled by water flowing through the tube. The current that passes through the coils creates a magnetic field that induces a current in the load inside the refractory. When the charge material is heated and the charge becomes completely molten, these magnetic fields continuously mix

the molten alloy and provide high purification in the structure. Due to the high mixing effect, finer grained structures can be obtained(Winkler D., 1971).

2.3.3 Production from the Gas State

For the production of high entropy alloys gaseous phase, all methods are basically based on the formation of thin films by depositing the formed metal vapors on a substrate. The physical vapor deposition (PVD) method offers various vacuum deposition techniques based on the evaporation of the target material desired to be deposited in the form of a thin film layer and condensation on the substrate. These techniques are: cathodic arc deposition, electron irradiation physical vapor deposition, volatile deposition, pulsed laser deposition, and sputter deposition (Gao et al., 2016).

Among these methods, the most common method used for deposition of films of high entropy alloys is magnetron sputtering. The most widely used method in vapor phase surface coating techniques is magnetron sputtering. The purpose of the production of thin film or layered high entropy alloys by coating techniques is to make the surfaces of materials such as low carbon steel and Al alloys used as substrates resistant to corrosion, oxidation and wear. In magnetron sputtering technique, for obtaining higher spraying at lower argon pressures, fields of magnetic and electric are used to increase the electron path length where both direct current and radio frequency are used (Y. Zhang et al., 2014).

2.4 Notation of High Entropy Alloys

Due to the basic definition of high entropy alloys which they are built on a multiple major element, there are many variations in the notations of HEA. There are differences in the representation of the constituent elements as chemical formulas. For the comparison of alloys belonging to the same or different systems, the primary elements are first listed in alphabetical order as a common method.

The concentration in the alloy can be expressed as a subscript based on atomic ratio or atomic percentage. For example, the notation AlCoCrFeNiTi, CrMnFeCoNi and AlCoCrFeNi for equiatomic high entropy alloys is appropriate (Firstov et al., 2016; Sun et al., 2022; R. Wang, Zhang, Davies, & Wu, 2017). The same notation applies to $Al_{0.5}Co_{1.5}CrFeNi_{1.5}Ti_{0.5}$ non-equiatomic alloys. The representation of this alloy according to atomic percentages is $Al_{8.3}Co_{25}Cr_{16.7}Fe_{16.7}Ni_{25}Ti_{8.3}$. The molar ratio is also easily used in the literature for high-entropy alloys because the molar ratio is equal to the atomic ratio. However, this rule can be neglected if compositional features of a component need to be emphasized. The most appropriate expression is used to reveal the desired feature. For example, the designation(denomination) of the $AlCoCrFeNiTi_X$ (X=0.0, 0.2, 0.4, 0.6, 0.8, 1.0) HEAs means that the Ti content varies between 0.0 and 1.0 (Güler, Alkan, & Alkan, 2022).

2.5 Solid solutions, intermetallics and intermetallic compounds in HEAs

High entropy alloys are more likely to form solid solutions such as BCC (B2), FCC (L_{12}) or HSP with irregular or ordered structure rather than forming intermetallic structures as generally mentioned. It can be said that Al, Cr, Fe, Ti, Mo, Nb, Ta, V and W elements are BCC structural elements. Unlike other elements in this group, aluminum has an FCC lattice structure. Aluminum has been used as an alloying element in most of the studies on HEAs to date (Murty, Ranganathan, Yeh, & Bhattacharjee, 2019). It is known that when aluminum is used in low amounts in the alloy, it stabilizes the FCC structure, and in high amounts, it stabilizes the BCC structure. The aluminum element has the ability to form a BCC structure. When aluminum is added in sufficient quantities, AlNi, AlFe, AlCo, and similar stable BCC compounds are formed. When titanium element is added, it has HCP structure at room temperature but turns into BCC structure with the increase in temperature. This is an element that stabilizes the BCC structure, similar to Aluminum in general. The element titanium is generally used to increase the corrosion resistance of the alloy. In addition, it is added to the alloy in order to increase the strength of the alloy by realizing solid solution hardening in the alloy (Murty et al., 2019).

Molybdenum element, also known as alloys in general, plays an active role in the formation of the sigma phase in the structure. The chromium element also contributes to the formation of the sigma phase when present together with iron, cobalt and nickel. In addition, it is known that elements such as cobalt, copper and nickel are elements with FCC structure and they behave towards stabilizing the FCC structure. Copper element generally tends to precipitate in the regions between dendrites. The reason for this situation is that the enthalpy values of the mixture between copper and other elements in the alloy are positive. When the concentration of copper in the alloy structure is low, it accumulates elementally in the interdendritic region, while copper-rich phases appear when the amount increases (Mary, S. J., Nagalakshmi, R., & Epshiba, R.,2015; Mishra, Samal, & Biswas, 2012).

2.5.1 B2 phases

Phase B2 is a regular BCC structure (with Pearson symbol cP2). Here, one type of atom fills the center of the volume, while another type of atom fills the corners of the crystal lattice structure. The most common compounds with this structure are CsCl, CuZn, and NiAl. The B2 phase has been observed as the primary phase or secondary phase in many high entropy alloys. In some cases it has also been observed that these alloys precipitate from a BCC crystal structure during heat treatment. Generally where the B2 phase is determined, the alloys contain Al together with 3d transition elements such as Ti, Cr, Mn, Fe, Co, Ni and Cu. Among these 3d transition elements, the element Al has a strong affinity with Fe, Co, and Ni to form the B2 phase (Murty et al., 2019).

2.5.2 $L1_2$ phases

The $L1_2$ phase (with Pearson symbol cP4) has a regular FCC structure, but the $L1_2$ phase is rarely observed in high entropy alloys. Al alloys containing $L1_2$ phase contain Al and Ni elements. However, in cases where the Al content is high, the $L1_2$ phase disappears and the FCC structure leaves its place to the BCC structure, and in this case, the B2 phase is formed (Murty et al., 2019).

2.5.3 Intermetallic

In high entropy alloys, binary element systems with high temperature often form more than two phases. For example, as shown in Table 2.4, while the Al element bonds strongly with Nickel, Co, Fe and Cr, the Cu element encounters a repulsive force against the aforementioned elements. In high entropy alloys, elements can form phases with different lattice structures due to these chemical bond interactions with each other at different temperatures. As a result of this situation, polyphase structures such as copper-rich multicomponent FCC structure, multicomponent FCC+BCC structure, B2 phase, and A2+B2 phases can occur in equiatomic AlFeCoCrCuNi alloys at temperatures above 600 °C (Wu et al., 2006).

Table 2.4 Binary mixture enthalpies of atom pairs in Al-Co-Cr-Cu-Fe-Ni alloys (kJ/mol) (Murty et al., 2019).

Al	-19	-10	-1	-11	-22
-19	**Co**	-4	6	-1	0
-10	-4	**Cr**	12	-1	-7
-1	6	12	**Cu**	13	4
-11	-1	-1	13	**Fe**	2
-22	0	-7	4	2	**Ni**

A high mixing entropy is not always sufficient for the formation of simple solid solutions. In the last 10 years, research on high entropy alloys has shown that these alloys have high atomic size differences and the differences between alloying elements. It has been observed that different intermetallic phases are formed in conditions where the attraction force (electro-negativity difference) is high. The most important of these intermetallic phases are the sigma (σ) and Laves phases (Murty et al., 2019; Y. Zhang, 2019).

2.5.4 Sigma phases

The sigma phase (σ) usually occurs in Cr-containing steels, and the equiatomic FeCr is tetragonal. In addition, the σ phase is also observed in CoCr and FeMo compounds with equiatomic composition in the Co-Cr and Fe-Mo binary alloy system. The σ phase is formed at various stages of the production of many high entropy alloys containing high amounts of Cr and Mo, as well as Fe and Co. In high entropy alloys, the σ phase is a multicomponent solid solution. In high entropy alloys, not only the mixing entropy is effective in the formation of the sigma phase. In addition, the different atomic sizes of the different elements in the alloy and their chemical interactions with each other are also effective in the formation of the sigma phase (Murty et al., 2019).

$AlCo_xCrFeMo_{0.5}Ni$ high entropy alloys with different cobalt content have also been studied in the literature. While the cobalt ratio is 0.5-1.0-1.5, there are regular BCC and σ phases in the microstructure, while the FCC structure is seen when the cobalt ratio is 2.0. This is explained by the fact that the cobalt element stabilizes the FCC structure. In this study, the σ phase is thought to be a solution consisting of mixtures of CoCr, FeCr, FeMo and NiMo compounds. When the Co ratio is 0.5, in the microstructure of the alloy includes dendritic DR, ID (without eutectic structure) and eutectic structures. When this ratio was 1.0 and 1.5, only DR and ID structures have been seen in the structure. While the Co ratio have been 2.0, a polycrystalline single-phase structure was obtained. The microstructure images obtained according to the changing Co content in the study of Hsu et al. are given in Figure 2.9(Murty et al., 2019).

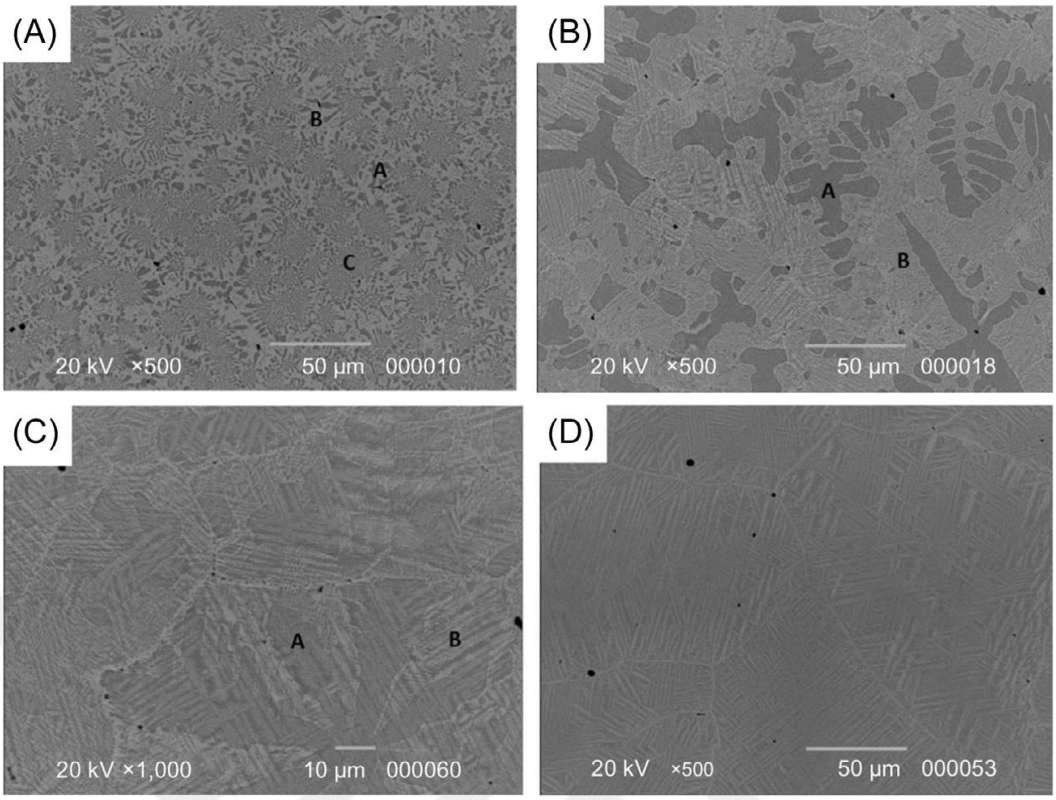

Figure 2.12 a) x = 0.5, b) x = 1.0, c) x = 1.5 and d) x = 2 SEM images of $AlCo_xCrFeMo_{0.5}Ni$ alloy (Murty et al., 2019).

At x=1.0 and 1.5, the (Ni,Al)-rich BCC structures DR and (Mo,Cr)-rich BCC structures ID have revealed structures that have been modulated. During the cooling step, they are made up through decomposition of BCC into ordered BCC(B2) and σ phase phase. When this alloy content x=2.0, a mixture of B2+FCC with σ phase along grain boundaries and beam-shaped σ phase in grain is observed.

2.5.5 Laves phases

Laves phase is an intermetallic compound with stoichiometry AB_2. The atomic size ratio is between 1.05 and 1.67. Laves phases are divided into 3 groups: C15 ($MgCu_2$-cubic), C14 ($MgZn_2$-hexagonal), and C36 ($MgNi_2$-hexagonal). In these compounds, A atoms in AB2 stoichiometry form diamond, hexagonal diamond or ordered arrangement, whereas B atoms form a tetrahedral arrangement around the A atoms. In addition, when the ratio of atomic sizes of A and B atoms to each other is about 1.225, they form tetrahedral closed-packed structures(Murty et al., 2019).

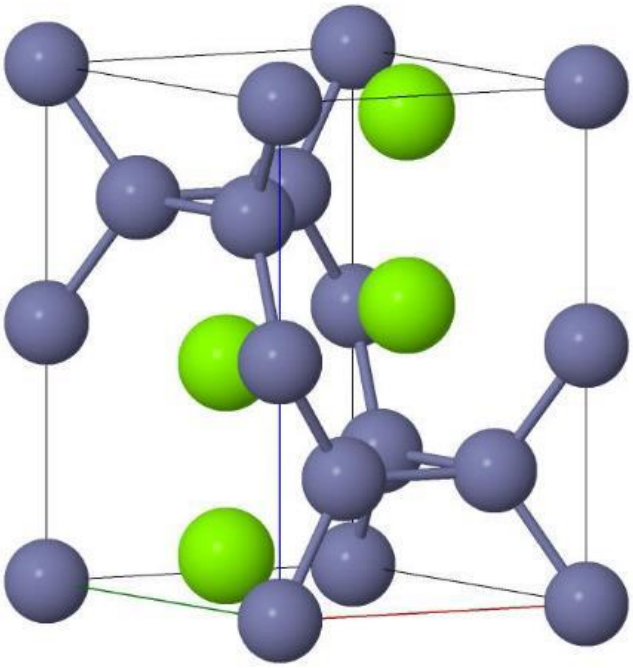

Figure 2.13 Unit cell of Laves phase with $MgZn_2$ structure (Mg atoms are green) (Murty et al., 2019)

Many studies show that the Laves phase is present in the structure of high entropy alloys as the main phase or the minor phase. The formation of Laves phase rich in terms of Ti and Co elements has been reported in $CoCrFeNiTi_{0.5}$ alloy produced by arc melting method. In another study, Ti2Co-type Laves phase was observed in CoCuFeNiTi alloy system. On the other hand, in the $CrMo_{0.5}NbTa_{0.5}TiZr$ alloy, the chromium-rich Laves phase was also observed along with the two BCC phases. For the alloys that are stated above, the Laves phase is formed by the presence of Ti element together with other transition elements. When x=0.8 in the AlxCoCrFeNiTi0.5 alloy system, a Laves phase was observed along with the FCC and BCC phases(Murty et al., 2019).

2.5.6 Intermediate Compounds

If sufficiently small atoms fill special interstitial spaces in the metal lattice, interstitial compounds are formed. For example, transition metals generally have a hexagonal close-packed or face-centered cubic structure. They also have tetrahedral

and octahedral spaces at different points. Typical stoichiometric ratios of these compounds are M_6X, M_3X, MX_2, M_2X, and MX. In this system, M can be elements such as Fe, Cr, V, Ti, Zr while "X" it can be N, C, B, H, elements (Brif, Thomas, & Todd, 2015).

The concept of high entropy alloys can be expanded to high entropy ceramics as oxides, nitrides, carbides, and combinations thereof. In a study conducted in 2012, the $(CrNbTiVW)_{50}C_{50}$ system with transition elements is the first high-entropy carbide synthesized by mechanical alloying and solid-state sintering. The sintered carbide consisted of a solid solution of NaCl type FCC, in which the five binary carbides were thermally stable. Nanopowder produced by mechanical alloying was successfully obtained by pressureless sintering at a low temperature of 1723 K in accordance with the mixing rule(Murty et al., 2019).

2.6 Application Areas of High Entropy Alloys

High entropy alloys have many uses as functional and structural materials. Some potential application areas of high entropy alloys are as follows :

1. High entropy alloys can be used as a transition layer between two different alloys. For example, High entropy brazing alloys are used as welding material between pure titanium and Cr-Ni-Ti stainless steel. As a brazing alloy, High entropy alloys are used as the welding material between carburized carbide and steel, providing a convenient manufacturing process with good flexibility.
2. Another study determined that high entropy alloys have very good super-paramagnetic, ferromagnetic and soft magnetic properties. It has been revealed that the material can be used in many different areas regarding its magnetic properties.
3. High entropy alloys can be used in the nuclear industry. High entropy alloys with high radiation and corrosion resistance are potential candidates for coating materials in nuclear fuels and high-pressure vessels.
4. High entropy alloys can be used as heat-resistant or wear-resistant coatings. However, new technologies need to be developed for coatings made of high entropy alloys to be more homogeneous and have higher bonding properties with the substrate.

5. High entropy alloys containing refractory metals can be used as thermal barrier coatings. New studies are being carried out in this area as well.

6. Carbides and nitrides of high entropy alloys are also interesting for their unique properties. It is available in both amorphous and solid solution structures with high hardness and strength properties. It has the potential to be used as a diffusion barrier and as a hard coating on cutting tool steels or high-speed steels. Recent studies show that high entropy carbide and nitrides could also be used in biomedical coatings.

7. Some physical properties of high-entropy alloys provide an advantage in using the materials for electronic applications. (eg $Al_{2.08}$CoCrFeNi HEAs exhibit almost constant resistivity). It is seen that research is concentrated on this subject.

8. Lightweight high-entropy alloys are used in portable devices, battery anode materials, and body materials for the transportation industry(Y. Zhang, 2019).

2.7 Design of High Entropy Alloys

While a wide composition universe of high entropy alloys greatly increases the composition amount of alloys that can be produced, it is very difficult to find alloys with desired properties among these compositions. Many methods have been developed to solve this situation. Studies have been carried out to predict the elements used in the production of alloys and the phases that will occur depending on the compositions of these elements. While some of these studies consist of empirical approaches, thermodynamic modeling and atomistic approaches are also frequently used.

2.7.1 Method of Empirical Calculation

The critical thermodynamic parameters used to describe the conditions of solid solutions in high entropy alloys have been mentioned above. ΔSmix and ΔHmix parameters are crucial in predicting solid solution formation in a multicomponent system. Yang et al., in a study they conducted in 2012, defined a new parameter in addition to these parameters. This parameter is Ω. Phase formation for multicomponent alloys was estimated by calculating Ω parameters in the study(Yang & Zhang, 2012).

$$\Omega = \frac{\mathrm{Tm}\Delta\mathrm{Smix}}{|\Delta\mathrm{Hmix}|} \quad (2.6)$$

The term “Tm” in the equation is an important term because the alloys to which the term entropy is applied form phases close to the melting temperature. This term is calculated according to the rule of mixtures.

$$\mathrm{Tm} = \sum_{i=1}^{n} Ci(Tm)i \quad (2.7)$$

In addition to basic thermodynamic criteria, the Ω term is a critical point for determining solid solution formation in a multicomponent alloy system. If $\Omega > 1$, it is anticipated that a solid solution phase will emerge in the alloy structure. In cases where this value is equal to or less than 1, it is predicted that intermetallic phases will form in the structure. Using these empirical calculations, all HEAs are designed(Yao et al., 2016; Zheng, Ding, Cao, Hu, & Huang, 2019).

2.7.2 Atomistic approaches

Ab-initio Molecular Dynamics (AIMD) is a technique based on Density Functional Theory (DFT) that combines simulations of molecular dynamics with computations of electronic structure. During the computation of the energy of a solid or molecule using DFT, this approach has been devised. Commonly, AIMD simulations are used to determine the thermodynamic characteristics, and the structural, dynamic, optimal geometries, electron band structures, total energies, and magnetization properties of materials at various temperatures(Kresse, 1995; Lin, Guo, & Ji, 2021). Before doing production, AIMD simulations are routinely used. The HEAs employed in AIMD simulations enable the investigation of a vast array of compositions. For example, in the study of Gao et al., AIMD simulations of selected high-entropy alloys were carried out in the first step(Gao & Alman, 2013).

2.7.3 Thermo-Calc Software

Thermo-Calc software based on the CALPHAD method is a computational approach used to estimate the material's composition, structure, and characteristics.

The computation is performed by combining thermodynamic and kinetic principles. The database of Thermo-Calc have been created by material engineers who are specialists in their domains by combining comprehensive scientific study, experimental data, and theoretical information. The CALPHAD approach is another method that allows obtaining information about the phase structure, composition, and microstructure of the HEA systems to be developed. Thanks to the thermodynamic extrapolation of the data obtained from the existing binary and triple equilibrium systems, the elements of the HEA system, quaternary, quintet, or even higher equilibrium systems can be made up(F. Zhang et al., 2014).

Computer software used today, based on thermodynamic calculations and the generation of phase diagrams for multi-component systems, applies the CALPHAD method. The understanding of this method is based on the mathematical description of the thermodynamic functions of the phases in the system and on reducing the Gibbs free energy. So as to calculate the total free energy value of each phase in the system, the sum of the free energy value of the pure component, the free energy value of the mixture in the ideal solution-forming state, and the residual free energy value of the solid solution mixture is used. The CALPHAD method has replaced traditional methods for generating phase diagrams because it allows the precise calculation of the phase balance of various materials with mixed chemical compositions. Calculation of phase diagrams requires extremely precise thermodynamic data. The collection, processing, and verification of data associated with thermodynamic properties and the calculation of equilibrium diagrams of metal alloys / slags / ceramic materials / molten salts / aqueous solutions are the tasks of teams formed by leading research centers. The SGTE database, created by the team of the Scientific Group Thermocata Europe - SGTE, constitutes the world standard for commercial software used in thermodynamic calculations. Thermo-Calc software includes several modules: the thermodynamic database (TDB) module; tabulation (TAB) module; POLY_3 module; Gibbs energy system (GES) module; POST module and PARROT experiment module(Zyska, Konopka, Łągiewka, & Kordas, 2017).

2.8 Literature survey

With the discovery of high entropy alloys, interest in thermodynamics, characterization, and manufacturability of these multicomponent alloys has increased. In the last 10 years, literature studies on HEA have increased 500 times. Many researchers have been continued investigating the potential production and feasibility evaluation of these alloys, their structural/functional properties, cost, machinability, and many properties (mechanical, thermal, magnetic, corrosion, etc.). In the literature, especially considering the cost-performance relationship, suitable alloy systems have been reported as AlCrCuFeMnNi, AlCrCuFeNi, AlCrFeNi, AlCrCuFeNiTi, AlCrFeMnNi, AlFeMoNi, CrCuFeMnNi, CrFeMnNi and CrFeNi(X. Fu, Schuh, & Olivetti, 2017).

Most of the studies in the literature are related to the formation of precipitate to increase the strength of the material with the effect of element type and amount on the properties in high entropy alloys. In a study by Gwalani et al., copper's role in increasing strength by precipitation hardening of FCC structured $Al_{0.3}CuCrFeNi_2$ alloys with high entropy was investigated(Gwalani et al., 2017).

In AlxCoCrFeNi high-entropy alloys studied by Rao et al., changes in the microstructure of these alloys caused by heat treatment or oxidation processes applied at different temperatures to high entropy alloys were investigated(Rao et al., 2017).

In a study investigating the effect of boron on the compositions of high entropy alloys, various proportions (x=0.0~1.0) of boron were added to the $Al_{0.5}CoCrCuFeNi$ alloy. According to the XRD results, while a simple FCC solid solution phase is formed in the alloy without boron, it has been reported that in addition to the FCC crystal structure, borit solution peaks are obtained in the boron-containing compositions. It was observed that as the boron content increased, the size of the boride structures increased, and the copper-rich dendritic phases did not disappear. Dendritic structure and FCC lattice constant did not change in the boron-free alloy; It has been

stated that borite precipitates increase the hardness and this increase is due to a strong correlation with the boron ratio (X. Liu et al., 2016).

Liu et al. conducted research on FeCoCuNi high entropy alloys by arc melting method in 2012. In their study, the effects of adding tin to the high entropy alloy on the microstructure and mechanical properties of the high entropy alloy were investigated. The findings indicate that alloys with low Sn concentration have a single FCC solution, whereas systems with growing Sn content have an FCC solution , Cu81Sn22 intermetallic compounds in their microstructure. These alloys were determined to have strong tensile and plastic strengths (L. Liu, Zhu, Zhang, Li, & Jiang, 2012).

Singh and Subramaniam (2014) studied Al-Cu-Co-Fe-Ni high entropy alloy. To comprehend the phase formation, certain ternary (CoFeNi, CrFeNi), quaternary (CoCrFeNi, CuCoFeNi, AlCrFeNi), and other (AlCuCoFeNi) alloys are selected for experimental research and the computation of various parameters. They used the vacuum induction melting method in this study, and annealing at 850 °C was applied. As a result of the study, they determined that two different FCC phases were formed in the structure of the alloy(A. K. Singh & Subramaniam, 2014).

Zhang et al. (2014), in their study, named microstructures and properties of high entropy alloys; The engineering properties of high entropy alloys are described. In this study, the formation criteria, thermodynamics, machining of high entropy alloys, It is briefly summarized of the kinetics, mechanical characteristics, and computer modeling of HEAs(Y. Zhang et al., 2014).

The microstructure and mechanical characteristics of AlCoCrFeNiZrx alloys generated by electric arc melting are investigated. The alloys have two distinct microstructures. The first is a periodic structure composed of the ordered BCC phase and BCC solid solution phase arising from spinodal decomposition, while the second is a mixture of the ordered BCC phase and Laves phase that alternately nucleate and grow. The coexistence of ordering and spinodal breakdown has been explained by the

introduction of a Zr element with a large atomic radius, which caused a lattice strain (J. Chen et al., 2016).

Unnikrishnan et al. (2017) investigated the effects of cobalt (Co), titanium (Ti), and silicon (Si) elements on AlCuNiFe high entropy alloys. It has been found that these elements are important factors in increasing the hardness of HEAs. In addition, the study found that the hardness of high entropy alloys is higher than conventional alloys, and the wear coefficient ratio is lower than conventional alloys(Unnikrishnan, Paul, Sellamuthu, & Arul, 2017).

Lee et al. (2017) discovered the effects of deformation and hot annealing on the microstructure of the alloy in their study on AlCoCrFeNi HEA. They have been determined that the alloy is rich in Cr and Fe, and when the temperature reaches 1100 ℃, it switches from BCC lattice structure to FCC lattice structure. In addition, high-temperature-compressed alloys have been demonstrated duplex microstructures composed of thin equiaxed FCC and BCC phases, whose average grain sizes fell dramatically to 1.54 and 1.97 m, respectively(Lee, Bae, Kang, Lim, & Na, 2017).

In recent years, many criteria such as mixing entropy (ΔSmix), atomic size difference (δ), mixing enthalpy (ΔHmix), and valence electron number (VEC) has been developed to indicate the phases that will form in high-entropy alloys. In the case where the VEC value, which is seen as an important parameter in the phase formation in HEAs in the literature, is " ≥ 8 ", the FCC phase; In case " < 6.87 ", BCC phase; When it is between these two values, it is stated that "FCC + BCC" phase tends to occur. A study that $(AlCoCrFeNi)_{100-X}Ni_X$ and $(CoCrCu\text{-}FeNi)_{100-X}Mo_X$ HEA by arc melting method has been observed when Ni element was added to the alloy, the VEC value increased, and FCC solid solutions were formed. Accordingly, it has been determined that the ductility of the alloy increased. When Mo element was added to the same alloy, it was observed that BCC solid solution formed due to low VEC value. When examining this alloy system in general, it was emphasized that the VEC value should be between 6.87 and 8 in practical applications where both high ductility and high strength properties are desired(R. Chen et al., 2018).

Another group of researchers working on the electron concentration-phase relationship has researched the lattice parameters, crystal lattices, phase and electron composition of more than 200 HEAs. As a result, it was revealed that the "6.7 < VEC < 7.3" condition should be met when %100 Laves phase is required in the structure(Gorban', Krapivka, & Firstov, 2017).

$AlCoCrFeNiTi_X$ high entropy alloy studies, which have been studied similarly in the literature within the scope of the thesis, are as follows:

Zhen et al., in their work in 2021, added Titanium element in different proportions to the structure of AlCoCrFeNi alloy by arc melting method. It was observed that the hardness value increased with the increase of titanium, and with the honeycomb-shaped indendritic structures formed from solid solution hardening. Furthermore, adding Ti seriously has increased AlCoCrFeNi HEAs resistance to sliding wear (Xu, Li, & Chen, 2021).

In their 2020 work, Qinglin et al. concocted a novel high entropy AlCoCrFeNiTi alloy using arc melting. The impacts of this alloys (1.0 weight percent, 2.0 weight percent, and 3.0 weight percent) on microstructure and mechanical characteristics of pure aluminum were investigated. The results indicate that the addition of HEA refined the aluminum's macrostructure and microstructure. Adding 3.0 wt.% of this alloy to the aluminum melt has been enhaced the tensile strength by 145.2%, from 62 MPa to 152 MPa, and the yield strength by 173.8%, from 42 MPa to 115 MPa(Q. Li et al., 2020).

In their study, Dang et al. investigated the effects of remelting and annealing on the wear resistance of AlCoCrFeNiTi0.5 HEAs. As seen in figure 2.10, the intensity of the diffraction peak of the BCC(A2) phase has been increased after remelting and annealing compared to the casting alloy(Kong et al., 2019).

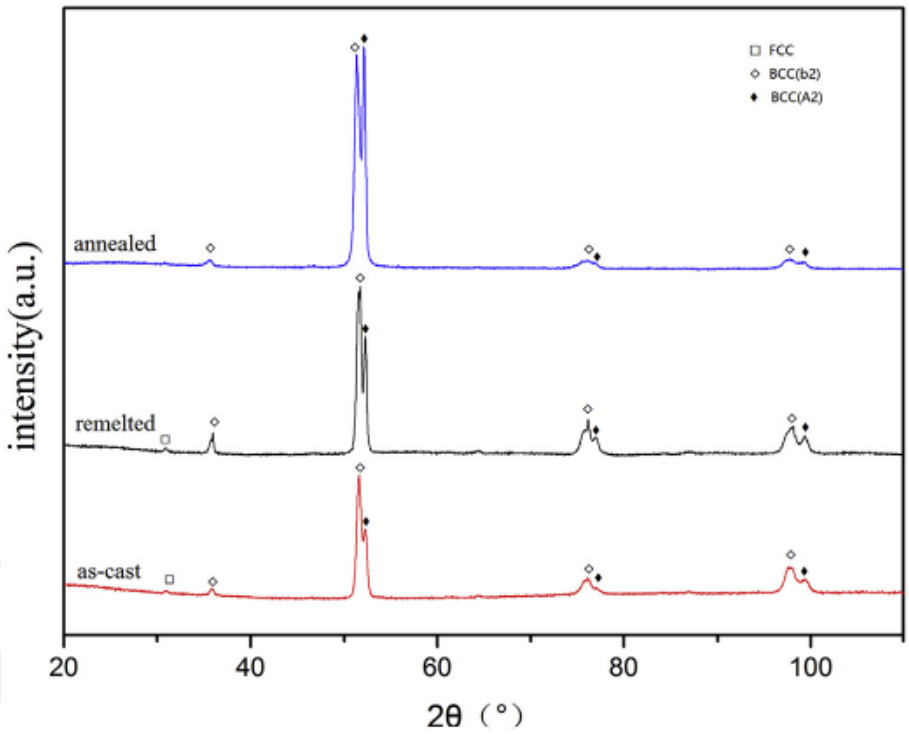

Figure 2.14 XRD results HEAs of $AlCoCrFeNiTi_{0.5}$(Kong et al., 2019)

After remelting & annealing, the microstructure distribution is homogenous. The dendritic gap diminishes, as shown by the findings in Figure 2.11. Moreover, the remelted and annealed $AlCoCrFeNiTi_{0.5}$ HEAs exhibited lower friction coefficients, higher hardness values, and less wear than the as-cast HEAs(Kong et al., 2019).

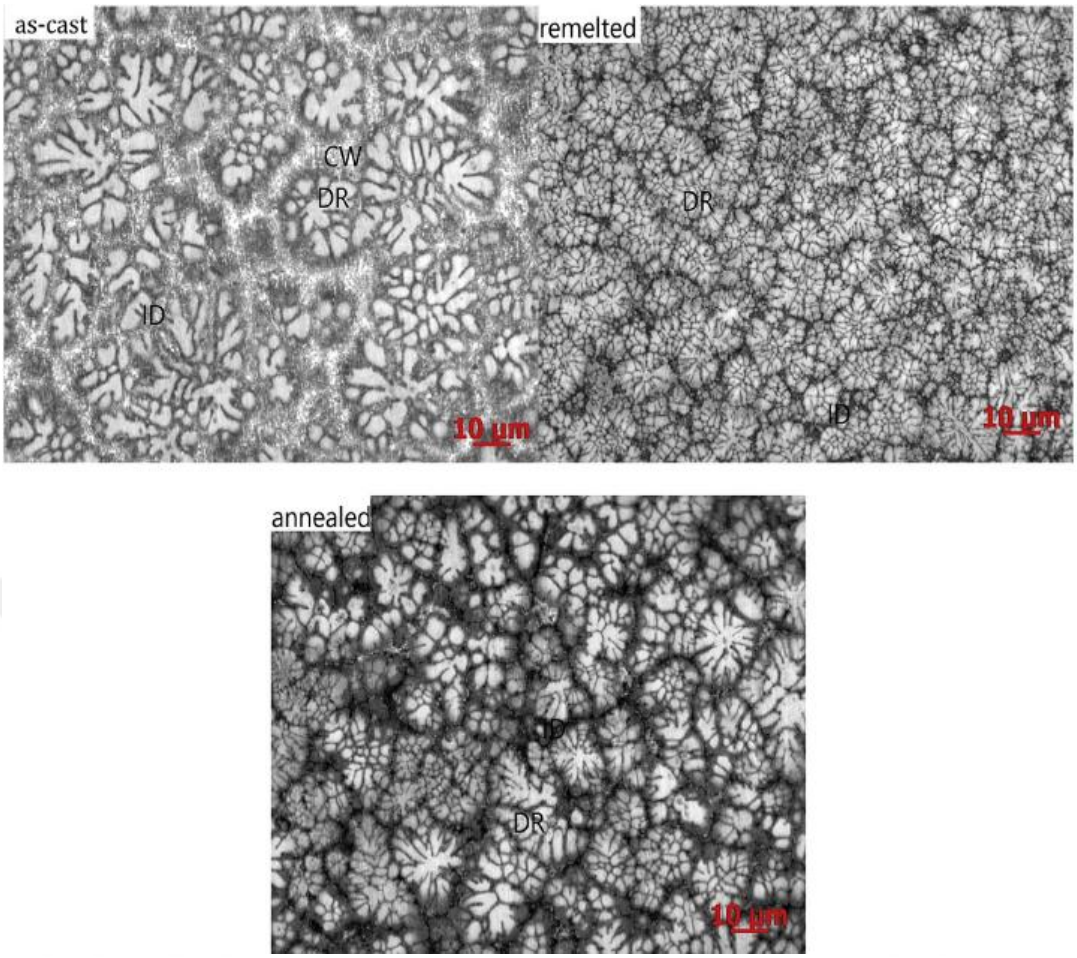

Figure 2.15 $AlCoCrFeNiTi_{0.5}$ HEA micrographs (DR: dendrite; ID:interdendrite; CW:cell wall) (Kong et al., 2019)

In the study of Young-Sang Na et al., the effect of adding up to 0.075% Ti to AlCoCrFeNi based high entropy alloy was investigated. It was determined that AlCoCrFeNi alloy undergoes spinodal decomposition into Al–Ni rich (B2) and Cr–Fe rich (A2) areas during solidification. Also, traces of Ti tend to separate along the grain boundary in the AlCoCrFeNi alloy. Therefore, it greatly refined the grain size of the AlCoCrFeNi alloy(Na, Lim, Chang, & Kim, 2016).

GiSu Ham et al. examined the impact of titanium addition on the microstructure and high temperature oxidation behavior of a high-entropy AlCoCrFeNi alloy. The titanium concentration is between 0 at% and 1 at%. It was established that both alloys had a BCC single phase and that the mean grain sizes of $AlCoCrFeNiTi_{0.0}$ and $AlCoCrFeNiTi_{1.0}$ were 47.2 m and 49.9 m, respectively. The XRD results in Figure

2.12 show the BCC phase formed in both alloys. In addition, the phase change from BCC to FCC was seen in AlCoCrFeNiTix (x=0.0,1.0) alloy as a consequence of oxidation (in Fig 2.13). Using this transition to investigated oxidation resistance was also examined. (Ham, Kim, Na, & Lee, 2021).

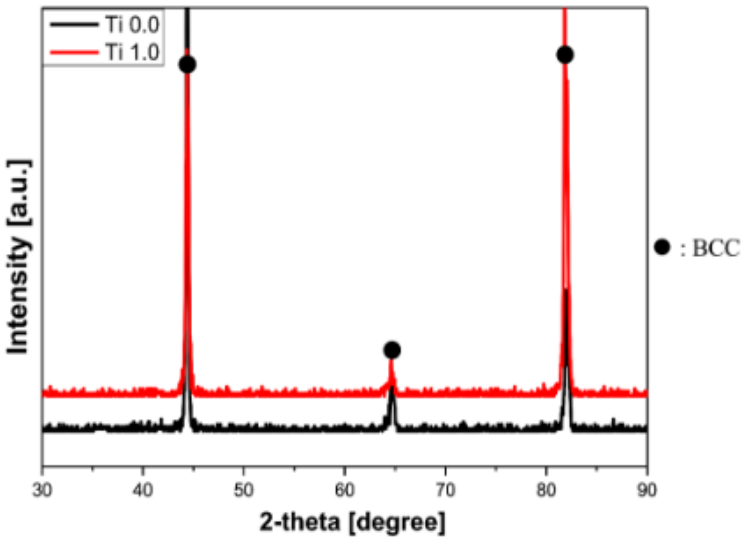

Figure 2.16 XRD analysis results of AlCoCrFeNiTix HEA before high temperature oxidation test(Ham et al., 2021)

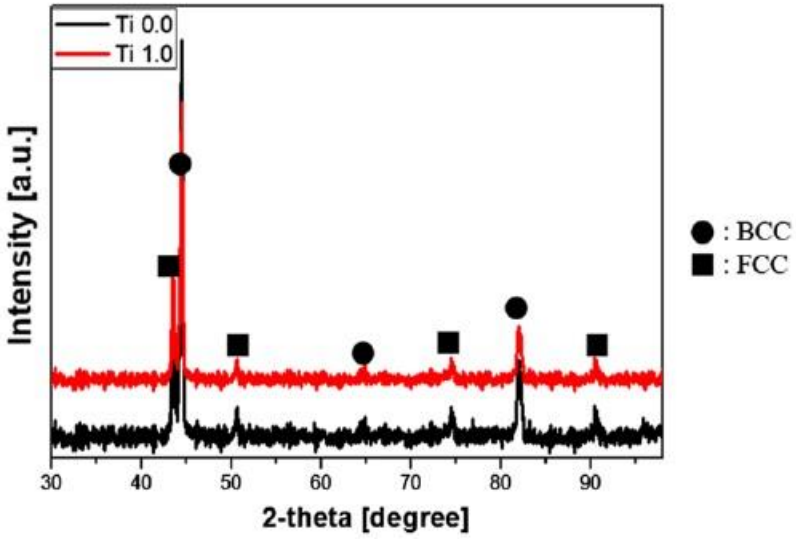

Figure 2.17 XRD analysis results of AlCoCrFeNiTix HEA after high temperature oxidation test(Ham et al., 2021)

Yuan et al.have investigated arc-melted AlCoCrFeNiTix high-entropy alloys.The developed alloys of microstructures and phases were examined. In high-entropy

AlCoCrFeNiTix alloys, BCC phases were found to equal FeCr and AlNi phases. As the Ti concentration increased, the single BCC phase has been showing transformed into BCC1 and BCC2 phases (ın Fig 2.14) (Yu, Wang, Li, Kou, & Liu, 2015).

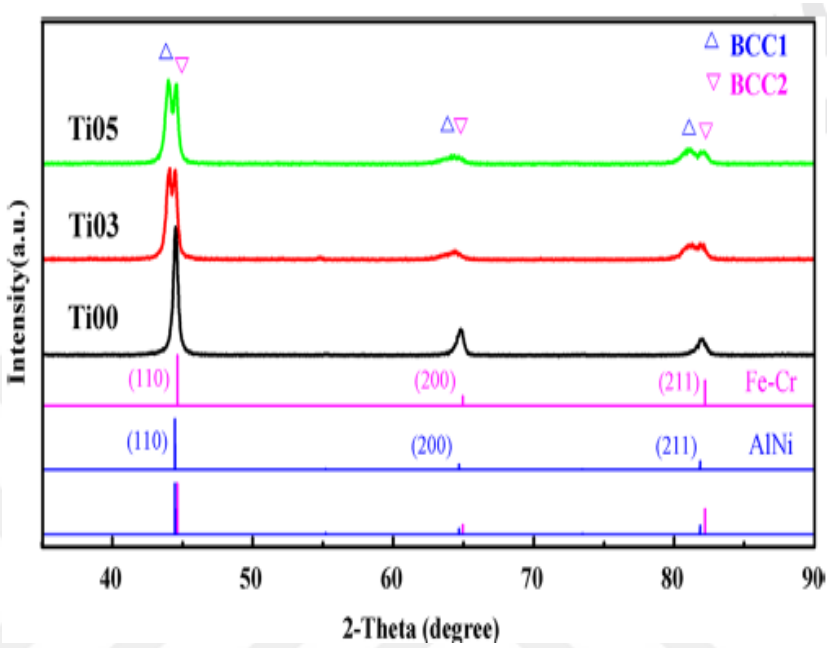

Figure 2.18 XRD analysis results of AlCoCrFeNiTix (Ti00, Ti03, Ti05)(Yu et al., 2015).

CHAPTER 3

MATERIALS AND METHOD

3.1 Materials

Aluminum, Cobalt, Chrome, Iron, Nickel, Titanium pure metal powders were purchased from three different companies. Fe, Cr, Al, Co, Ni were purchased from Molchem technologies, Ti powders from Alfa Aesar. High purity metal powders are used as raw materials in VAM studies. In the preparation of the alloys, powder raw materials with a grain size of -325 mesh (less than 45 μm) and 99.95% purity were used.

Table 3.1 Physical characteristics of chosen elements for the multi-principle alloying system.

Property	**Al**	**Co**	**Cr**	**Fe**	**Ni**	**Ti**
Atomic number	13	27	24	26	28	22
Molar mass	26.982	58.933	51.996	55.845	58.693	47.867
Density(g/cm^3)	2.7	8.9	7.15	7.87	8.90	4.5
Melting Point(°C)	660.3	1495	1907	1538	1455	1668

AlCoCrFeNiTix (x=0.0, 0.2, 0.4, 0.6, 0.8 and 1.0) Before preparing the high entropy alloys for production, the weights and alloy compositions of the samples were calculated according to their molar ratios. Calculated alloy compositions are shown in Table 3.2 and initial weights are shown in Table 3.3. The weights of the prepared pellets are given in Table 3.4.

Table 3.2 Calculated alloy composition ratios

X	**Al**	**Co**	**Cr**	**Fe**	**Ni**	**Tix**
0.0	0.2	0.2	0.2	0.2	0.2	0.0
0.2	0.1923	0.1923	0.1923	0.1923	0.1923	0.0384
0.4	0.1851	0.1851	0.1851	0.1851	0.1851	0.0740
0.6	0.1785	0.1785	0.1785	0.1785	0.1785	0.1071
0.8	0.1724	0.1724	0.1724	0.1724	0.1724	0.1379
1.0	0.1666	0.1666	0.1666	0.1666	0.1666	0.1666

Table 3.3 Initial weights of powders prepared by pelleting

X	**Al**	**Co**	**Cr**	**Fe**	**Ni**	**Tix**
0.0	0.5344	1.1672	1.0898	1.1061	1.1624	0.0
0.2	0.5148	1.1245	0.9922	1.0656	1.1199	0.1826
0.4	0.4967	1.0849	0.9572	1.0281	1.0805	0.3524
0.6	0.4782	1.0479	0.9246	0.9931	1.0437	0.5107
0.8	0.4624	1.0135	0.8942	0.9604	1.0093	0.6585
1.0	0.4492	0.9812	0.9297	0.9297	0.9772	0.7969

Table 3.4 Initially weight of the pellet

x	**0.0**	**0.2**	**0.4**	**0.6**	**0.8**	**1.0**	**Total**
Set 1	4.999	4.998	4.997	4.999	4.998	4.999	5
Set 2	4.998	4.997	4.998	4.999	4.999	4.999	5

3.2 Thermo-Calc Software for AlCoCrFeNiTix HEAs

The microstructure and phase behavior of an alloy is crucial to understanding its ultimate qualities. In order to predict the microstructure at any temperature, phase diagrams are usually utilized in the pre-production stages. ThermoCalc is used to draw phase diagrams using the CALculation of PHAse Diagram (CALPHAD) approach(Senkov et al., 2019; N. Zhou et al., 2019). First of all, the definition is made in our system to be created. The TCHEA4 (High Entropy Alloys v4.0) database to be used is selected. After the elements in the alloy were selected, the relevant mole fractions were calculated and entered.

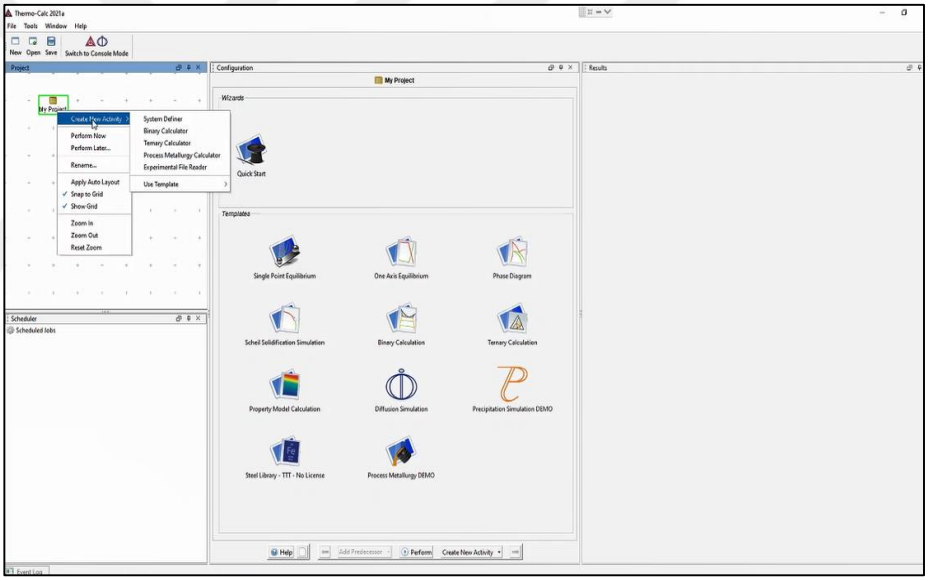

Figure 3.1 The process of creating the model tree for calculations.

TCHEA4 is a thermodynamic resource on multi-principal element alloys, often known as high entropy alloys. TCHEA4 is developed in the style of CALPHAD by assessing all binary and many ternary systems critically. Using a combination of researchers, first-principle calculations, and CALPHAD modeling, accurate thermodynamics descriptions of BCC, FCC, intermetallics, and HCP solutions have been obtained. This permits the prediction of multi-component alloy systems, particularly HEAs. In this module, approximately 307 binary systems can be evaluated according to all composition and temperature ranges and calculated with the BINARY Module. In terms of triple systems, 493 systems are evaluated. Of these, 192 can be

resolved over the entire composition and temperature range. It can be calculated with the TERNARY Module in the program. These modules are used to extrapolate to higher order systems, and predict phase formation, phase fractions, and phase compositions. Additionally, it helps to understand the phase equilibrium in high entropy alloys to calculate the driving force to form a phase. The SCHEIL GULLIVER module in Thermo-Calc may also be used to estimate the solidification behavior of HEAs using the database. For the majority of the phases, all relevant molar volume and high thermal behaviour have been evaluated(Andreoli et al., 2021; Zyska et al., 2017).

The model tree is created by selecting the module to be used in the program. Here, the mole fractions of the elements that make up the alloy are entered into the system. These stages are shown in Figure 3.1 and Figure 3.2. In the study, cooling behavior is resolved faster in equilibrium conditions. The transformation points and temperatures of the formed phases are obtained in graphic and table form. Then, the analysis perform to examine the cooling behavior of the alloy under Equlibirium (Fig.3.3) and non-Equlibirium conditions(Fig 3.4).

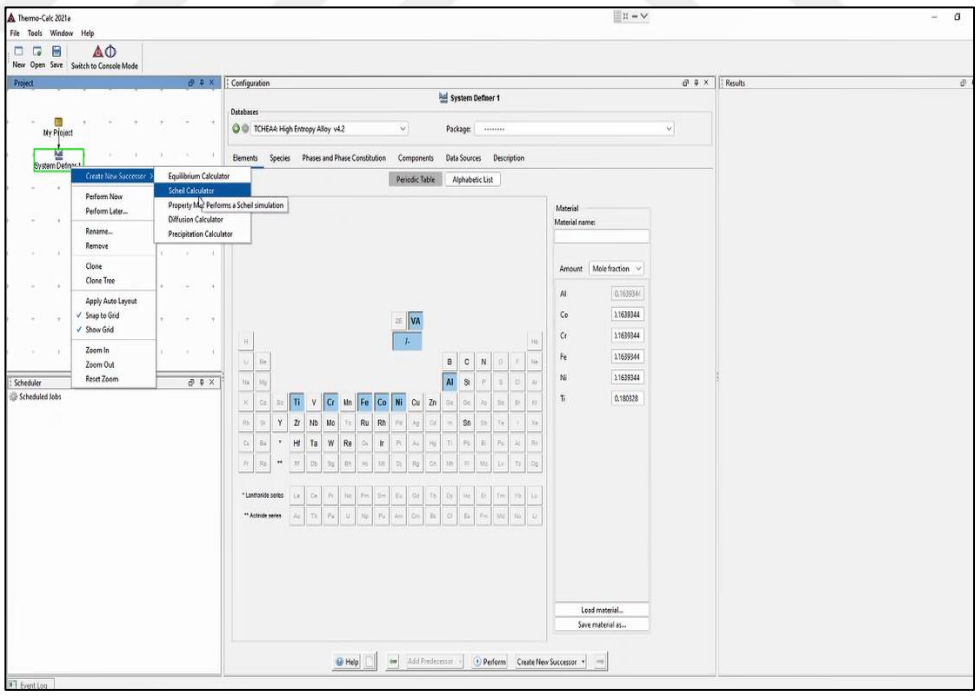

Figure 3.2 Entering boundary conditions into the model tree created for the calculations.

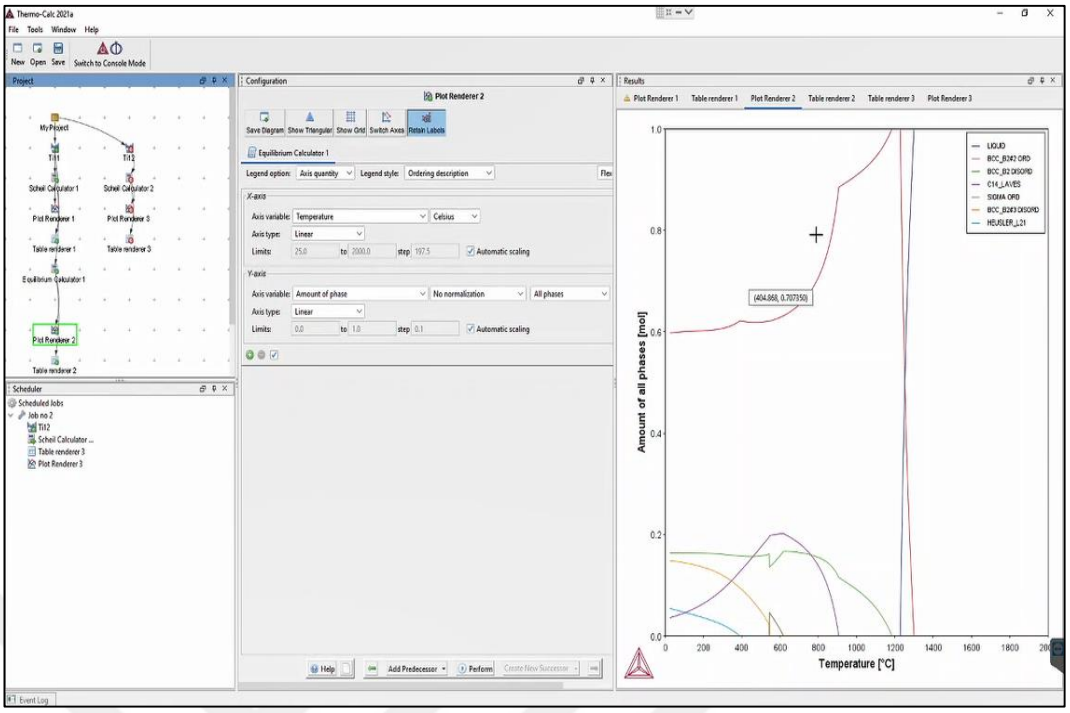

Figure 3.3 The cooling behavior occurring at equilibrium conditions

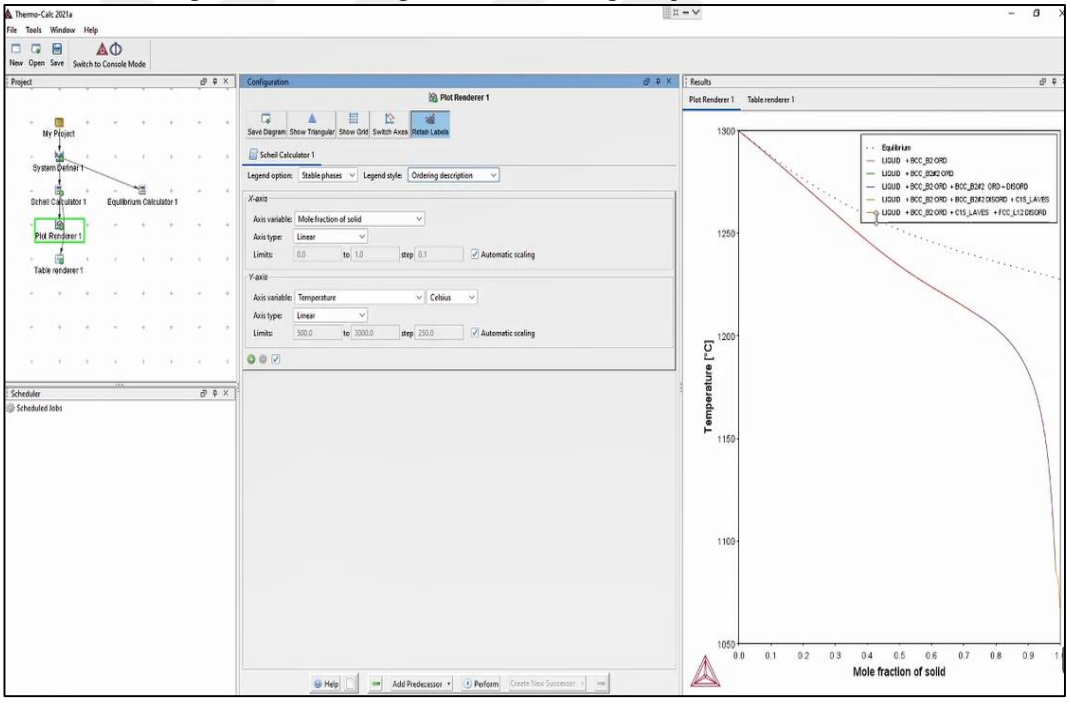

Figure 3.4 The cooling behavior occurring at non-equilibrium conditions

3.3 Production of AlCoCrFeNiTi$_x$ HEAs

The weights of metal powder mixtures prepared according to target alloys were measured with precision balance. Metal powder mixtures were mixed in Emor brand

powder mixer at 250-300 rpm for 30 minutes to produce a homogeneous alloy (In Figure 3.5).

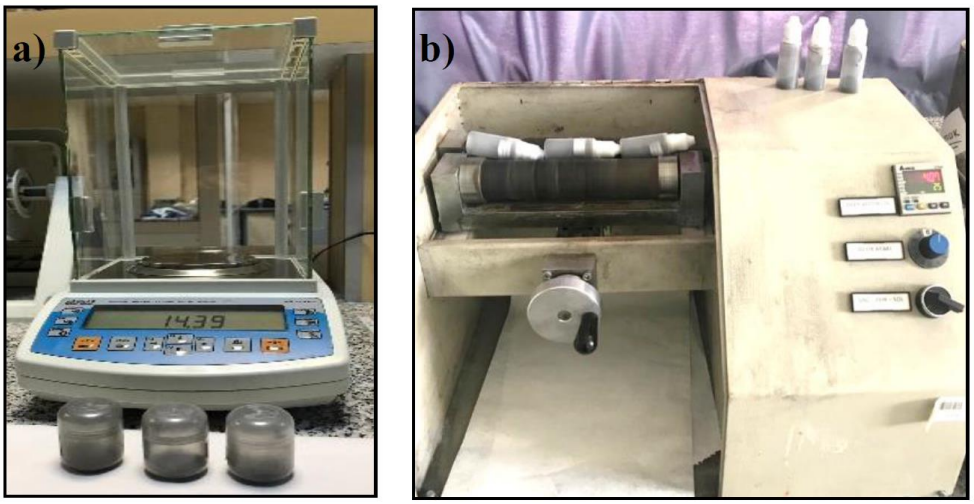

Figure 3.5 a) Weighing process of the prepared powders and b) Mixture of the prepared powders

Since the powder sample could not be melted directly in the arc melting device, the powder mixture of 5 grams has been turned into pellets. Powder mixtures prepared for the pelleting process were turned into pellets by applying approximately 30 bar pressure in the hydraulic press. The initial weights of the prepared pellets have been measured. Pelletizing apparatuses made of stainless steel were ultrasonically cleaned with ethyl alcohol and dried before each process. This process was repeated for the powder mixes in each composition. Then they were placed in the melting crucibles of the device for vacuum melting. A high-purity titanium metal was also placed inside the device to prevent oxidation. Before melting, the chamber was cleaned with argon gas 3 times, then the system was put into the vacuum. Melting experiments were carried out in Edmund Bühler brand VAM device operating in argon gas atmosphere in a water-cooled copper mold (Figure 3.6). To assure chemical uniformity, each samples were remelted five times by inversion. The final weights of the melted pellets were measured (Table 3.5.)

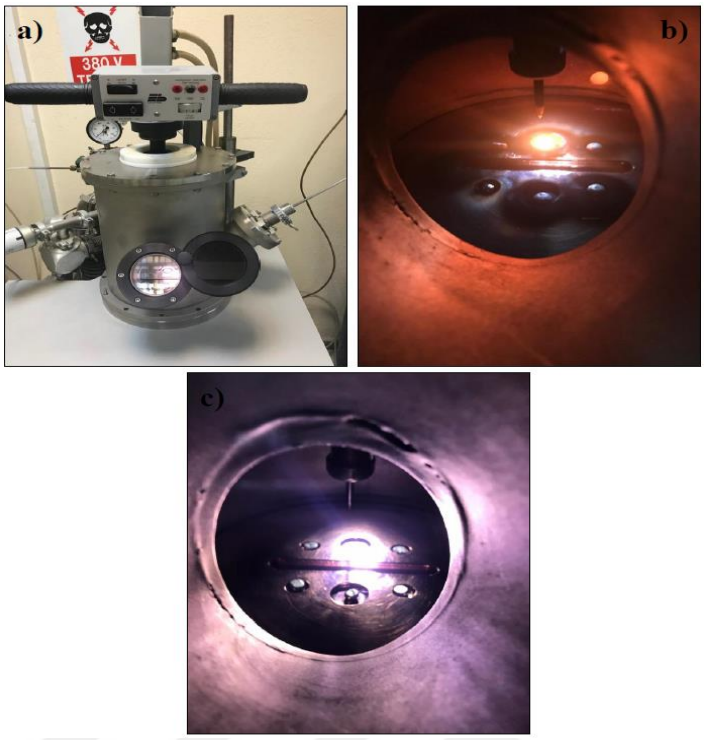

Figure 3.6 a)Edmund Bühler brand VAM device, b)arc melting process, and c)cooling of melted samples

Table 3.5 Average of the final weights of the melted alloy series

x	0.0	0.2	0.4	0.6	0.8	1.0
Set 1	4.838	4.899	4.774	4.786	4.756	4.748

After the weights of the melted pellets were measured with a precision balance, the pellets were brought together in the form of sticks. Metal ingots were cut into slices with a thickness of approximately 1.0 mm (Fig.3.7.).

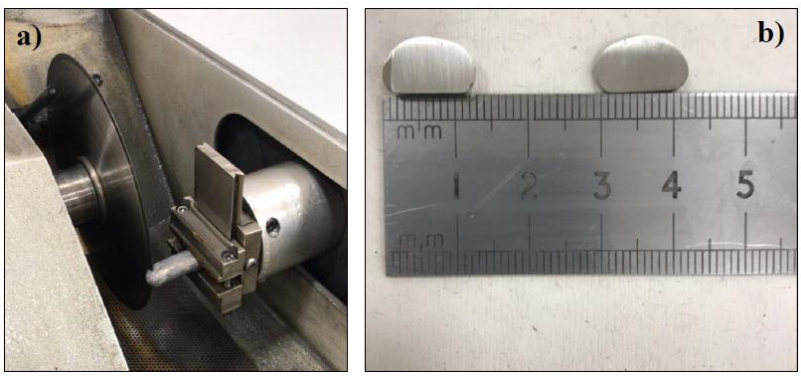

Figure 3.7 a) Cutting samples, and b) measuring the dimensions of the cut samples

After the cut samples were cleaned in an ultrasonic bath with a mixture of ethyl alcohol and water, they were made ready for heat treatment. The operations for heat treatment (H-T) were carried out in a resistance furnace at a heating rate of 10 degrees Celsius per minute. Heat treatments have been done to $AlCoCrFeNiTi_X$-based HEAs with X=0.0, X=0.2, and X=1.0 across all of the samples. These heat treatments have been carried out in quartz capsules that were hermetically sealed and evacuated. In a Protherm PLF 150/15 chamber furnace with a heating rate of 10°C per minute, the samples have been kept to temperatures of 500°C, 750°C, and 1000°C for a period of two hours each (Fig.3.8.). The samples that were maintained at temperatures of 500°C and 750°C were solely cooled in water, whereas the samples that were maintained at a temperature of 1000 °C cooled to room temperature using both water and the atmosphere of the furnace.

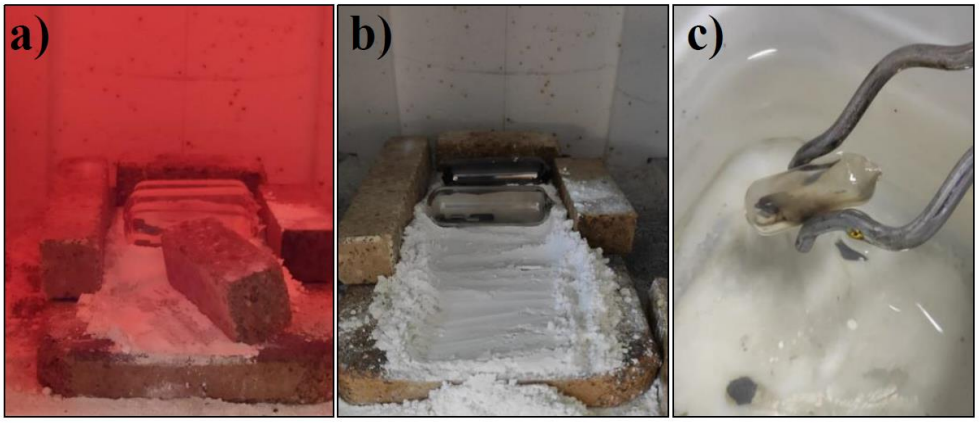

Figure 3.8 Heat treatment stages of the produced samples. a) holding process, b) cooling in the furnace c) cooling in water

For microstructure analysis and other analyses, the samples taken from the products produced by VAM method and heat treatment process have been sanded with 120, 320, 600, 800, and 1200, 1500, 2000 grit emery papers respectively in the sample preparation laboratory, and the polishing.

3.4 Characterization of produced $AlCoCrFeNiTi_X$ HEAs

The X-ray diffraction pattern (XRD) was made with the Rigaku ULTIMA 3–Rint 2200/PC system and Cu-Kα radiation (λ-Kα=1.54 Å) from 20° to 80°. X'pert High-

Score Plus software and also the ICDD and ICSD databases were utilized to look at the XRD results. A JEOL-JSM 6060 scanning electron microscope (SEM) was used to look at the microstructures of the AlCoCrFeNiTi$_X$-based HEAs. AlCoCrFeNiTi$_X$-based HEAs element was investigated after casting and heat treatment with the IXRF System-500 Energy Scattering Spectrometer (EDS) detector connected to the SEM device. The Perkin Elmer STA 8000 TG/DTA and the LABSYS evo DTA/DSC were used to do the thermal analysis. To avoid oxidation, samples were heated from room temperature to 1200 °C at a rate of 10 °C/min in a N_2 atmosphere. The mechanical properties were looked at with the Sinowon HV-1000D microhardness (micro-vickers) device. A load of 0.2 kg was applied to each sample for 10 seconds and 12 measurements were made. The average of these numbers was calculated, and the standard deviation was figured out.

CHAPTER 4

RESULTS AND DISCUSSION

4.1 CALPHAD Results

The phases that AlCoCrFeNiTi$_X$ high entropy alloys will form under balanced cooling conditions at different mole fractions were investigated using the CALPHAD program. Figure 4.1 depicts the potential phases and their quantities created under equilibrium cooling circumstances, beginning with 1 mole of liquid in these alloys.

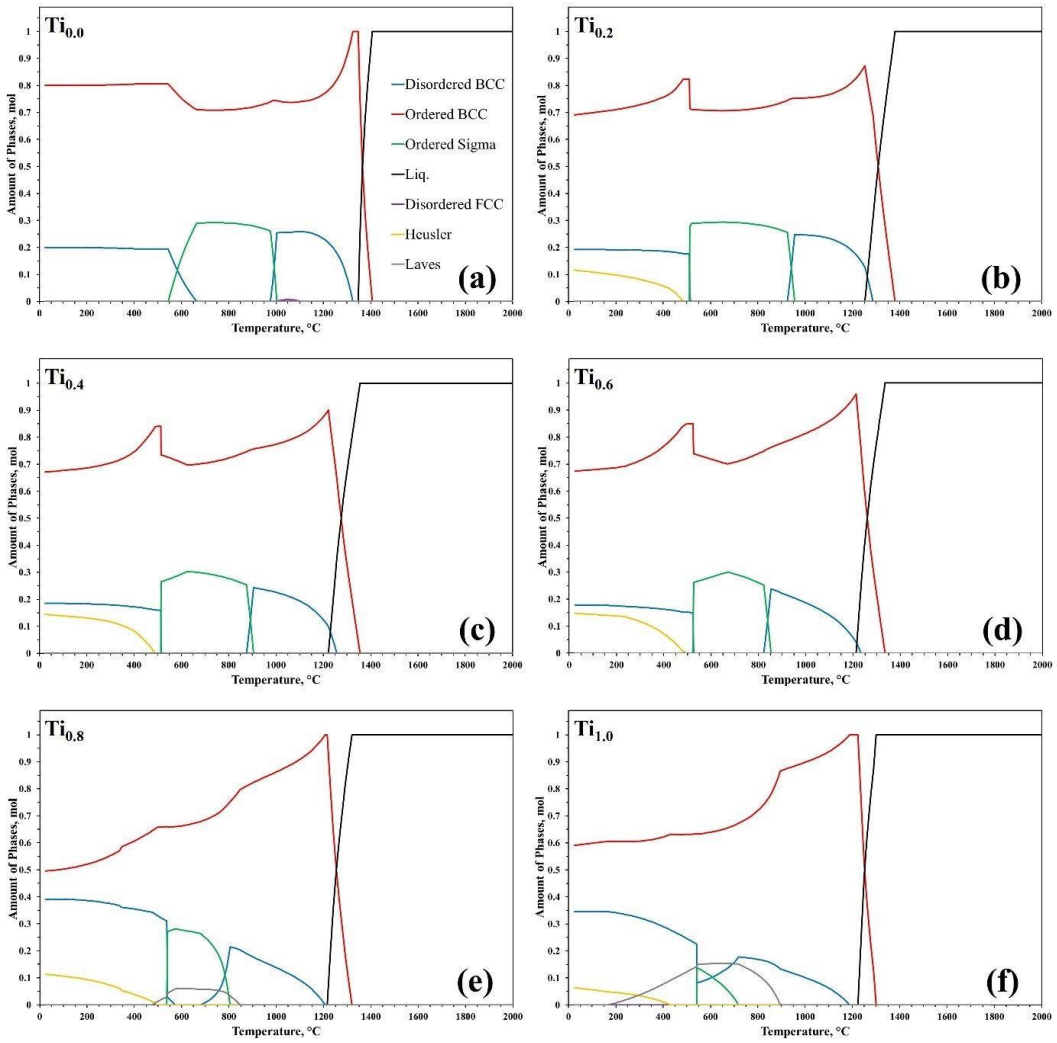

Figure 4.1 Possible phases to occur under balanced cooling conditions and their quantities a) x=0.0, b) x=0.2, c) x=0.4, d) x=0.6, e) x=0.8, and f) x=1.0 in AlCoCrFeNiTi$_X$ HEAs

As a result of the thermodynamic analysis, the ratios of the theoretical phases formed with the temperature change and the compositions of the phases were also calculated. As shown in Figure 4.1, the structure of HEAs can form many phases. It is seen that the main phase in the microstructure of these HEAs is the sequential BCC phase (B2). The same phases were obtained in the study of Zhen et al. in 2021(Xu et al., 2021). Other phases in alloy structures include the irregular BCC phase, the disordered FCC phase, the ordered Sigma phase (intermetallic σ-phase), the the $L2_1$ structure of X_2YZ type full-Heusler phase, and the C14 type hexagonal Laves phase. Depending on the titanium element added to the AlCoCrFeNiTix HEAs structure, the initial solidification temperature in the structure also changed. It is seen that the ordered BCC phase, which first solidified from the liquid in the Ti0.0 alloy structure, solidified at approximately 1375°C. Due to this situation, it was observed that the first solidified sequential BCC phase from the liquid was formed at approximately 1255°C with the increase of titanium. It was determined that the solidification temperature decreased with the addition of titanium to the structure. In the study of Ferrari et al., it was observed that similar regular and irregular BCC phases were formed in the microstructure when AlCoCrFeNiTix x=0.0 (Ferrari et al., 2019). In addition, it was observed that some additional phases (Laves and Heusler) were formed with the titanium element included in the structure. The compositions of the formed phases changed with the increase in Ti content at stable temperature ranges. The compositions of the formed phases changed with the increase in Ti content at stable temperature ranges. Two B2 phases (B2#2 and B2#4) solidified from liquid were obtained in Ti1.0, which contains the most titanium element in the alloy series. The Ti contents of these phases were determined to be approximately from 12.90 mol% to 3.39×10^{-3} mol%. Ti1.0 alloy is developed two ordered BCC (B2) , two disordered BCC phases during equilibrium solidification. According to CALPHAD software, the Al-Co-Ni-Ti-based B2#2 phase forms around 1306°C. When the temperature was at 1187°C, the disordered B2 phase (Cr-based) was formed. At about 544°C, the disordered B2#3 phase (Fe-based) was formed. In Figure 4.1, the sums of phases with the same crystallographic structure but different composition ratios are given under equilibrium cooling conditions.

Since the cooling behavior of the alloy produced in the VAM process could not be controlled, the alloys showed a behavior of cooling under non-equilibrium conditions. Especially in metals and alloys produced by melting, the cooling behavior of the material determines the state of the phases that will occur in the structure. With this point of view, Scheil Solidification Simulations are used to identify possible formations of phases and non-equilibrium transformations. The phase diagram obtained according to the result of the Scheil Solidification module in Termo-Calc software is given in Figure 4.2. Utilizing the Scheil Calculator, the microstructure, solidification range, and segregation degree of a material may be determined more precisely. Guan et al. used Scheil's solidification simulation to analyze the AlCoCrFeNiTi0.5 high entropy alloy in detail. They determined the phases to be obtained as a result of this solidification(Guan et al., 2019).

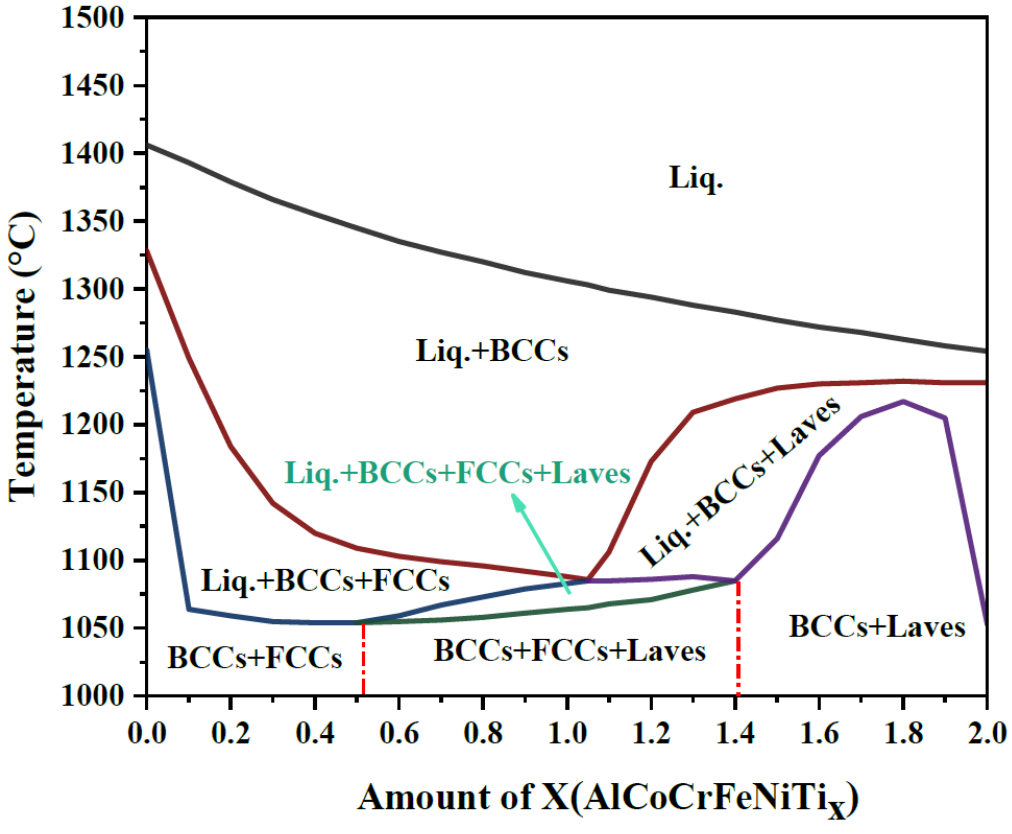

Figure 4.2 Phase diagram of AlCoCrFeNiTi$_X$ high-entropy alloy formed according to Scheil Solidification Simulations under non-eqilibrium conditions

The phases shown in figure 4.2 above are as follows: BCC phases describe a mixture of ordered BCC (B2) and disordered BCC phases with different compositions. The FCC phase structure is described by the different compositions of the disordered FCC and ordered FCC ($L1_2$) phases. According to phase diagram of $AlCoCrFeNiTi_X$ HEAs, the temperature at which solidification begins declines with increasing titanium content. When the titanium content is above approximately 0.50, the Laves phase occurs in the structure during solidification. The Laves phase has two different structures. One of these structures is C14 (hexagonal structure), and the other is C15 (cubic structure). According to Scheil Solidification Simulations, the C15 Laves phase in the structure indicates that it is formed the titanium content is above 0.50. The C14 Laves phase, on the other hand, states it is formed when the titanium content is above 1.21. As for investigating the phase diagram, eutectic transformation can occur during non-equilibrium cooling. Eutectic transformation occurs at the point where the temperature is approximately 1085 °C and the titanium content is 1.05. This reaction is defined as Liquid = FCCs+Laves. This is the first phase diagram of $AlCoCrFeNiTi_X$ high entropy alloys in the literature, created by Scheil Solidification simulation under non-equilibrium conditions. Thanks to this created phase diagram, the phases formed in the structure were predicted. In addition, by looking at the phases formed by the produced alloy between 1000°C and 1450°C, it is estimated that these alloys can be used in the aviation industry (high temperature applications, etc.).

4.2 Arc Melting Result of $AlCoCrFeNiTi_X$ HEAs

4.2.1 XRD Results

In Figure 4.8, the phases formed in the $AlCoCrFeNiTi_X$ alloy system were determined by X-ray diffraction. 5 phases have been determined in this alloy series. These are as follows: ordered BCC (B2), disordered BCC (BCC), disordered FCC (FCC) phases, Sigma phases, and Laves phases. It has been observed that Ti0.0 alloy consists of ordered BCC (B2) phase. The highest intensity (main peak) formed in this alloy system is between about 43.15° and 45.15°.With the increase of titanium content in the alloy structure, phases have increased. In solid solutions, the peaks move as the elements and the amount of mass they make up a change.

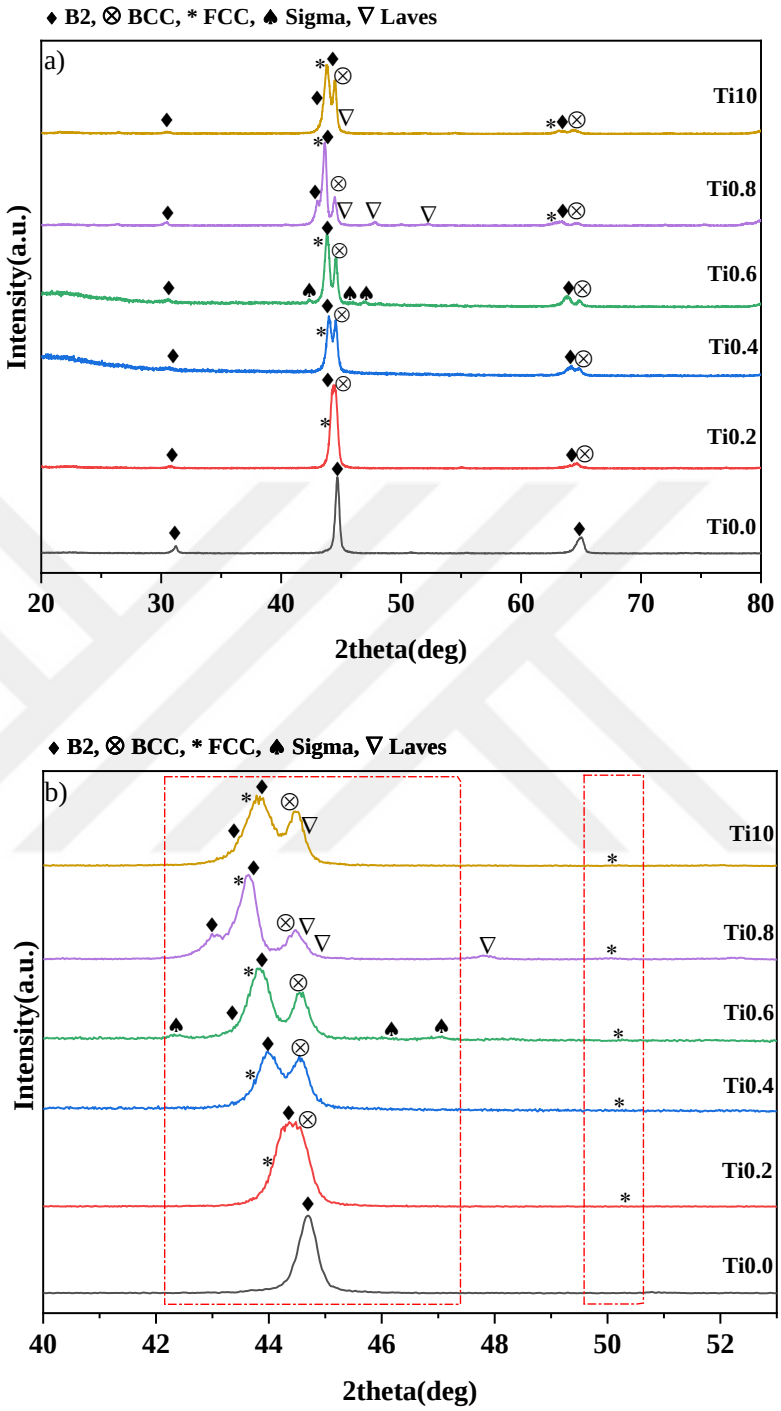

Figure 4.3 XRD analysis of as-cast AlCoCrFeNiTi$_X$-based HEAs: a) full scan, b) magnified sections

To determine the existence of ordered BCC (B2), disordered BCC (BCC), and disordered FCC (FCC) phases, diffraction points from certain angles and planes have analyzed rather than the peak with the maximum intensity. The existence of phase B2

is indicated by the peak {100} at about 31.02°, whereas the FCC phase is indicated by the peak {200} at approximately 51.03°. Additionally, the space groups of the chosen patterns were utilized to demonstrate the probable phases. The patterns in the $Pm\bar{3}m$, $Im\bar{3}m$, and $Fm\bar{3}m$ space groups were accepted to be the B2, BCC, and FCC phases, respectively. The space groups of the phases formed in this alloy system were also determined as $Pm\bar{3}m$ (B2 phase), $Im\bar{3}m$(BCC phase), and $Fm\bar{3}m$ (FCC phase). As shown in Figure 4.3, the peaks of the phases (particularly the B2 phase) generated as the titanium concentration of the alloy increased shifted towards lower angles.

The reason for these shifts in the XRD peaks is that the titanium content has a larger atomic radius than the other elements involved in the solid solution phases. While the atomic radii of elements other than titanium are (1.241×10^{-10} – 1.432×10^{-10} m), the atomic radius of the element titanium is (2.150×10^{-10} m). This situation causes the lattice to be distorted and the lattice structure to deteriorate(H. L. Chen, Mao, & Chen, 2018). When examined in Figure 4.3.b, the highest peak of the B2 phase {110} in the alloy shifted towards lower angles (from 44.67° to 43.63°) with the increase of titanium content. This has been observed in several studies(Dong et al., 2014; Ham et al., 2021; Yu et al., 2020).

The intermetallic Laves phase, which was seen to be formed by AB_2 stoichiometry, was also detected in Ti0.8 and Ti1.0 HEA. The Laves phase principally comprises the elements Fe, Ti, and Co. It was also observed that the B2 phase shifted towards a higher angle in the Ti1.0 alloy. This situation occurred with the increase in the amount of Laves phase formed in the structure. The Laves phases might form in non-equilibrium circumstances when the stoichiometric quantity of titanium is more than 0.5, as seen in Fig. 4.3. Yet, Laves phase was not observed in the Ti0.6 HEA, in Figure 4.3. It is considered that this event arises due to the comparatively little quantity of Laves phase generated in the structure compared to the other phases.

FCC phases in the alloy structure are also formed during non-equilibrium cooling (Fig. 4.2), even in the alloy series containing low titanium (Ti0.2). This phase in the alloy is also consistent with the XRD result (Fig 4.3).

As for all series of alloys examined, it was determined by XRD analysis that the Sigma phase was formed only in Ti0.6 alloy. When the studies in the literature are examined, the formation of the sigma phase in the structure of the alloy is explained with certain parameters(Tsai, Chang, Li, Tsai, & Cheng, 2015; X. J. Wang, Xu, Liu, & Liu, 2021). These parameters are paired sigma phase forming elements (PSFE) and valence electron concentration (VEC) that make up the alloy. These 2 parameters of the alloy can divide the high entropy alloy into 3 different groups. In Ti0.6 alloy, these parameters (VEC and PSFE values) were determined as 6.861% and 35.72%. These values indicate that there is a possibility of the formation of the Sigma phase in the alloy. It is also seen in Figure 4.2 that sigma phase can be seen during solidification under balanced cooling conditions. In line with these analyses, the formation of the Sigma phase can be explained as follows. It is the phase transformation of some of the first B2 and BCC mixture phases formed during the solidification of the alloy. With the phase transformation, FCC and sigma mixed phases were formed in the structure.

4.2.2 SEM/EDS Results

The microstructure of the Ti0.0 alloy is compatible with the XRD analysis. A single-phase microstructure image was obtained. The only phase in the alloy is the B2 phase (in Figure 4.3). Zhou et al. also obtained similar microstructure images in their study(Y. J. Zhou, Zhang, Wang, & Chen, 2007). With the increase of titanium content in the $AlCoCrFeNiTi_X$ alloy system, new phase morphologies were formed in the structure. The phase formations obtained by the XRD result are also supported by the SEM analysis.

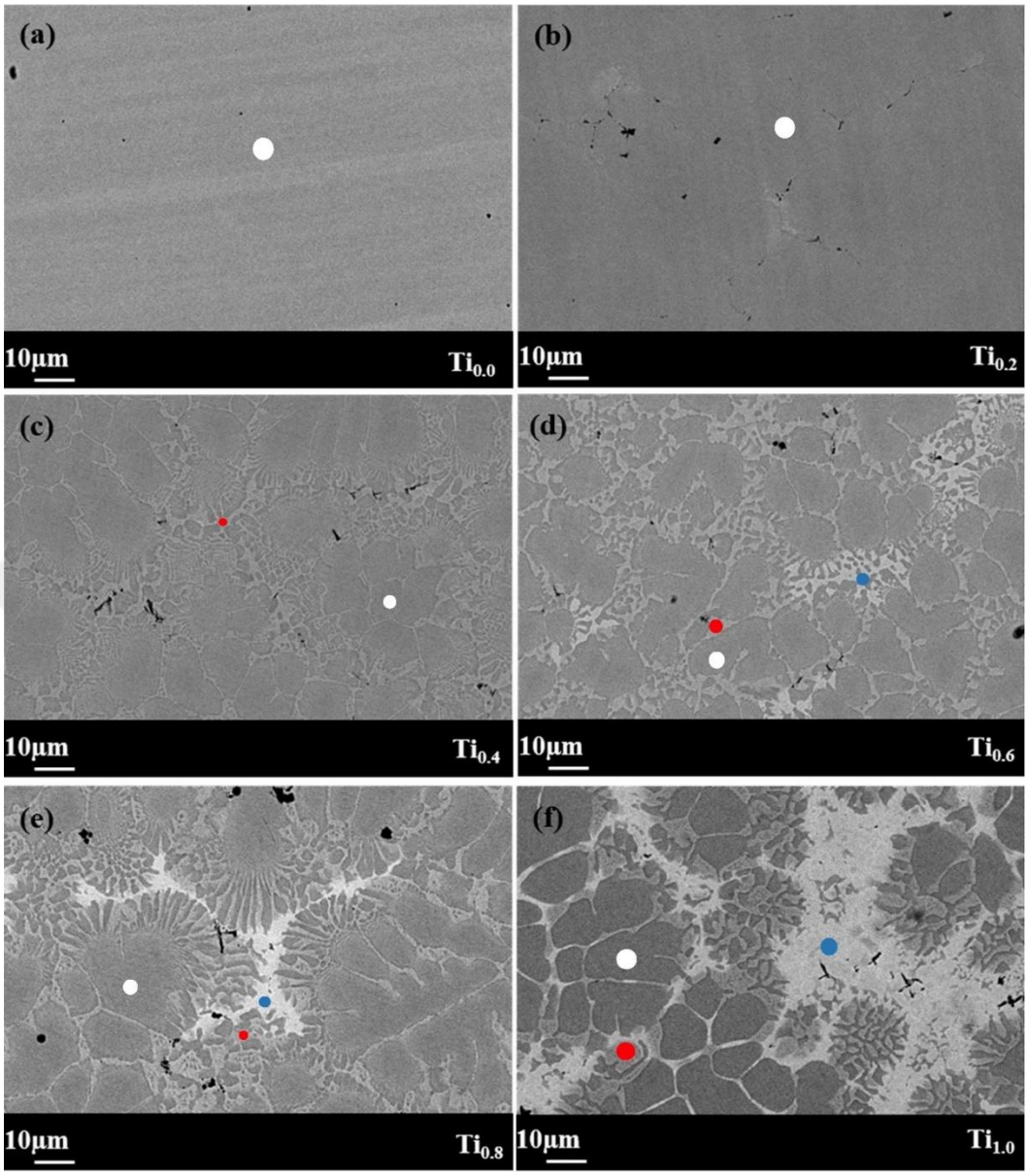

Figure 4.4 SEM micrographs of as-cast AlCoCrFeNiTi_X based HEAs where (a) X = 0.0, (b) X = 0.2, (c) X = 0.4, (d) X = 0.6, (e) X = 0.8, and (f) X = 1.0

In the Figure 4.4 above, it is seen that eutectic-like structures are formed in all of the other series, except for Ti0.0 and Ti0.2 alloys. The phase diagram in Figure 4.2 shows that eutectic transformations occur in Ti0.6, Ti0.8, and Ti1.0 alloys with titanium content between about 0.51 and 1.40. Scheil Solidification Simulation was used to investigate why a eutectic-like microstructure was detected (Fig. 4.c) in the microstructure of HEA at X=0.4, which is outside of these constraints. The titanium element chosen as the fast diffuser showed that the Laves and FCC phases in the structure consisted of the liquid phase at a temperature of about 1057 °C. In the

literature review, Chen et al. stated that the titanium element has a lower diffusion coefficient from the Al-Co-Cr-Fe-Ni based high entropy alloy than the other elements. This is in line with our analysis. Therefore, titanium elements cannot act as a fast diffuser in AlCoCrFeNi based high entropy alloy systems. In other words, the titanium element does not show rapid solidification in the structure(S. Chen, Li, Zhong, Xing, & Zhang, 2019). According to Scheil solidification calculation in the casting method, it was observed that there are several different reasons why the elements forming the alloy form different phases. The reasons for this differentiation are the formation of back diffusion in solid phases, diffusion not fast enough in liquid structure, and the absence of probable phases due to the high nucleation energy of the structure. It has also been described in the literature in this way(H. L. Chen et al., 2018). So to better comprehend the distribution of components in the structure of Al-Co-Cr-Fe-Ni-Ti-based high entropy alloys, X-ray mapping analysis using the EDS method at various magnifications was done.

As seen in the EDS analysis in Figure 4.5, the microstructure differentiation has occurred by the addition of the titanium element to the structure. This differentiation also proves that new phases are formed in the structure. When the distribution of all elements is examined in detail here, dendritic structures have been obtained in the microstructure starting from the Ti0.4 alloy in Figure 4.5.c. After the alloys were produced by arc melting, dendritic formations occurred in the morphology of the alloy due to the solidification behavior. This behavior is compatible to microstructures in the study of Ham et al (Ham et al., 2021). Likewise, Löbel et al. obtained similar dendritic microstructures (Löbel, Lindner, Mehner, & Lampke, 2018). This situation is completely related to the solidification behavior of the elements that make up the alloy. In the arc melting method, this solidification behavior cannot be controlled. Due to fast or slow solidification, inhomogeneous dendritic structures were obtained in the structure of the alloy. The phase composition calculated under the equilibrium and non-equilibrium cooling conditions obtained with Thermo-Calc software is given to compare the EDS results. As an example, different regions have been selected in the Ti1.0 alloy. These regions are shown in figure 4.4.f with dots of different colors. The EDS data of the first phase (white dot) involved in the structure of the alloy was similar

to the ordered+ disordered mixture composition analyzed with the Scheil module in Thermo-Calc software. The light-colored region in this microstructure image is the BCC + B2 mixture phase. Scheil's modulus, shows that phase transformation can occur at about 1210°C of the alloy. At this temperature, peritectic transformation can occur (BCC_B2+Liquid = BCC_B2#2). The compositions of the BCC phases at this point differ from each other. The structure is composed of both an ordered and a disordered structure. During the peritectic transformation, according to Scheil calculator, it was determined that the amount of Al-Ni in the content of the newly formed BCC_B2#2 phase would decrease. However, it was determined that the amount of Cr-Fe in the alloy would increase. The differences in the amount of Al-Ni and Cr-Fe in the structure of the alloy were determined by the EDS result of the 2 different regions seen in Figure 4.4.f. When these regions were examined in detail, the phase in the red dotted region was estimated to be the BCC_B2#2 phase.

According to Scheil calculator, Ti1.0 alloy performs eutectic phase transformation at 1086°C. The theoretically calculated composition of the alloy at this temperature is 1.23 at.% Al, 29.06 at.% Co, 19.16 at.% Cr, 27.81 at.% Fe, 6.83 at.% Ni, and 15.52 at.% Ti. EDS analysis of the eutectic region (blue point) was measured 1.87 at.% Al, 13.62 at.% Co, 27.28 at.% Cr, 30.62% at.% Fe, 9.87 at.% Ni, and 14.96 at.% Ti.

According to the results of the EDS analysis, light-colored dendritic regions and dark-colored block regions were demonstrated in Ti0.0 alloy. The dendritic structures in the alloy indicate a eutectic solidification that occurs during the casting process. The same microstructure images were obtained in many studies in the literature (L. Ma et al., 2017; W. R. Wang et al., 2012; S. cheng Zhou et al., 2018). It is seen that Co-Cr-Fe elements are clear in the light-colored region. Other region Al-Ni elements are obvious. In Ti0.2 alloy, thin shiny dendrites and very dark regions are seen. Titanium element added to the content of the alloy is seen as accumulated in the very dark region. In addition, in the region of thin dendrites in the alloy, Cr-Co and Fe elements are more dominant. Dark phase precipitates dispersed in brighter coarse columnar grains were observed in Ti0.4 alloy. Dark phase sediments are regions rich in Al-Co-Ni-Ti. Coarse columnar grains show the region rich in Cr-Fe. With the increase in titanium content,

the distribution of titanium started to show a homogeneous behavior. In Ti1.0 alloy, with the increase of titanium content, light-colored region, dark colored region, and medium dark (grey) region were observed in the microstructure. It can be stated that elements precipitated in the inner part of the medium-dark region. It has been understood that more advanced characterization techniques should be used to analyze the amount and crystal structure of these precipitated elements. These techniques have not been realized at this stage.

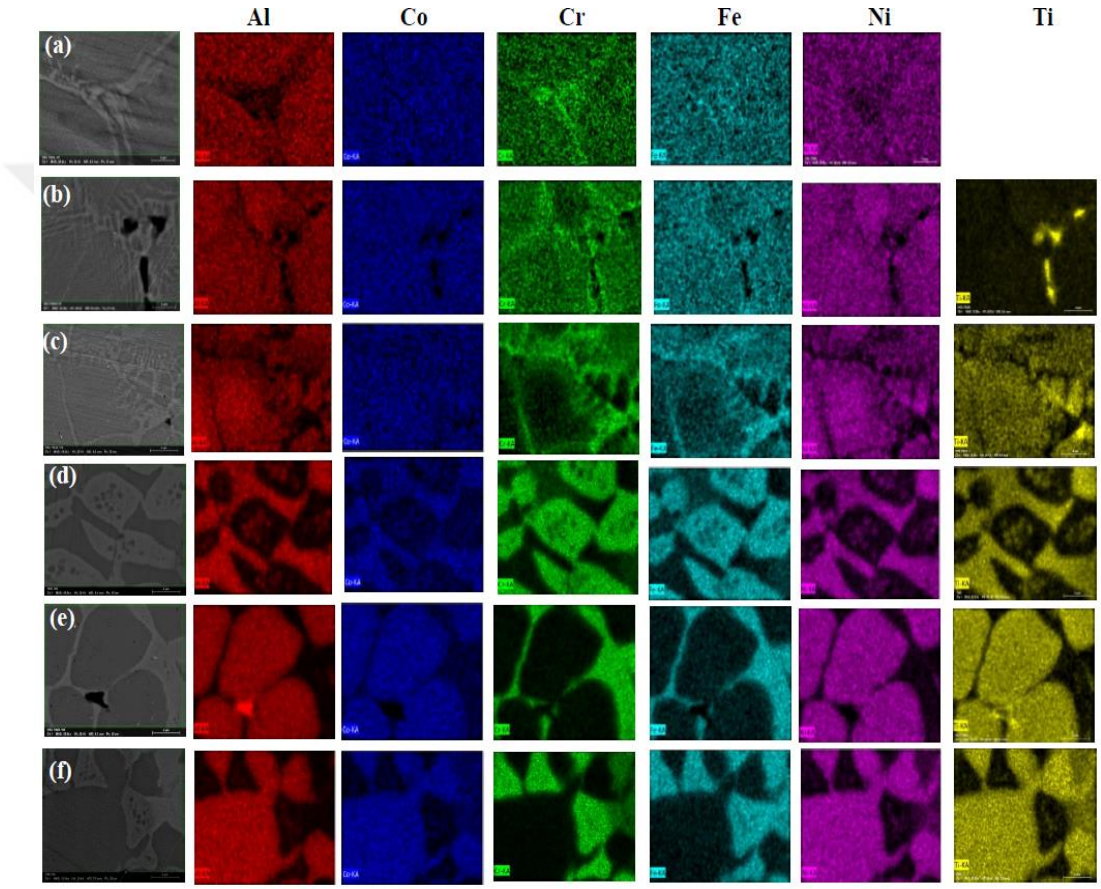

Figure 4.5 Image depicting the microstructure and phase compositions of the AlCoCrFeNiTix alloy as recognized via EDS a)Ti0.0, b) Ti0.2, c) Ti0.4, d) Ti0.6, e) Ti0.8, and f) Ti1.0 magnification 15.00Kx

4.2.3 DTA Results

DTA analysis was performed to predict the melting point of the alloy and the reactions that would occur. As seen in Figure 4.6, a significant endothermic peak formation was observed in the Ti0.0 alloy at a temperature of about 620°C. This peak may indicate that there is melting in the structure of the alloy at this temperature and

that a new phase formation begins. It has been observed that a small amount of melting will occur in the structure of the alloy up to about 1200°C. Similarly, melting points were determined by DTA analysis in the study of Liu et al(Y. Liu et al., 2020).

When examined Fig. 4.6, Fig. 4.7, and Fig.4.8, there are distinct endothermic peaks for each curve. These peaks represent the initial melting points of AlCoCrFeNiTi based HEAs. With the increase of titanium content in this alloy series, the melting point of the alloy reached higher temperatures. While its initial point was 620°C, it reached approximately 914°C with the addition of titanium. This is theoretically due to the high melting point of the titanium element. A temperature range for the transformation of the phases formed in the structure can be determined by looking at these graphs.

In the study of Fan et al., Ag element added to $BiSbTe_{1.5}Se_{1.5}$ HEAs had the opposite effect(Fan, Wang, Wu, Liu, & Lu, 2016). It lowered the melting point. Based on this situation, the melting points of the elements that make up the alloy are highly important. By looking at the result of the DTA analysis, the heat treatment parameters to be applied to the alloy were determined. The critical temperatures were determined by looking at the endothermic peaks. In this case, heat treatment was carried out to determine the phase transformations in the structure and the different microstructures that will occur. According to the endothermic peaks in the DTA graph, the heat treatment temperatures were determined as 500°C, 750°C, and 1000°C. Here, the lower, intermediate, and upper parts of the peaks at approximately 600 °C and 900 °C were examined. Wang et al. also applied heat treatment at the same temperatures using a similar alloy series(Y. Wang et al., 2013).

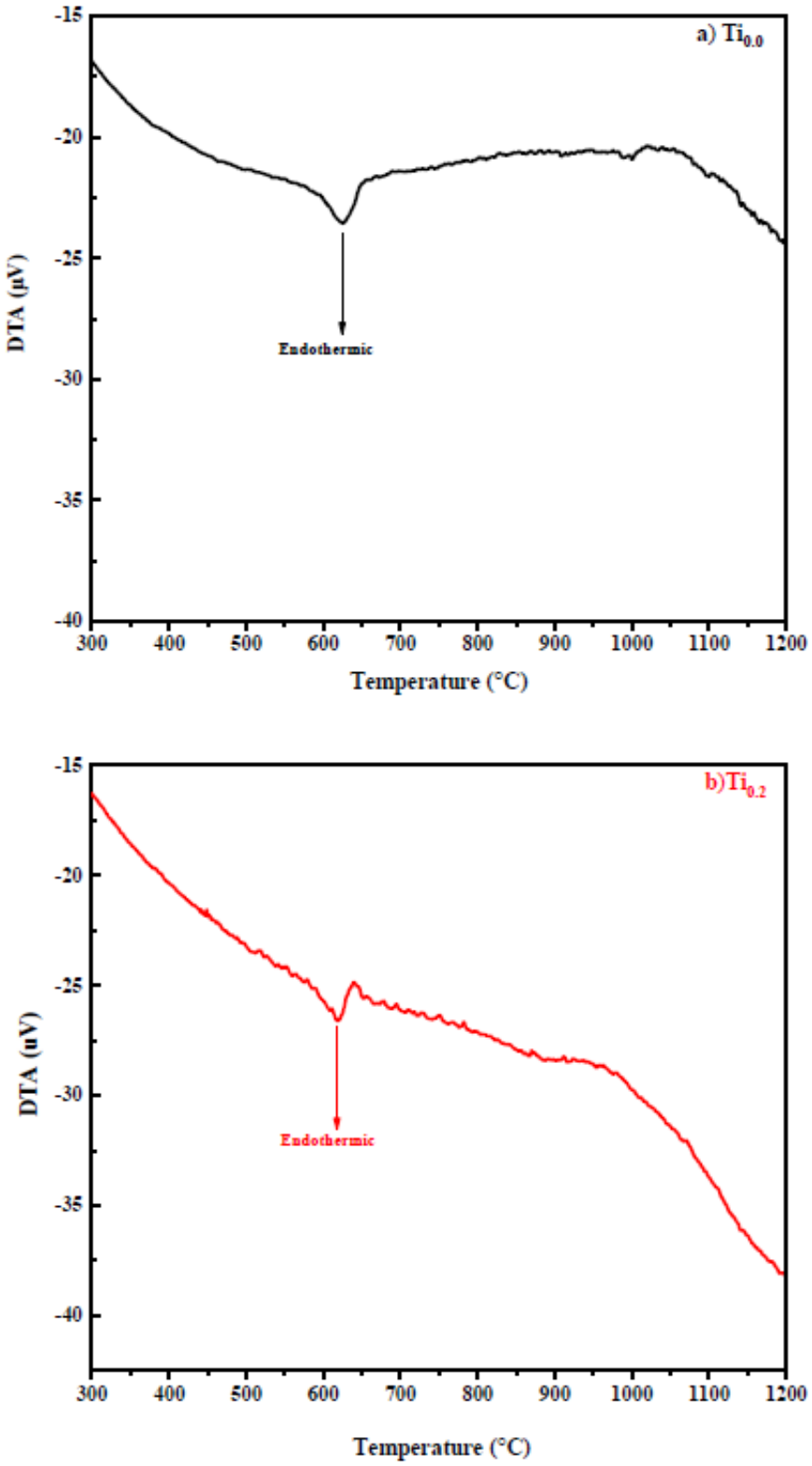

Figure 4.6 Differential thermal analysis (DTA) curves a)Ti0.0 and b)Ti0.2 based HEAs

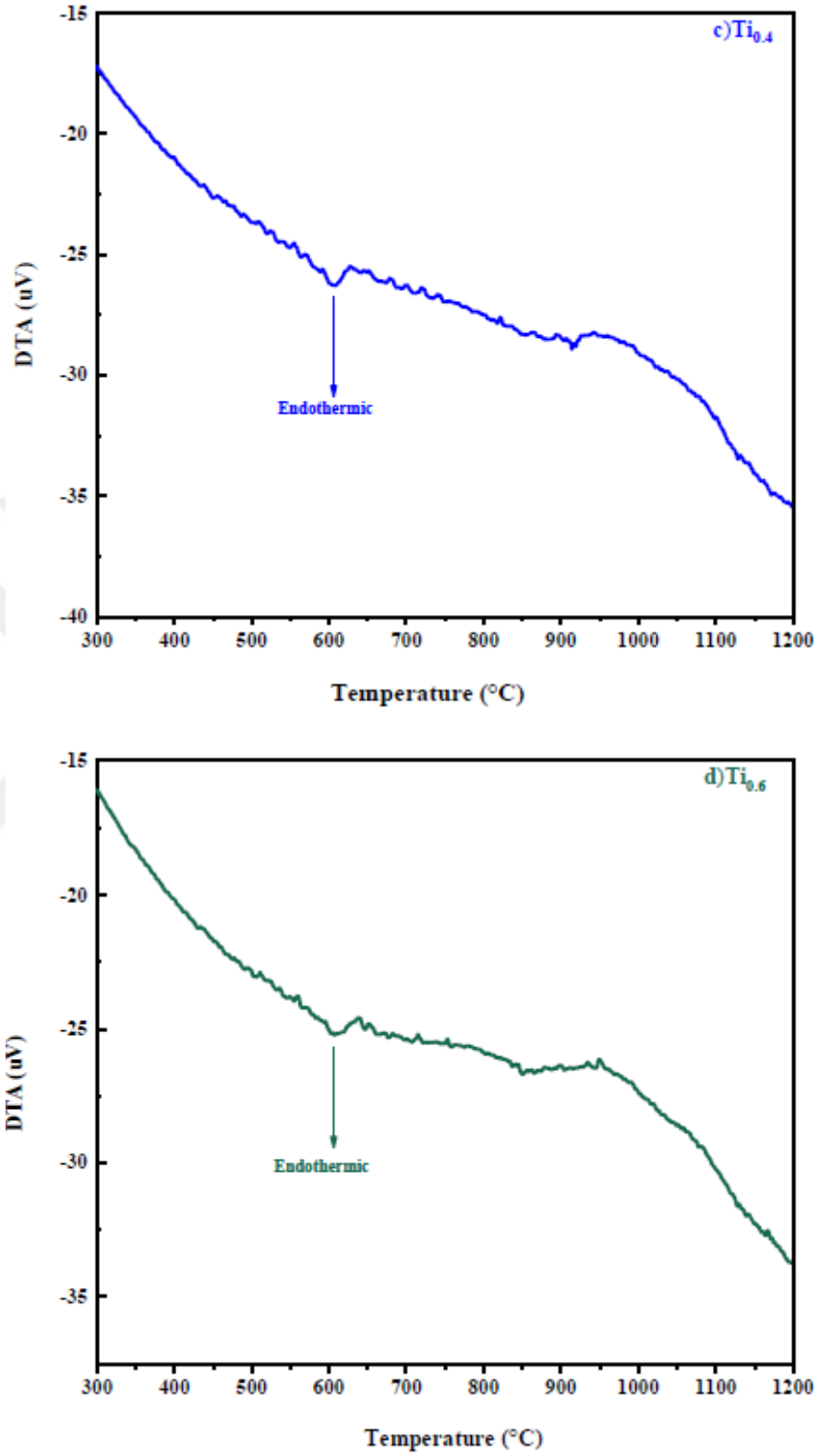

Figure 4.7 Differential thermal analysis (DTA) curves c)Ti0.4 and d)Ti0.6 based HEAs

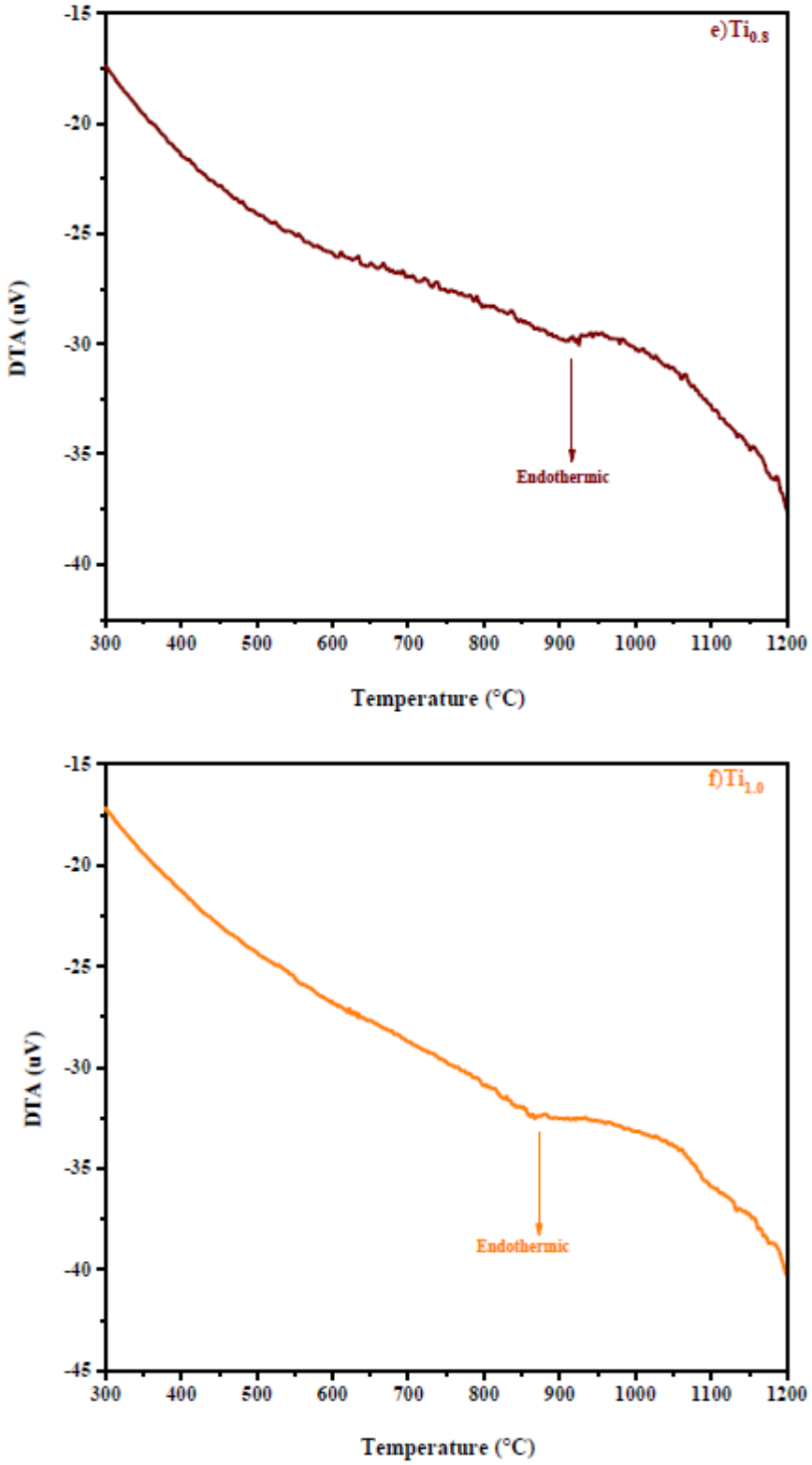

Figure 4.8 Differential thermal analysis (DTA) curves e)Ti0.8 and f)Ti1.0 based HEAs

4.2.4 Hardness Results

In Figure 4.9, 0.2 kg load was applied to the surfaces of AlCoCrFeNiTix high entropy alloys prepared after metallographic processes for about 10 seconds. Regions with different microstructures (as light and dark regions) in the alloy system were analyzed separately. Approximately 12 measurements were taken from each region. In line with the result obtained, the mean and standard deviation of 12 measurements were calculated.

It was seen in both XRD and SEM analyzes that Ti0.0 alloy has single-phase ordered BCC (B2) phase. During the hardness analysis, measurements were taken from the alloy with a single-phase microstructure image. As a result of the measurements, the average hardness value of the alloy was calculated as 519 ±4 HV. With the addition of titanium element to the alloy system, the hardness value of the alloy increased. In the study of Wang et al., it was observed that the number of phases increased with the increase of aluminum content in AlxCoCrFeNi based HEAs. Similarly, the hardness value of the alloy increased after casting(W. R. Wang et al., 2012). In the high entropy study of AlCoCrFeNi produced by Zheng et al. produced by laser melting deposition method, AlCoCrFeNi HEAs was observed hardness value as approximately 548HV at a load of 0.3 kilograms(J. Zhao et al., 2022).

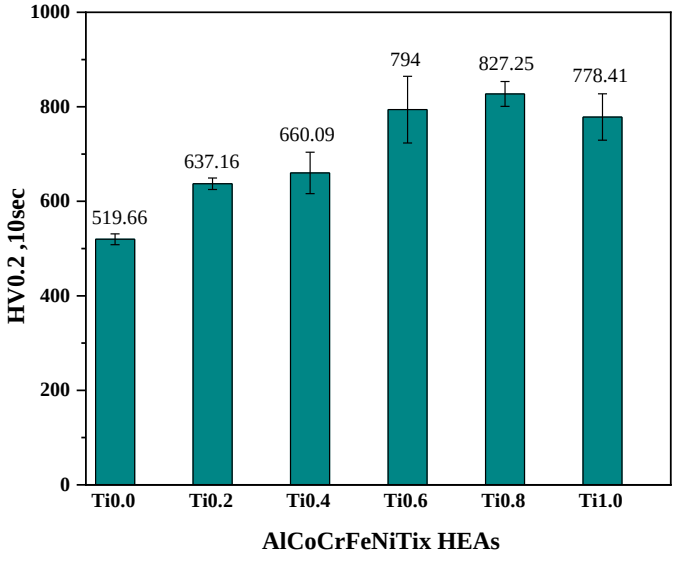

Figure 4.9 The microhardness values of AlCoCrFeNiTix HEAs

In particular, the hardness value reached 794±38 HV. HV with the formation of the Sigma phase in addition to the B2, BCC, FCC phases in the Ti0.6 alloy. In Ti0.8 alloy, on the other hand, the hardness value due to the formation of Laves phase(C15) in the structure and the phases in the alloy reached the highest value of 827±15 HV.

In the Ti1.0 alloy, the hardness value decreased to 778 ±22 HV, due to forming a different type of Laves phase (C14). This phase structures compare with the Scheil solidification modulus in Figure 4.2. With the increase of titanium content from 0.8 to 1.0, the C15 laves structure formed in the alloy turned into C14 laves. C14 laves phase contains less titanium composition. In Table 4.2, hardness results from different parts of all alloy series are given. It was observed that the hardness increased with the effect of eutectic-like structures and different phases formed from Ti0.4.

Table 4.1 Microhardness values of AlCoCrFeNiTix HEAs from different phase regions (Area 1:Dark area, and Area 2: bright area)

Sample	Area 1	Area 2
Ti0.0	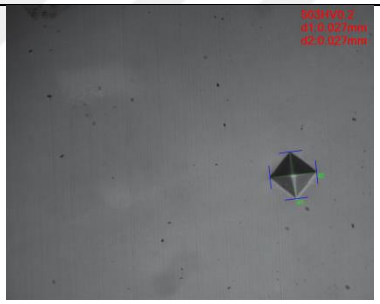	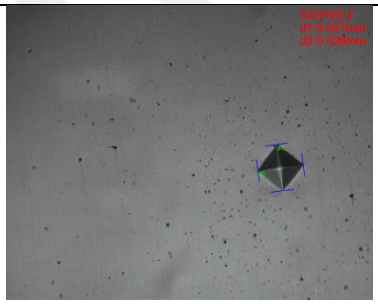
Ti0.2	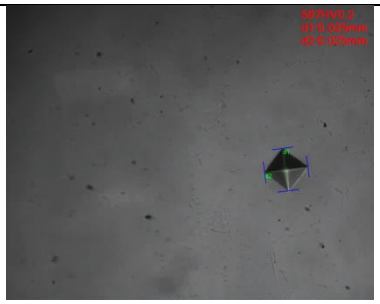	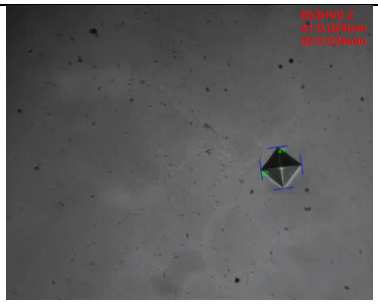

Table 4. 1 Contiunes

Ti0.4	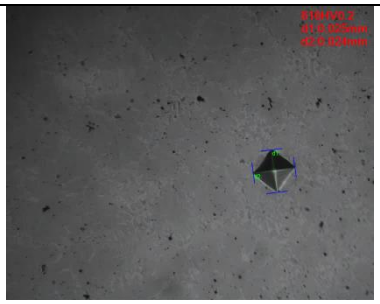	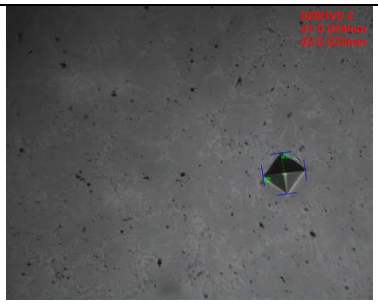
Ti0.6	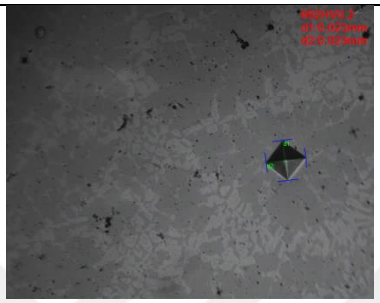	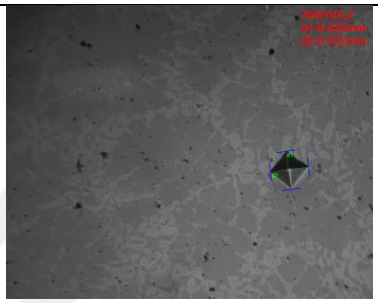
Ti0.8	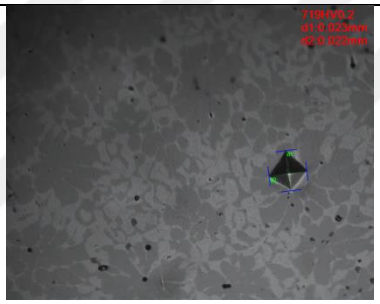	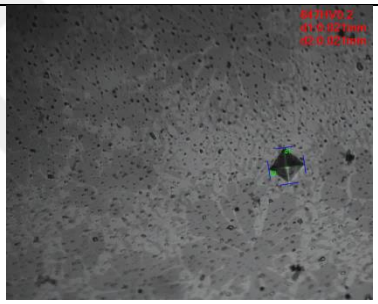
Ti1.0	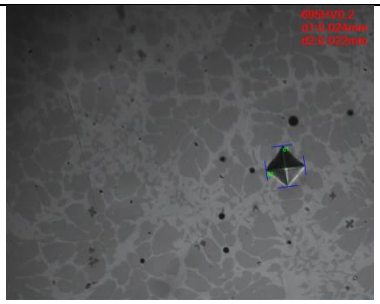	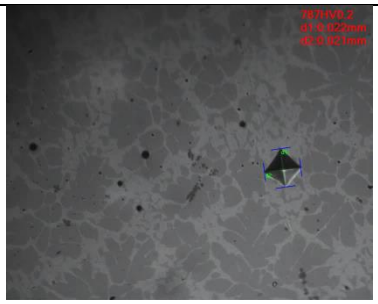

4.3 Heat Treatment Result of AlCoCrFeNiTi$_x$ HEAs

4.3.1 XRD Results

Heat treatment was applied to Ti0.0, Ti0.2 and Ti1.0 high entropy alloys at temperatures determined as a result of DTA analysis (500°C, 750°C and 1000°C). After the heat treatment, the phases in the structure were determined by XRD analysis (In Fig.4.10). According to the Ti0.0 casting alloy, no phase transformation occurred in the water cooling process after the heat treatment at 500°C. Only the B2 phase was seen in Ti0.0 alloy structure. After the heat treatment at 750°C, as a result of the phase transformation in the water cooling process, besides the B2 phase, FCC and Sigma phases were formed. Sigma phase disappeared from the structure in the process at 1000°C as a result of further increasing the temperature. Only the B2 and FCC phases were obtained. Likewise, B2 and FCC phases were obtained at similar angles in the sample, which was cooled in the furnace atmosphere after the heat treatment at 1000°C. In this study, the phase transformations that occur after the heat treatment processes in the Ti0.0 alloy are similar to the results of other studies (He et al., 2014; C. Li, Li, Zhao, & Jiang, 2010; Sistla, Newkirk, & Frank Liou, 2015; J. Zhao et al., 2022).

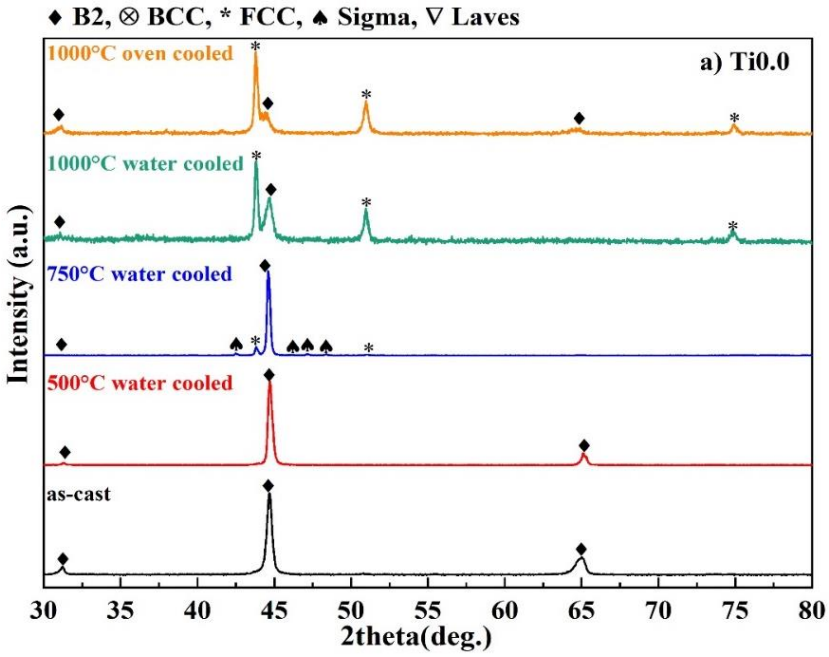

Figure 4.10 The XRD patterns of as-heat treated a)Ti0.0-based HEA

When Figure 4.11 is examined, the same phases obtained from casting resulting from the heat treatment carried out at 500°C in the Ti0.2 alloy are seen. Different stages did not occur. However, it was observed that the Sigma phase was formed in the structure of the alloy as a result of heat treatment at 750°C. The formation of the Sigma phase in the Ti0.2 alloy at this temperature is supported by DTA analysis. In DTA analysis, it can be expressed by the formation of distinct endothermic and exothermic peaks in the Ti0.2 alloy at a temperature of about 620°C to 1000°C. In the heat treatment procedure carried out at 1000°C, it was determined that there were similar phases under different cooling conditions. (B2, BCC, FCC and Sigma phase).

As for Ti1.0 alloy, as a result of XRD obtained after casting, B2, FCC, BCC, and Laves phases in the structure of the alloy were determined. However, as a result of the heat treatment at 500°C, it was determined that there was no Laves phase in the structure. It can be said that a phase transformation takes place at this temperature. If it is evaluated according to the heat treatment of Ti0.0 alloy at 500°C, BCC and FCC phases were formed in the structure with the increase in titanium content. Similar phases were formed at 750°C as in the other alloy series. When the temperature reaches 1000°C, the sigma phase in the structure disappears, instead, there are only B2, BCC, FCC phases.

In order to observe these phase differences resulting from heat treatment in more detail, SEM-EDS analysis was performed on these 3 selected alloys. The resulting microstructures are shown in detail under 4.3.2 SEM results.

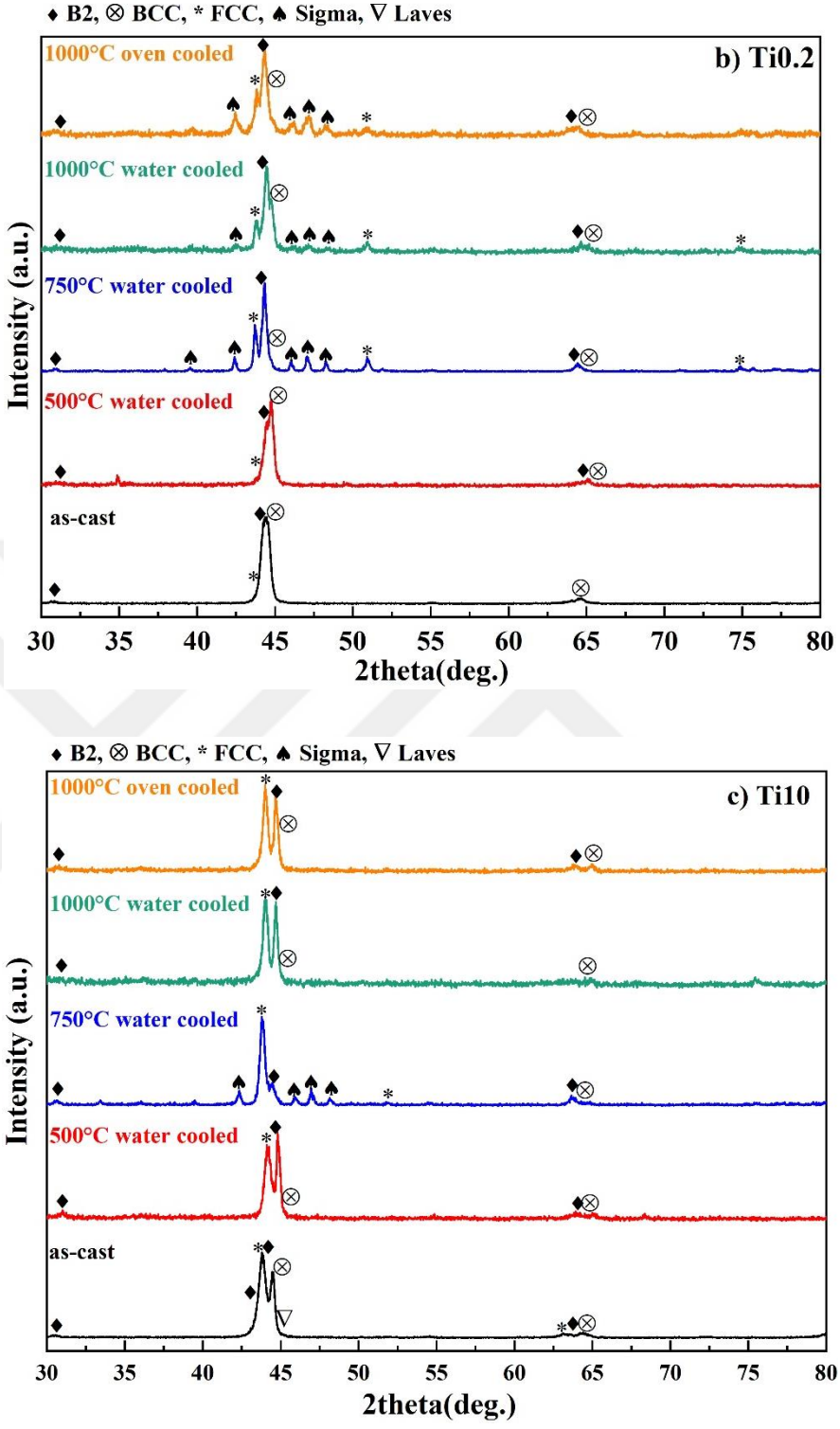

Figure 4.11 The XRD patterns of as-heat treated b)Ti0.2, and c)Ti1.0-based HEA

4.3.2 SEM Results

Microstructure images formed as a result of heat treatment are shown in Figure 4.12. Compared to the post-cast condition (Fig. 4.4), changes in the microstructure could be noticed. In the Ti0.0 alloy, differentiation occurred from 750°C. This was also seen when the XRD analysis after heat treatment was examined. As a result of XRD, it was determined that Sigma and FCC phases were formed in addition to the B2 phase in the structure. When the heat treatment temperature reaches 1000°C, it is seen that the coarse columnar bright grains in the microstructure turn into a more regular structure.

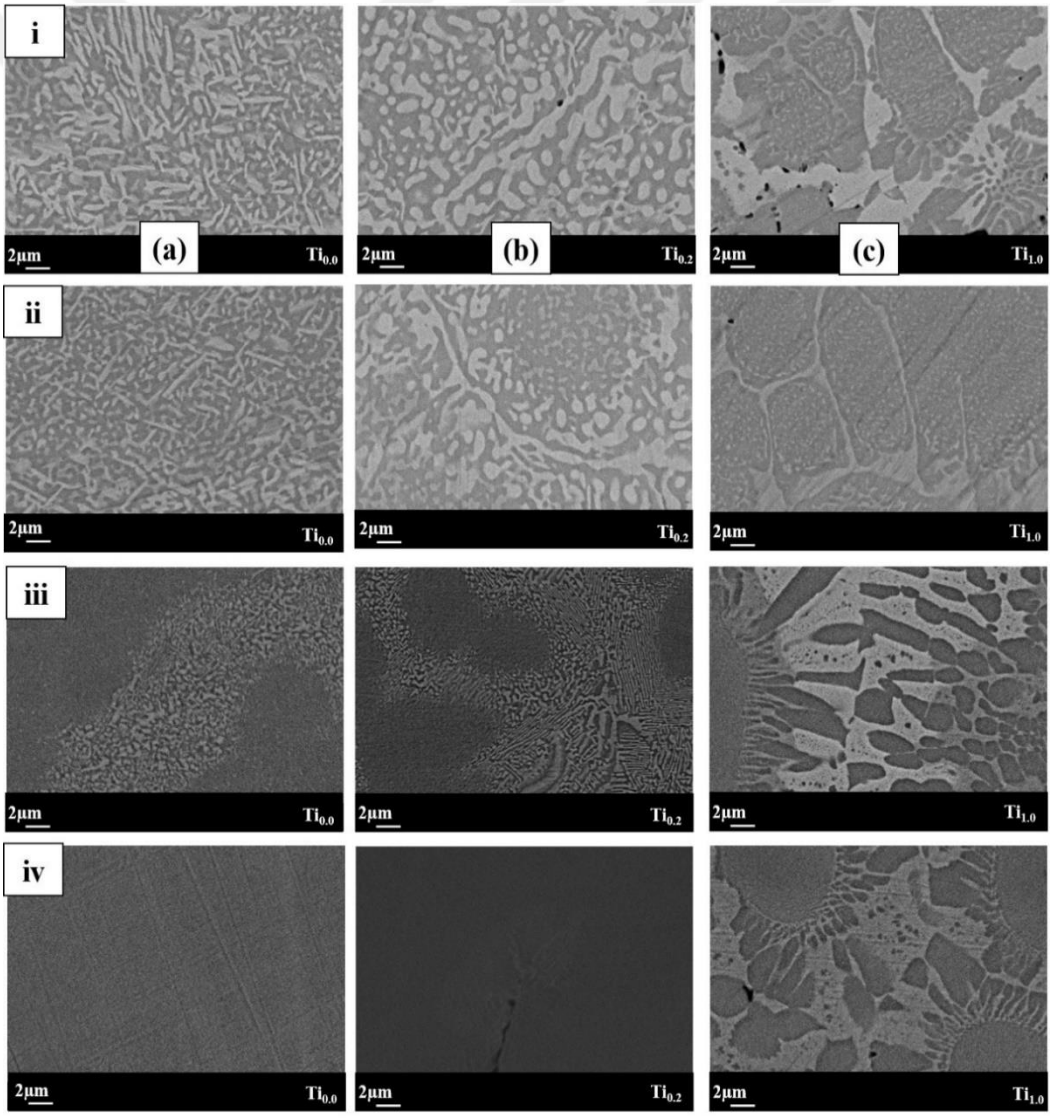

Figure 4.12 The SEM micrographs of as-heat treated Ti0.0, Ti0.2, and Ti1.0-based HEA

When the Ti0.2 alloy is examined in the figure above (Fig4.12.b), dendritic bright regions formed in the structure with increased heat treatment temperature. It is known that the effect of the Sigma phase, which is also seen as a result of XRD, is in these regions. Similar microstructures were obtained from cooling both in water and in the oven at 1000°C. It is estimated that the formed phases have a more homogeneous distribution. Similar microstructure images were obtained as a result of heat treatment in a study by Cheng et al(L. Chen et al., 2018).

In the Ti1.0 alloy, on the other hand, the effect of sigma and laves phases formed by the increase in titanium content is observed. It is known that this situation coincides with the XRD result. Some sediments were observed inside the coarse dendritic structures, which are light in color. It is observed that the Laves phase transforms into a different phase at 500°C, thus increasing the dark columnar regions in the structure. It was observed that the light-colored dendritic regions increased in volume after cooling in water at 750°C. As a result of cooling in the oven at 1000°C, it is seen that the dendritic regions decrease, and the structure exhibits a homogeneous distribution.

When all alloy series were evaluated, it was determined that the phase in the bright (light color) region formed in all microstructure images as a result of the heat treatment performed with water cooling at 750°C was the sigma phase. In the EDS analysis, the compositions of these bright regions were found to be close to the theoretical composition of the Sigma phases seen under equilibrium conditions. For instance, the chemical composition of the bright (light colored) region at 750 °C in the Ti0.0 alloy after heat treatment was measured by EDS analysis as 9.41% Co, 44.76% Cr, and 37.85% Fe. The average of the theoretical composition of the Sigma phase obtained under equilibrium cooling conditions using the Thermo-Calc software is 5.75% Co, 53.46% Cr, and 40.24% Fe.

4.3.3 DSC Results

DSC analysis was performed to determine the thermal stability of AlCoCrFeNiTix high entropy alloys. So as to determine the thermal stability of AlCoCrFeNiTix high entropy alloys and the transformations in the structure, DSC analysis was performed on the samples. The endothermic peaks at the transformation points of the alloys that were heated up to approximately 1000°C and cooled were determined. Microstructure images obtained from SEM analysis were added to the graph to understand these transformation points more easily.

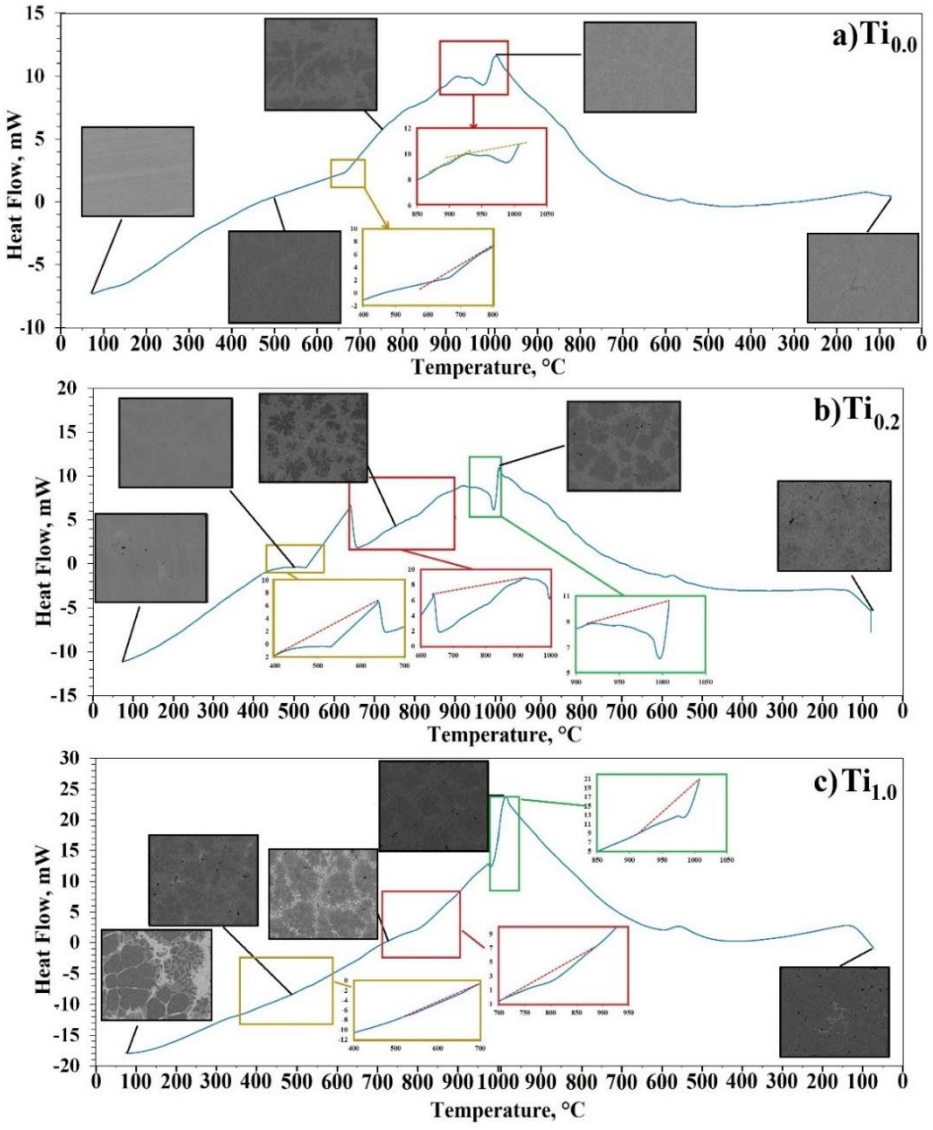

Figure 4.13 DSC curve of Ti0.0, Ti0.2, and Ti1.0-based HEAs

In the Ti0.0 alloy, the DSC curve 1 (Fig4.13.a) exhibits two major endothermic peaks around 680°C and 980°C. The endothermic peak at 680°C corresponds to Al melting (Tm = 660°C), while the second peak at 980°C is predicted to coincide with the melting of the entire AlCoCrFeNi high entropy alloy composition. AlCoCrFeNi HEAs can be explained by the differentiation of internal stresses resulting from low and wide exothermic peaks (at 895-925-955 °C), lattice stress and structural deformation, etc. in the temperature range of about 895-1000°C. In this case, N.F. The research of Shkodich et al. has also been observed in the CoCrFeNiCu HEA(Shkodich et al., 2022).

In the Ti0.2 alloy, the DSC curve 1 (Fig. 4.13.b) exhibits three major endothermic peaks around 540°C and 998°C. Endothermic peaks are observed at 550°C, 650°C, and 997°C. In addition, it was compared with the microstructure images formed as a result of heat treatment in this temperature range. The phase transformation resulting from the heat treatment started in the region close to 750°C and continued up to 1000°C. With the effect of the Sigma phase formed, the endothermic peaks became deeper. Also, in Ti1.0 alloy, the DSC curve (Fig. 4.13.c) exhibits three main endothermic peaks around 680°C and 990°C. Endothermic peaks were observed at approximately 680°C, 810°C, and 990°C. A slight shift was observed in the endothermic peaks with increasing titanium content. In general, having a high melting point of the titanium element gave the alloy an advantage. It increased the melting temperature of the alloy.

4.4 Phase Diagram Result of AlCoCrFeNiTi$_x$ HEAs

Thermo-calc was calculated for the AlCoCrFeNiTix high entropy alloy system with Thermo-Calc software. The phase diagram, including the transformations depending on the titanium content and the temperature of the alloy under balanced cooling conditions, is given in Figure 4.14. Here, the ranges in which the phases formed in the alloy structure are demonstrated from about 1600°C to 25°C. Using Thermo-Calc software, phase diagrams of AlCoCrFeNiTix alloys were produced for the first time. There is no phase diagram in the literature describing the phases that will occur with the addition of titanium elements into AlCoCrFeNi HEA systems. Within the scope of this thesis, phase diagrams of AlCoCrFeNiTix high entropy alloys were obtained in light of both theoretical and experimental data. A contribution to the literature has been made. In this way, the usage areas of these alloy series in industrial applications will be increased.

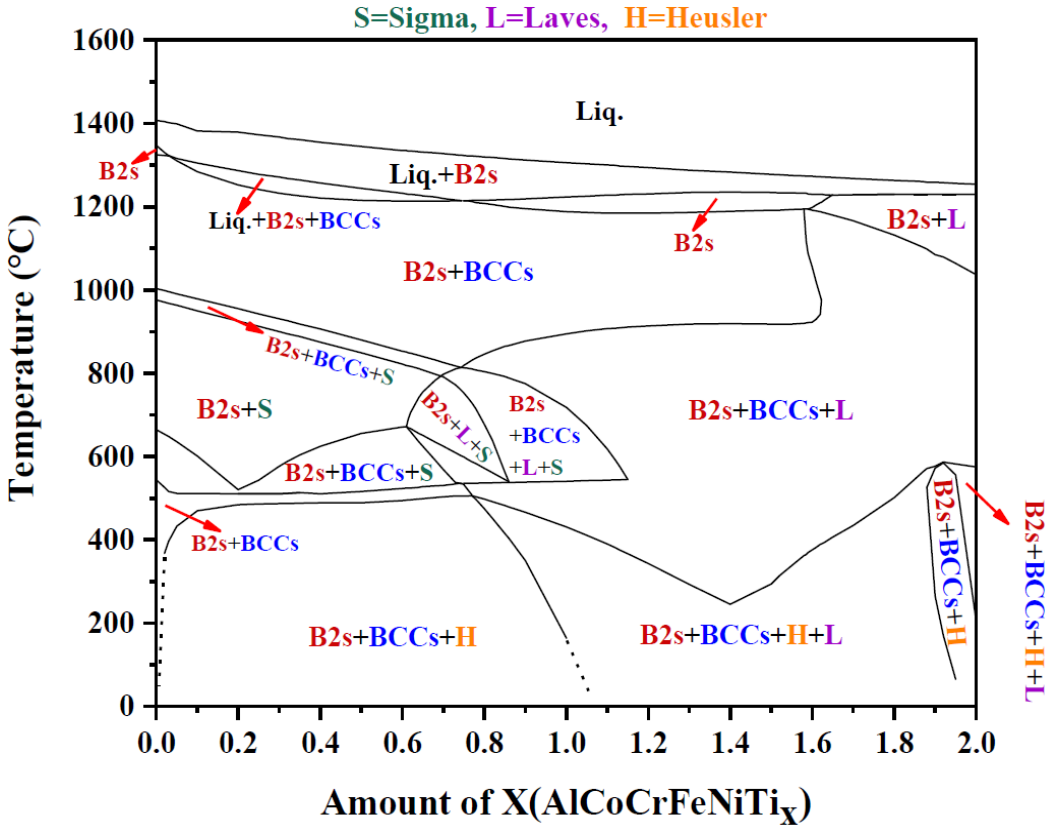

Figure 4.14 The phase equilibrium diagram of the AlCoCrFeNiTi$_X$ (0<x<2) system (Thermo-Calc software calculations)

In according within Fig. 4.14, the melting temperature of HEAs is decreasing as the titanium concentration rises. According to the phase diagram of HEAs consisting of Al-Co-Cr-Fe-Ni-Ti elements, the first solidified phase from the liquid phase is the BCC(B2) phase. At about 1400°C, the BCC phase occurs. In cases where the titanium content added to the Al-Co-Cr-Fe-Ni alloy was above about 1.62, the Laves phase in the structure was the second solidified phase at 1225°C. When the titanium content is below about 1.62, it is seen that the disorder structure of BCC phase is formed in the structure. This phase diagram shows that the alloy may undergo two peritectic and two eutectoid transformations. It was observed that at about 1320°C and titanium content of 0.03, a peritectic transformation to Liq. + B2s = BCCs phase could occur. It was observed that at approximately 1213°C and 0.74 titanium content, a peritectic transformation to Liq. + B2s = BCCs phase could happen. The temperature and composition at which eutectoid transformations can occur are as follows. It can occur at approximately 1187°C where the titanium content is 1.60 (B2s = BCCs + Laves). Another eutectoid transformation can occur at 814°C, where the titanium content is 0.74 (BCCs = Laves + Sigma).

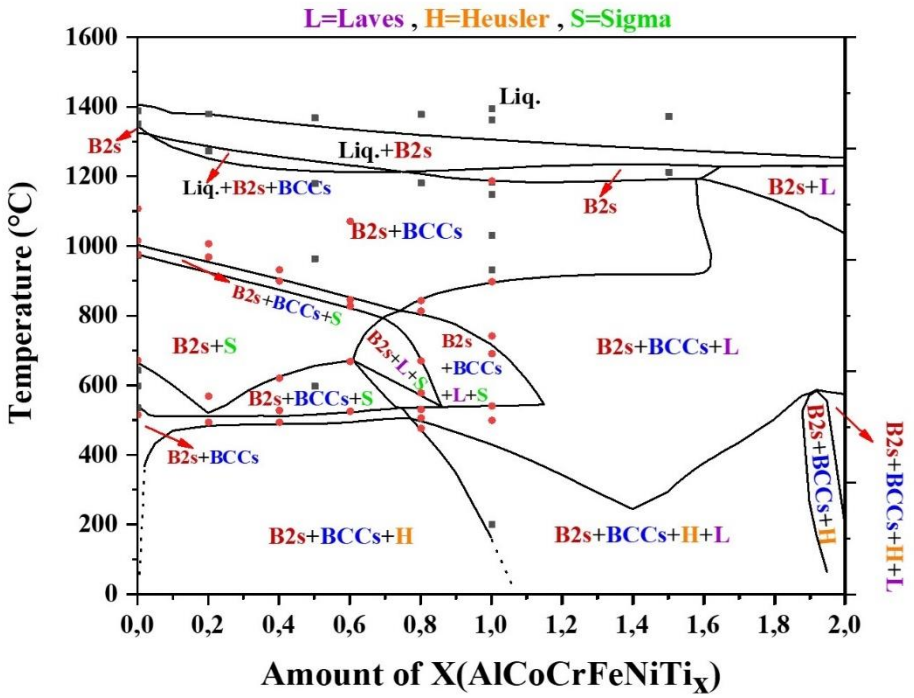

Figure 4.15 The phase equilibrium diagram of the AlCoCrFeNiTiX (0 < x < 2) system (■ = literature articles with ● = experimental findings)

The data obtained in the studies with the AlCoCrFeNiTix based system and the thermal analyzes (red dots) performed in this study are shown together in Figure 4.15. The results obtained here are compared. The difference between the liquidus and solidus temperatures of the experimental data (black dots) obtained in the studies was higher than in our study(Z. Fu & Koc, 2017; W. H. Guo, Li, Qi, Xu, & Ezatpour, 2021; Löbel et al., 2018; Strumza & Hayun, 2021; Uporov, Bykov, Pryanichnikov, Shubin, & Uporova, 2017; D. Zhao, Yamaguchi, Shu, Tokunaga, & Danjo, 2020)

CHAPTER 5

CONCLUSION

In this thesis, AlCoCrFeNiTix was produced by high entropy vacuum arc melting method. In addition, AlCoCrFeNiTix high entorpy alloy was designed by thermodynamically modeling with TermoCalc software. In line with the data obtained, heat treatment was applied to AlCoCrFeNiTix alloys. The phase morphology, microstructure images, thermal behavior and mechanical properties of the alloys were investigated. With the software used, the phase diagram of the AlCoCrFeNiTix alloy series ($0 < x < 2$) was revealed both theoretically and experimentally. In this context, AlCoCrFeNiTix is the first study of high entropy alloys in the literature. All the data obtained as a result of this study are presented below.

The following are the general findings of this research based on the outcomes of the tests conducted:

1. The phase amounts of AlCoCrFeNiTix high entropy alloys and the temperatures at which they formed were determined under non-equilibrium and balanced cooling conditions obtained by using TermoCalc software. These determined diagrams are also compatible with phase data obtained experimentally.
2. A single-phase ordered BCC solid solution was detected in the Ti0.0 alloy.As the percentage of titanium in the alloys rises,irregular BCC and irregular FCC phases were also formed. These observations were made in the XRD results of the cast HEAs. In addition to the B2, FCC, and BCC phases formed in the structure of Ti0.6 alloy, the Sigma phase was formed. 2 parameters explained this in high entropy alloys. The sigma phase forming elements (PSFE) and valence electron concentration (VEC) values in the alloy were investigated with TermoCalc software. VEC and PSFE are calculated at 6.86% and 35.7%. It was stated that the formation of the sigma phase in the alloy is likely. Low density newly formed Laves phases were

detected in Ti0.8 and Ti1.0 alloys. No sigma phase was observed except for Ti0.6 alloy.

3. Microstructure images were examined by SEM analysis of Ti-doped AlCoCrFeNi high entropy alloys produced by arc melting method. The microstructure images of the formed phases were similar to the XRD results. A single matrix phase was seen in the microstructure in Ti0.0 HEA. It was determined that with the increase of titanium content in the alloy, multiple phases with different contents were formed. Eutectic-like structures (X=0.4, 0.6, 0.8, and 1.0) and peritectic-like structures (X=0.8 and 1.0) were seen in the microstructures by SEM analysis. According to the EDS results, the content of the first solidified phase matched the content of the ordered BCC and disordered BCC mixture phases. The composition of the peritectic-like structure was found to belong to the mixed phase of regular BCC and irregular BCC with different content. In addition, the content of the eutectic-like structure was found to be compatible with the content of Laves, disordered FCC and disordered BCC mixture phases. These eutectic and peritectic transformations are congruous perfectly with the phase diagram that was obtained using the Scheil Calculator under circumstances of non-equilibrium cooling.
4. Endothermic peaks were observed in the DTA results of all AlCoCrFeNiTix high entropy alloys produced by arc melting. According to the DTA results, shifts were observed in the endothermic peaks with the increase of the titanium content in the alloy. This supported the formation of new phases by adding the element of titanium to the phases forming the alloy. It was thought that phase transformation took place at temperatures with these endothermic peaks.
5. As a result of the measurements, the average hardness value of the Ti0.0 alloy was calculated as 519 ±10 HV. With the addition of titanium element to the alloy system, the hardness value of the AlCoCrFeNİTix alloy system reached a maximum 827±15 HV.
6. According to the DTA results, the alloys and temperatures for the heat treatment experiments were determined. The heat treatment was carried out

at 3 different temperatures (500 °C, 750 °C, and 1000 °C) and under different ambient conditions (water cooling, oven cooling). When XRD analyzes were examined after heat treatment, no significant phase change was observed in the structure of Ti0.0, Ti0.2, and Ti1.0 alloys at 500 °C. It was determined that the Sigma phase was formed at 750 °C in all heat-treated alloys. No different phases were determined in the alloys in the heat treatment carried out at 1000 °C with both water cooling and furnace cooling.

7. By DSC analysis, the melting point of the alloy and the temperatures at which the phases forming the alloy can undergo structural deformation were determined. The structures of the endothermic and exothermic peaks in alloys allowed us to comment on the phase transformations that may occur. It was determined that phase transformations would occur in the temperature range of approximately 550 to 998°C in these 3 selected alloy series.
8. The phase equilibrium diagram calculated by the CALPHAD method under equilibrium cooling conditions was plotted. The predictions for the phase transformations were made with the help of this phase diagram. The findings of both the previous studies and present study were compared with the phase diagram proposal. It was determined that the formation and dissolution temperatures of the Sigma phases are in good agreement with the theoretical calculations.In addition, it was observed that the Sigma and Laves phases that would form in the structure were formed with the increase in titanium content. Critical transformation points of all phases in the alloy were determined and this phase diagram was drawn.

CHAPTER 6

FUTURE RECOMMENDATIONS

This study is a pioneering study in its field with the design and production of AlCoCrFeNiTix-based high entropy alloys in Turkey and revealing the phase diagram. This work's findings might be examined in the following areas:

The use of the AlCoCrFeNiTix high entropy alloy system, produced within the scope of the thesis, in various applications for medical biomaterial tools is investigated. In this context, biocompatibility tests were carried out on the alloy produced. The results showed that the biocompatibility was high. In the future, it is planned to produce alloys in which biocompatible phases can be formed by looking at the phase diagram we have created.

In addition, the produced AlCoCrFeNiTix was applied to Ti0.0 alloy, one of the high entropy alloy series, by pack boriding method. The surface hardness values that may occur due to the boron atom that may occur in these alloys were examined. An increase in the hardness values of the alloy was detected. In this context, it is predicted at which temperatures surface modification can be made using the Ti0.0 alloy system. The results of the study will be brought to the literature as a research article in the near future.

Considering all these, knowing the phase diagrams formed depending on the elements forming the alloy in detail will enable the estimation of the phases to be formed in other studies. It is thought that the usage areas of high entropy alloys can be increased by estimating the phases to be formed.

REFERENCES

Alshataif, Y. A., Sivasankaran, S., Al-Mufadi, F. A., Alaboodi, A. S., & Ammar, H. R. (2020). Manufacturing methods, microstructural and mechanical properties evolutions of high-entropy alloys: a review. *Metals And Materials International*, *26*(8), 1099–1133. https://doi.org/10.1007/S12540-019-00565-Z/FIGURES/36

Andreoli, A. F., Mendes, R. G., Witusiewicz, V. T., Shuleshova, O., van Huis, M. A., Nielsch, K., & Kaban, I. (2021). Phase constitution and microstructure of the NbTiVZr refractory high-entropy alloy solidified upon different processing. *Acta Materialia*, *221*, 117416. https://doi.org/10.1016/J.ACTAMAT.2021.117416

Bhattacharjee, P. P., Sathiaraj, G. D., Zaid, M., Gatti, J. R., Lee, C., Tsai, C. W., & Yeh, J. W. (2014). Microstructure and texture evolution during annealing of equiatomic CoCrFeMnNi high-entropy alloy. *Journal of Alloys and Compounds*, *587*, 544–552. https://doi.org/10.1016/J.JALLCOM.2013.10.237

Brif, Y., Thomas, M., & Todd, I. (2015). The use of high-entropy alloys in additive manufacturing. *Scripta Materialia*, *99*, 93–96. https://doi.org/10.1016/J.SCRIPTAMAT.2014.11.037

Butler, T. M., & Weaver, M. L. (2016). Oxidation behavior of arc melted AlCoCrFeNi multi-component high-entropy alloys. *Journal of Alloys and Compounds*, *674*, 229–244. https://doi.org/10.1016/J.JALLCOM.2016.02.257

Cantor, B., Chang, I. T. H., Knight, P., & Vincent, A. J. B. (2004). Microstructural development in equiatomic multicomponent alloys. *Materials Science and Engineering: A*, *375–377*(1-2 SPEC. ISS.), 213–218. https://doi.org/10.1016/J.MSEA.2003.10.257

Chen, H. L., Mao, H., & Chen, Q. (2018). Database development and Calphad calculations for high entropy alloys: Challenges, strategies, and tips. *Materials Chemistry and Physics*, *210*, 279–290. https://doi.org/10.1016/J.MATCHEMPHYS.2017.07.082

Chen, J., Niu, P., Liu, Y., Lu, Y., Wang, X., Peng, Y., & Liu, J. (2016). Effect of Zr content on microstructure and mechanical properties of AlCoCrFeNi high entropy alloy. *Materials & Design*, *94*, 39–44. https://doi.org/10.1016/J.MATDES.2016.01.033

Chen, L., Bobzin, K., Zhou, Z., Zhao, L., Öte, M., Königstein, T., et.al. (2018). Effect of heat treatment on the phase composition, microstructure and mechanical properties of Al0.6CrFeCoNi and Al0.6CrFeCoNiSi0.3 high-entropy alloys. *Metals 2018, 8, 974*, *8*(11), 974. https://doi.org/10.3390/MET8110974

Chen, R., Qin, G., Zheng, H., Wang, L., Su, Y., Chiu, Y. L., et.al.Fu, H. (2018). Composition design of high entropy alloys using the valence electron concentration to balance strength and ductility. *Acta Materialia*, *144*, 129–137. https://doi.org/10.1016/J.ACTAMAT.2017.10.058

Chen, S., Li, Q., Zhong, J., Xing, F., & Zhang, L. (2019). On diffusion behaviors in face centered cubic phase of Al-Co-Cr-Fe-Ni-Ti high-entropy superalloys. *Journal of Alloys and Compounds*, *791*, 255–264. https://doi.org/10.1016/J.JALLCOM.2019.03.286

Cheng, C. Y., Yang, Y. C., Zhong, Y. Z., Chen, Y. Y., Hsu, T., & Yeh, J. W. (2017). Physical metallurgy of concentrated solid solutions from low-entropy to high-entropy alloys. *Current Opinion in Solid State and Materials Science*, *21*(6), 299–311. https://doi.org/10.1016/J.COSSMS.2017.09.002

Cui, H. B., Wang, H. Y., Wang, J. Y., & Fu, H. Z. (2011). Microstructure and microsegregation in directionally solidified FeCoNiCrAl high entropy alloy. *Advanced Materials Research*, *189–193*, 3840–3843. https://doi.org/10.4028/WWW.SCIENTIFIC.NET/AMR.189-193.3840

Dong, Y., Lu, Y., Kong, J., Zhang, J., & Li, T. (2013). Microstructure and mechanical properties of multi-component AlCrFeNiMox high-entropy alloys. *Journal of Alloys and Compounds*, *573*, 96–101. https://doi.org/10.1016/J.JALLCOM.2013.03.253

Dong, Y., Zhou, K., Lu, Y., Gao, X., Wang, T., & Li, T. (2014). Effect of vanadium addition on the microstructure and properties of AlCoCrFeNi high entropy alloy. *Materials & Design*, *57*, 67–72. https://doi.org/10.1016/J.MATDES.2013.12.048

Fan, Z., Wang, H., Wu, Y., Liu, X. J., & Lu, Z. P. (2016). Thermoelectric high-entropy alloys with low lattice thermal conductivity. *RSC Advances*, *6*(57), 52164–52170. https://doi.org/10.1039/C5RA28088E

Ferrari, V., Wolf, W., Zepon, G., Coury, F. G., Kaufman, M. J., Bolfarini, C., et.al. (2019). Effect of boron addition on the solidification sequence and microstructure of AlCoCrFeNi alloys. *Journal of Alloys and Compounds*, *775*, 1235–1243. https://doi.org/10.1016/J.JALLCOM.2018.10.268

Firstov, S. A., Rogul', T. G., Krapivka, N. A., Ponomarev, S. S., Kovylyaev, V. V., Danilenko, N. I., et.al. (2016). Structural features and solid-solution hardening of high-entropy CrMnFeCoNi alloy. *Powder Metallurgy and Metal Ceramics*, *55*(3–4), 225–235. https://doi.org/10.1007/S11106-016-9797-9/TABLES/5

Fu, X., Schuh, C. A., & Olivetti, E. A. (2017). Materials selection considerations for high entropy alloys. *Scripta Materialia*, *138*, 145–150. https://doi.org/10.1016/J.SCRIPTAMAT.2017.03.014

Fu, Z., & Koc, R. (2017). Processing and characterization of TiB2-TiNiFeCrCoAl high-entropy alloy composite. *Journal of the American Ceramic Society*, *100*(7), 2803–2813. https://doi.org/10.1111/JACE.14814

Fujieda, T., Shiratori, H., Kuwabara, K., Kato, T., Yamanaka, K., Koizumi, Y., & Chiba, A. (2015). First demonstration of promising selective electron beam melting method for utilizing high-entropy alloys as engineering materials. *Materials Letters*, *159*, 12–15. https://doi.org/10.1016/J.MATLET.2015.06.046

Gao, M. C., & Alman, D. E. (2013). Searching for Next Single-Phase High-Entropy Alloy Compositions. *Entropy*, *15*(10), 4504–4519. https://doi.org/10.3390/E15104504

Gao, M. C., Liaw, P. K., Yeh, J. W., & Zhang, Y. (2016). *High-Entropy Alloys*. (M.

C. Gao, J.-W. Yeh, P. K. Liaw, & Y. Zhang, Eds.), *High-Entropy Alloys: Fundamentals and Applications*. Cham: Springer International Publishing. https://doi.org/10.1007/978-3-319-27013-5

Gorban', V. F., Krapivka, N. A., & Firstov, S. A. (2017). High-entropy alloys: Interrelations between electron concentration, phase composition, lattice parameter, and properties. *Physics of Metals and Metallography 2017 118:10*, *118*(10), 970–981. https://doi.org/10.1134/S0031918X17080051

Guan, S., Solberg, K., Wan, D., Berto, F., Welo, T., Yue, T. M., & Chan, K. C. (2019). Formation of fully equiaxed grain microstructure in additively manufactured AlCoCrFeNiTi0.5 high entropy alloy. *Materials & Design*, *184*, 108202. https://doi.org/10.1016/J.MATDES.2019.108202

Güler, S., Alkan, E. D., & Alkan, M. (2022). Vacuum arc melted and heat treated AlCoCrFeNiTiX based high-entropy alloys: Thermodynamic and microstructural investigations. *Journal of Alloys and Compounds*, *903*. https://doi.org/10.1016/J.JALLCOM.2022.163901

Guo, S., & Liu, C. T. (2011). Phase stability in high entropy alloys: Formation of solid-solution phase or amorphous phase. *Progress in Natural Science: Materials International*, *21*(6), 433–446. https://doi.org/10.1016/S1002-0071(12)60080-X

Guo, W. H., Li, J., Qi, M., Xu, Y., & Ezatpour, H. R. (2021). Effects of heat treatment on the microstructure, mechanical properties and corrosion resistance of AlCoCrFeNiTi0.5 high-entropy alloy. *Journal of Alloys and Compounds*, *884*, 161026. https://doi.org/10.1016/J.JALLCOM.2021.161026

Gwalani, B., Choudhuri, D., Soni, V., Ren, Y., Styles, M., Hwang, J. Y., et.al. (2017). Cu assisted stabilization and nucleation of L12 precipitates in Al0.3CuFeCrNi2 fcc-based high entropy alloy. *Acta Materialia*, *129*, 170–182. https://doi.org/10.1016/J.ACTAMAT.2017.02.053

Ham, G. S., Kim, Y. K., Na, Y. S., & Lee, K. A. (2021). Effect of ti addition on the microstructure and high-temperature oxidation property of AlCoCrFeNi high-

entropy alloy. *Metals and Materials International*, *27*(1), 156–165. https://doi.org/10.1007/S12540-020-00708-7/FIGURES/10

He, J. Y., Liu, W. H., Wang, H., Wu, Y., Liu, X. J., Nieh, T. G., & Lu, Z. P. (2014). Effects of Al addition on structural evolution and tensile properties of the FeCoNiCrMn high-entropy alloy system. *Acta Materialia*, *62*(1), 105–113. https://doi.org/10.1016/J.ACTAMAT.2013.09.037

Kong, D., Guo, J., Liu, R., Zhang, X., Song, Y., Li, Z., et.al. (2019). Effect of remelting and annealing on the wear resistance of AlCoCrFeNiTi0.5 high entropy alloys. *Intermetallics*, *114*, 106560. https://doi.org/10.1016/J.INTERMET.2019.106560

Kresse, G. (1995). Ab initio molecular dynamics for liquid metals. *Journal of Non-Crystalline Solids*, *192–193*, 222–229. https://doi.org/10.1016/0022-3093(95)00355-X

Lee, K. S., Bae, B., Kang, J., Lim, K. R., & Na, Y. S. (2017). Multi-phase refining of an AlCoCrFeNi high entropy alloy by hot compression. *Materials Letters*, *198*, 81–84. https://doi.org/10.1016/J.MATLET.2017.03.181

Li, C., Li, J. C., Zhao, M., & Jiang, Q. (2010). Effect of aluminum contents on microstructure and properties of AlxCoCrFeNi alloys. *Journal of Alloys and Compounds*, *504*(SUPPL. 1), S515–S518. https://doi.org/10.1016/J.JALLCOM.2010.03.111

Li, K., & Chen, W. (2021). Recent progress in high-entropy alloys for catalysts: synthesis, applications, and prospects. *Materials Today Energy*, *20*, 100638. https://doi.org/10.1016/J.MTENER.2021.100638

Li, Q., Zhao, S., Bao, X., Zhang, Y., Zhu, Y., Wang, C., et.al. (2020). Effects of AlCoCrFeNiTi high-entropy alloy on microstructure and mechanical properties of pure aluminum. *Journal of Materials Science & Technology*, *52*, 1–11. https://doi.org/10.1016/J.JMST.2020.04.008

Lin, G., Guo, J., & Ji, P. (2021). Molecular dynamics study on the diffusion process

of AuAgCuNiPd high-entropy alloy metallurgy induced by pulsed laser heating. *Physical Chemistry Chemical Physics*, *23*(35), 19482–19493. https://doi.org/10.1039/D1CP02181H

Liu, L., Zhu, J. B., Zhang, C., Li, J. C., & Jiang, Q. (2012). Microstructure and the properties of FeCoCuNiSnx high entropy alloys. *Materials Science and Engineering: A*, *548*, 64–68. https://doi.org/10.1016/J.MSEA.2012.03.080

Liu, X., Lei, W., Ma, L., Liu, J., Liu, J., & Cui, J. (2016). Effect of boron on the microstructure, phase assemblage and wear properties of Al0.5CoCrCuFeNi high-entropy alloy. *Rare Metal Materials and Engineering*, *45*(9), 2201–2207. https://doi.org/10.1016/S1875-5372(17)30003-6

Liu, Y., Pu, L., Yang, Y., He, Q., Zhou, Z., Tan, C., et.al. (2020). A high-entropy alloy as very low melting point solder for advanced electronic packaging. *Materials Today Advances*, *7*, 100101. https://doi.org/10.1016/J.MTADV.2020.100101

Löbel, M., Lindner, T., Mehner, T., & Lampke, T. (2018). Influence of titanium on microstructure, phase formation and wear behaviour of AlCoCrFeNiTix high-entropy alloy. *Entropy*, *20*(7), 1–11. https://doi.org/10.3390/E20070505

Ma, L., Wang, L., Nie, Z., Wang, F., Xue, Y., Zhou, J., et.al. (2017). Reversible deformation-induced martensitic transformation in Al0.6CoCrFeNi high-entropy alloy investigated by in situ synchrotron-based high-energy X-ray diffraction. *Acta Materialia*, *128*, 12–21. https://doi.org/10.1016/J.ACTAMAT.2017.02.014

Ma, S. G., Zhang, S. F., Gao, M. C., Liaw, P. K., & Zhang, Y. (2013). A successful synthesis of the CoCrFeNiAl0.3 single-crystal, high-entropy alloy by Bridgman solidification. *JOM*, *65*(12), 1751–1758. https://doi.org/10.1007/S11837-013-0733-X/FIGURES/5

Mary, S. J., Nagalakshmi, R., & Epshiba, R. (2015). High entropy alloys properties and its applications–An overview. *European Chemical Bulletin*, *4*(6), 279-284.

Miracle, D. B., Miller, J. D., Senkov, O. N., Woodward, C., Uchic, M. D., & Tiley, J. (2014). Exploration and development of high entropy alloys for structural

applications. *Entropy 2014, Vol. 16, Pages 494-525*, *16*(1), 494–525. https://doi.org/10.3390/E16010494

Mishra, A. K., Samal, S., & Biswas, K. (2012). Solidification behaviour of Ti-Cu-Fe-Co-Ni high entropy alloys. *Transactions of the Indian Institute of Metals*, *65*(6), 725–730. https://doi.org/10.1007/S12666-012-0206-X

Murty, B. S., Ranganathan, S., Yeh, J. W., & Bhattacharjee, P. P. (2019). *High-entropy alloys*. *High-Entropy Alloys*. Elsevier. https://doi.org/10.1016/C2017-0-03317-7

Na, Y. S., Lim, K. R., Chang, H. J., & Kim, J. (2016). Effect of trace additions of ti on the microstructure of AlCoCrFeNi-Based high entropy alloy. *Science of Advanced Materials*, *8*(10), 1984–1988. https://doi.org/10.1166/sam.2016.2793

Nayan, N., Singh, G., Murty, S. V. S. N., Jha, A. K., Pant, B., George, K. M., & Ramamurty, U. (2014). Hot deformation behaviour and microstructure control in AlCrCuNiFeCo high entropy alloy. *Intermetallics*, *55*, 145–153. https://doi.org/10.1016/J.INTERMET.2014.07.019

Ng, C., Guo, S., Luan, J., Shi, S., & Liu, C. T. (2012). Entropy-driven phase stability and slow diffusion kinetics in an Al0.5CoCrCuFeNi high entropy alloy. *Intermetallics*, *31*, 165–172. https://doi.org/10.1016/J.INTERMET.2012.07.001

Rao, J. C., Diao, H. Y., Ocelík, V., Vainchtein, D., Zhang, C., Kuo, C., et.al. (2017). Secondary phases in AlxCoCrFeNi high-entropy alloys: An in-situ TEM heating study and thermodynamic appraisal. *Acta Materialia*, *131*, 206–220. https://doi.org/10.1016/J.ACTAMAT.2017.03.066

Senkov, O. N., Wilks, G. B., Miracle, D. B., Chuang, C. P., & Liaw, P. K. (2010). Refractory high-entropy alloys. *Intermetallics*, *18*(9), 1758–1765. https://doi.org/10.1016/J.INTERMET.2010.05.014

Senkov, O. N., Zhang, C., Pilchak, A. L., Payton, E. J., Woodward, C., & Zhang, F. (2019). CALPHAD-aided development of quaternary multi-principal element refractory alloys based on NbTiZr. *Journal of Alloys and Compounds*, *783*, 729–742. https://doi.org/10.1016/J.JALLCOM.2018.12.325

Shkodich, N. F., Kovalev, I. D., Kuskov, K. V., Kovalev, D. Y., Vergunova, Y. S., Scheck, Y. B., et.al. (2022). Fast mechanical synthesis, structure evolution, and thermal stability of nanostructured CoCrFeNiCu high entropy alloy. *Journal of Alloys and Compounds*, *893*, 161839. https://doi.org/10.1016/J.JALLCOM.2021.161839

Singh, A. K., & Subramaniam, A. (2014). On the formation of disordered solid solutions in multi-component alloys. *Journal of Alloys and Compounds*, *587*, 113–119. https://doi.org/10.1016/J.JALLCOM.2013.10.133

Singh, S., Wanderka, N., Murty, B. S., Glatzel, U., & Banhart, J. (2011). Decomposition in multi-component AlCoCrCuFeNi high-entropy alloy. *Acta Materialia*, *59*(1), 182–190. https://doi.org/10.1016/J.ACTAMAT.2010.09.023

Sistla, H. R., Newkirk, J. W., & Frank Liou, F. (2015). Effect of Al/Ni ratio, heat treatment on phase transformations and microstructure of AlxFeCoCrNi2−x (x = 0.3, 1) high entropy alloys. *Materials & Design*, *81*, 113–121. https://doi.org/10.1016/J.MATDES.2015.05.027

Srivatsan, T. S., & Gupta, M. (2020). *High Entropy Alloys*. (T. S. Srivatsan & M. Gupta, Eds.). Boca Raton : CRC Press, 2020.: CRC Press. https://doi.org/10.1201/9780367374426

Strumza, E., & Hayun, S. (2021). Comprehensive study of phase transitions in equiatomic AlCoCrFeNi high-entropy alloy. *Journal of Alloys and Compounds*, *856*, 158220. https://doi.org/10.1016/J.JALLCOM.2020.158220

Sun, Z. H., Zhang, J., Xin, G. X., Xie, L., Yang, L. C., & Peng, Q. (2022). Tensile mechanical properties of CoCrFeNiTiAl high entropy alloy via molecular dynamics simulations. *Intermetallics*, *142*, 107444. https://doi.org/10.1016/J.INTERMET.2021.107444

Tsai, M. H., Chang, K. C., Li, J. H., Tsai, R. C., & Cheng, A. H. (2015). A second criterion for sigma phase formation in high-entropy alloys. *Http://Mc.Manuscriptcentral.Com/Tmrl*, *4*(2), 90–95.

https://doi.org/10.1080/21663831.2015.1121168

Tsai, M. H., & Yeh, J. W. (2014). High-entropy alloys: A critical review. *Materials Research Letters*, *2*(3), 107–123. https://doi.org/10.1080/21663831.2014.912690

Unnikrishnan, T. G., Paul, C., Sellamuthu, R., & Arul, S. (2017). An investigation on the effects of Co, Ti and Si on microstructure, hardness and wear properties of AlCuNiFe based entropy alloys. *Materials Today: Proceedings*, *4*(2), 178–187. https://doi.org/10.1016/J.MATPR.2017.01.011

Uporov, S., Bykov, V., Pryanichnikov, S., Shubin, A., & Uporova, N. (2017). Effect of synthesis route on structure and properties of AlCoCrFeNi high-entropy alloy. *Intermetallics*, *83*, 1–8. https://doi.org/10.1016/J.INTERMET.2016.12.003

Vaidya, M., Muralikrishna, G. M., & Murty, B. S. (2019). High-entropy alloys by mechanical alloying: A review. *Journal of Materials Research 2019 34:5*, *34*(5), 664–686. https://doi.org/10.1557/JMR.2019.37

Wang, R., Zhang, K., Davies, C., & Wu, X. (2017). Evolution of microstructure, mechanical and corrosion properties of AlCoCrFeNi high-entropy alloy prepared by direct laser fabrication. *Journal of Alloys and Compounds*, *694*, 971–981. https://doi.org/10.1016/J.JALLCOM.2016.10.138

Wang, W. R., Wang, W. L., Wang, S. C., Tsai, Y. C., Lai, C. H., & Yeh, J. W. (2012). Effects of Al addition on the microstructure and mechanical property of AlxCoCrFeNi high-entropy alloys. *Intermetallics*, *26*, 44–51. https://doi.org/10.1016/J.INTERMET.2012.03.005

Wang, X. J., Xu, M., Liu, N., & Liu, L. X. (2021). The formation of sigma phase in the CoCrFeNi high-entropy alloys. *Materials Research Express*, *8*(7), 076514. https://doi.org/10.1088/2053-1591/AC0A5C

Wang, Y., Ma, S., Chen, X., Shi, J., Zhang, Y., & Qiao, J. (2013). Optimizing mechanical properties of AlCoCrFeNiTi x high-entropy alloys by tailoring microstructures. *Acta Metallurgica Sinica (English Letters) 2013*, 277–284. https://doi.org/10.1007/S40195-012-0174-5

Winkler D., B. R. (1971). *Thermodynamics and Kinetics in Vacuum Metallurgy*. Vacuum Metallurgy Books

Wu, J. M., Lin, S. J., Yeh, J. W., Chen, S. K., Huang, Y. S., & Chen, H. C. (2006). Adhesive wear behavior of AlxCoCrCuFeNi high-entropy alloys as a function of aluminum content. *Wear*, *261*(5–6), 513–519. https://doi.org/10.1016/J.WEAR.2005.12.008

Xu, Z., Li, D. Y., & Chen, D. L. (2021). Effect of Ti on the wear behavior of AlCoCrFeNi high-entropy alloy during unidirectional and bi-directional sliding wear processes. *Wear*, *476*, 203650. https://doi.org/10.1016/J.WEAR.2021.203650

Yang, X., & Zhang, Y. (2012). Prediction of high-entropy stabilized solid-solution in multi-component alloys. *Materials Chemistry and Physics*, *132*(2–3), 233–238. https://doi.org/10.1016/J.MATCHEMPHYS.2011.11.021

Yao, H. W., Qiao, J. W., Gao, M. C., Hawk, J. A., Ma, S. G., Zhou, H. F., & Zhang, Y. (2016). NbTaV-(Ti,W) refractory high-entropy alloys: Experiments and modeling. *Materials Science and Engineering: A*, *674*, 203–211. https://doi.org/10.1016/J.MSEA.2016.07.102

Yeh, J.-W. (2016). Physical Metallurgy. In *High-Entropy Alloys* (pp. 51–113). Cham: Springer International Publishing. https://doi.org/10.1007/978-3-319-27013-5_3

Yeh, J. W. (2006). Recent progress in high-entropy alloys. *Annales de Chimie: Science Des Materiaux*, *31*(6), 633–648. https://doi.org/10.3166/ACSM.31.633-648

Yeh, J. W. (2013). Alloy design strategies and future trends in high-entropy alloys. *JOM*, *65*(12), 1759–1771. https://doi.org/10.1007/S11837-013-0761-6

Yeh, J. W., Chen, S. K., Lin, S. J., Gan, J. Y., Chin, T. S., Shun, T. T., et.al. (2004). Nanostructured high-entropy alloys with multiple principal elements: novel alloy design concepts and outcomes. *Advanced Engineering Materials*, *6*(5), 299–303. https://doi.org/10.1002/ADEM.200300567

Yu, Y., Shi, P., Feng, K., Liu, J., Cheng, J., Qiao, Z., et.al. (2020). effects of ti and cu on the microstructure evolution of AlCoCrFeNi high-entropy alloy during heat treatment. *Acta Metallurgica Sinica (English Letters)*, *33*(8), 1077. https://doi.org/10.1007/S40195-020-01002-6

Yu, Y., Wang, J., Li, J., Kou, H., & Liu, W. (2015). Characterization of BCC phases in AlCoCrFeNiTix high entropy alloys. *Materials Letters*, *138*, 78–80. https://doi.org/10.1016/J.MATLET.2014.09.100

Zhang, F., Zhang, C., Chen, S. L., Zhu, J., Cao, W. S., & Kattner, U. R. (2014). An understanding of high entropy alloys from phase diagram calculations. *Calphad*, *45*, 1–10. https://doi.org/10.1016/J.CALPHAD.2013.10.006

Zhang, K., & Fu, Z. (2012). Effects of annealing treatment on phase composition and microstructure of CoCrFeNiTiAlx high-entropy alloys. *Intermetallics*, *22*, 24–32. https://doi.org/10.1016/J.INTERMET.2011.10.010

Zhang, Y. (2019). *High-Entropy Materials : a Brief Introduction*. High Entropy Materials Books.

Zhang, Y., Zhou, Y. J., Lin, J. P., Chen, G. L., & Liaw, P. K. (2008). Solid-solution phase formation rules for multi-component alloys. *Advanced Engineering Materials*, *10*(6), 534–538. https://doi.org/10.1002/ADEM.200700240

Zhang, Y., Zuo, T. T., Tang, Z., Gao, M. C., Dahmen, K. A., Liaw, P. K., & Lu, Z. P. (2014). Microstructures and properties of high-entropy alloys. *Progress in Materials Science*. Elsevier Limited. https://doi.org/10.1016/j.pmatsci.2013.10.001

Zhao, D., Yamaguchi, T., Shu, J., Tokunaga, T., & Danjo, T. (2020). Rapid fabrication of the continuous AlFeCrCoNi high entropy alloy coating on aluminum alloy by resistance seam welding. *Applied Surface Science*, *517*, 145980. https://doi.org/10.1016/J.APSUSC.2020.145980

Zhao, J., Jiang, Z., Dobrzá, A., Lee, C. S., Pang, Z., Yang, J., et.al. (2022). Effect of high-temperature heat treatment on strengthening mechanism of AlCoCrFeNi

component fabricated by LMD. *Metals 2022,. 12*, *767*, *12*(5), 767. https://doi.org/10.3390/MET12050767

Zheng, M., Ding, W., Cao, W., Hu, S., & Huang, Q. (2019). A quick screening approach for design of multi-principal element alloy with solid solution phase. *Materials & Design*, *179*, 107882. https://doi.org/10.1016/J.MATDES.2019.107882

Zhou, N., Jiang, S., Huang, T., Qin, M., Hu, T., & Luo, J. (2019). Single-phase high-entropy intermetallic compounds (heics): bridging high-entropy alloys and ceramics. *Science Bulletin,17*. https://doi.org/10.48550/arxiv.1902.10420

Zhou, S. Cheng, Zhang, P., Xue, Y. Fei, Wang, F. Chi, Wang, L., Cao, T. Qing, et.al. (2018). Microstructure evolution of Al0.6CoCrFeNi high entropy alloy powder prepared by high pressure gas atomization. *Transactions of Nonferrous Metals Society of China*, *28*(5), 939–945. https://doi.org/10.1016/S1003-6326(18)64728-4

Zhou, Y. J., Zhang, Y., Wang, Y. L., & Chen, G. L. (2007). Solid solution alloys of AlCoCrFeNiTix with excellent room-temperature mechanical properties. *Applied Physics Letters*, *90*(18), 181904. https://doi.org/10.1063/1.2734517

Zyska, A., Konopka, Z., Łągiewka, M., & Kordas, P. (2017). Thermocalc application for the assessment of binary alloys non-equilibrium solidification. *Archives of Foundry Engineering*, *17*(1), 163–168. https://doi.org/10.1515/afe-2017-0030